Carbon Nanotube-Based Thermoelectric Materials and Devices

Jeffrey L. Blackburn, Andrew J. Ferguson,* Chungyeon Cho,* and Jaime C. Grunlan**

Conversion of waste heat to voltage has the potential to significantly reduce the carbon footprint of a number of critical energy sectors, such as the transportation and electricity-generation sectors, and manufacturing processes. Thermal energy is also an abundant low-flux source that can be harnessed to power portable/wearable electronic devices and critical components in remote off-grid locations. As such, a number of different inorganic and organic materials are being explored for their potential in thermoelectric-energy-harvesting devices. Carbon-based thermoelectric materials are particularly attractive due to their use of nontoxic, abundant source-materials, their amenability to high-throughput solution-phase fabrication routes, and the high specific energy (i.e., W g^{-1}) enabled by their low mass. Single-walled carbon nanotubes (SWCNTs) represent a unique 1D carbon allotrope with structural, electrical, and thermal properties that enable efficient thermoelectric-energy conversion. Here, a detailed review of the progress made toward understanding the fundamental thermoelectric properties of SWCNTs, nanotube-based composites, and thermoelectric devices prepared from these materials is provided. This progress illuminates the tremendous potential that carbon-nanotube-based materials and composites have for producing high-performance next-generation devices for thermoelectric-energy harvesting.

1. Introduction

The United States Energy Information Administration predicts that annual global energy consumption will increase by as much as 48% (relative to 2012 values) by the year 2040.[1] Of the estimated 97.3 quadrillion Btu's (British thermal units) consumed in the United States in 2016, Lawrence Livermore National Laboratory estimates that ≈66% of this energy was wasted, primarily as heat.[2] There are many strategies being explored for reducing the fraction of this wasted energy, including increasing consumption efficiency across multiple sectors (transportation, electricity generation, manufacturing, etc.) and increasing the percentage of generation by sustainable sources (e.g., solar, wind, geothermal). Another important strategy relies upon recovering some portion of this waste heat to do useful work. A variety of broad strategies exist for thermal energy conversion, including phase-change cycles such as Rankine cycles (steam engines), single-phase cycles based on gases (e.g., Carnot engines) or liquids (e.g., Malone engines), and solid-state heat engines such as those based on the thermoelectric (TE) effect.

The thermoelectric effect describes the conversion of a temperature gradient, typically across a doped semiconductor or metal, into an electrical voltage (Seebeck effect) or vice versa (Peltier effect). While TE energy conversion devices represent a potentially promising strategy for recovering energy from waste heat sources across a broad range of temperatures, many of the semiconductors that currently deliver the best TE efficiencies are costly to manufacture and are based on elements that are relatively scarce and/or toxic. As examples, the most widely used thermoelectric materials are inorganic semiconductors and their alloys, including Bi_2Te_3, PbTe, and Sb_2Te_3.[3] As such, the cost per Watt of delivered electricity is prohibitively high and there is currently no major commercial market for TE energy conversion devices. Other important potential applications for TE devices include the generation of electricity in remote locations (e.g., military field deployments) and/or powering small mobile wireless devices that require low power (e.g., health sensors for athletes or emergency responders). In these applications, device weight and form factor (e.g., flexible and conformable devices) become just as important as cost and efficiency. All of these issues have contributed to a growing interest in "soft" TE systems that are based on light, nontoxic organic (or hybrid) materials that can be deposited inexpensively from solution onto flexible substrates of widely varying form factors.[4]

In 1993, Hicks and Dresselhaus published two seminal papers with a theoretical framework capturing the dramatic improvements that both nanoscale interfaces and quantum-confined "nanomaterials" should offer to the thermoelectric figure of merit, zT (defined in detail below).[5] As shown in **Figure 1**, reprinted from the recent commentary by Heremans et al.,[3b] these publications sparked a new era of TE research,

Dr. J. L. Blackburn, Dr. A. J. Ferguson
Chemistry and Nanoscience Center
National Renewable Energy Laboratory
Golden, CO 80401-3305, USA
E-mail: jeffrey.blackburn@nrel.gov; andrew.ferguson@nrel.gov
Dr. C. Cho, Prof. J. C. Grunlan
Department of Mechanical Engineering
Texas A&M University
College Station, TX 77843-3003, USA
E-mail: cycho78@tamu.edu; jgrunlan@tamu.edu
The ORCID identification number(s) for the author(s) of this article can be found under https://doi.org/10.1002/adma.201704386.

DOI: 10.1002/adma.201704386

© 2017 WILEY-VCH Verlag GmbH & Co. KGaA, Weinheim

Pursuant to the DOE Public Access Plan, this document represents the authors' peer-reviewed, accepted manuscript. The published version of the article is available from the relevant publisher.

where nanoscale materials and nanoengineered interfaces helped to nearly double the performance of a number of the most heavily studied TE materials. Importantly, the calculations of Hicks and Dresselhaus led them to an intriguing conclusion: "These results indicate that a significant increase in zT can be achieved by going to lower dimensions, with the highest zT occurring in one dimension," an increase that they noted was "due mainly to the change in the density of states."[5b] It was noted that a particular new (at that time) 1D class of materials, carbon nanotubes, may hold particular promise, due to their small diameters (≈1.5 nm).[5b]

In the same year of the Hicks/Dresselhaus reports, Iijima et al. and Bethune et al. independently discovered single-walled carbon nanotubes (SWCNTs) experimentally.[6] A few computational studies had already suggested interesting dimensionality-dependent SWCNT electronic structures,[7] but these calculations remained to be tested experimentally. Following their discovery in 1993, researchers embarked on a number of fundamental studies, confirming that SWCNTs could indeed be semiconducting or metallic,[8] had diameter-dependent optical and electrical band gaps,[8b,9] and had many attractive properties such as incredibly high charge carrier mobilities.[10] In 2002, O'Connell et al. developed the critical advance of dispersing isolated individual SWCNTs in aqueous dispersions with micelle-forming surfactants.[9c] This advance set the stage for the rigorous assignment of structurally dependent band gaps[11] and the subsequent development of numerous enrichment strategies that successfully separated polydisperse as-synthesized SWCNT samples into pure semiconducting or metallic SWCNT populations and even populations dominated by a few or one specific SWCNT electronic structure.[12] These easily manipulated colloidal dispersions of individualized nanotubes established SWCNTs as a versatile electronic material, paving the way toward the integration of these unique 1D materials into high-performance applications, such as transistors,[13] biological imaging fluorophores,[14] photovoltaics,[15] and thermoelectrics.[16]

This review covers the significant progress made toward understanding the fundamental thermoelectric properties of SWCNTs and the performance metrics of nanotube-based TE materials and devices. The TE properties of random networks of SWCNTs are discussed first, with a focus on how electronic structure, charge carrier doping, and temperature influence these properties. After discussing the properties of "neat" SWCNT systems, the use of SWCNTs and few-walled CNTs in composite TE materials is reviewed. From these studies, it is clear that SWCNTs can be viewed on their own as a high-performance organic TE material, with performance on par with semiconducting polymers and the potential to enable lightweight and flexible TE devices. Importantly, the convergence of these two fields, the study of the TE performance of highly pure SWCNT samples and the study of TE composites containing CNTs, sets the stage for some dramatic performance gains in CNT-based TE materials in the years to come. The understanding of (1) the intrinsic performance metrics of pure SWCNT samples and (2) emergent phenomena that improve TE performance in CNT-based composites can provide a platform for the rational development of high-performance TE materials based on CNTs.



Jeffrey L. Blackburn received his Ph.D. in analytical chemistry from the University of Colorado, Boulder, in 2004. He worked as a postdoctoral researcher at the National Renewable Energy Laboratory (NREL) from 2004 to 2007, and is currently a senior scientist and group manager at NREL. His research interests include the fundamental understanding of optical and electrical properties and processes in low-dimensional materials (SWCNTs, graphene, 2D semiconductors, and semiconductor quantum dots), and the integration of these materials into sustainable energy technologies.



Andrew Ferguson is a Senior Scientist in the Chemistry & Nanoscience Center at the NREL. He received his Ph.D. in Physical Chemistry from Imperial College, United Kingdom, followed by a three-year term as a postdoctoral researcher at NREL. His current research focuses on exploring strategies to control exciton, carrier, and heat transport in nanoscale and organic semiconductors, including single-walled carbon nanotubes, and on the development and application of techniques to probe these transport properties over many decades in both time and length scale.



Jaime C. Grunlan is the Linda & Ralph Schmidt '68 Professor in the Department of Mechanical Engineering at Texas A&M University. He received his Ph.D. in Materials Science and Engineering from the University of Minnesota. His research focuses on thermal and transport properties of nanocomposite materials, especially in the areas of thermoelectric energy generation, gas barrier, and fire prevention. Dr. Grunlan also holds joint appointments in the Department of Chemistry and the Department of Materials Science and Engineering at Texas A&M University.

2. Basic Performance Metrics for Thermoelectrics

The TE effect enables the harvesting of thermal energy, where a temperature difference across a semiconductor induces the movement of charge carriers, producing electrical current and voltage. Whereas minority carriers, excited across the bandgap

© 2017 WILEY-VCH Verlag GmbH & Co. KGaA, Weinheim

Pursuant to the DOE Public Access Plan, this document represents the authors' peer-reviewed, accepted manuscript. The published version of the article is available from the relevant publisher.

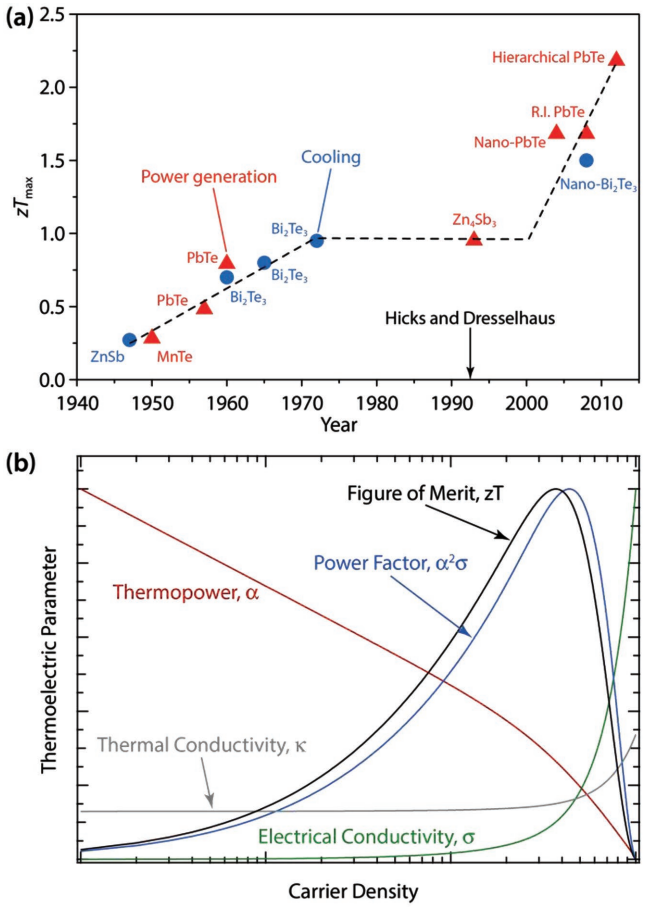

Figure 1. a) Progress in the material zT over time for low/intermediate-temperature inorganic TE materials, illustrating the advances brought about through material nanostructuring. Materials for TE cooling applications are shown as blue circles and for TE power generation as red triangles. Adapted with permission.[3b] Copyright 2013, Nature Publishing Group. b) Schematic showing the interdependence of the various TE properties with carrier density (over three orders of magnitude), illustrating the challenge of trying to optimize the material zT. The shapes of the individual curves are extracted from actual data on s-SWCNT networks.

by incident photons, are the predominant source of current in PV devices, typical (unipolar) TE devices are based on the electromotive diffusion and extraction of majority carriers, either electrons or holes, that are intentionally introduced into semiconductors by doping. Since they are majority carrier devices, a key factor in optimizing the performance of any TE material is the careful tuning of carrier density. Importantly, the carrier density directly affects the three critical material properties that define the TE figure of merit (zT): the electrical conductivity (σ), the Seebeck coefficient (α), and the thermal conductivity (κ_t). The TE figure of merit is defined by

$$zT = \frac{\alpha^2\sigma}{\kappa_t}T \quad (1)$$

It should be noted here that we use lowercase zT to denote the material figure of merit, following a previously employed convention,[3a] whereas the device figure of merit defined later will use uppercase ZT.

The electrical conductivity is related to the majority charge carrier density, n, and the charge carrier mobility, μ, through Equation (2)

$$\sigma = ne\mu \quad (2)$$

where e is the elementary charge. The Seebeck coefficient is the voltage generated in a material for a given temperature difference

$$\alpha = \frac{\Delta V}{\Delta T} \quad (3)$$

This "Seebeck voltage," or thermopower, is related to the entropy of charge carriers within the material—carriers move from the hot side of the material (high entropy) to the cold side of the material (low entropy), establishing a steady-state voltage once at equilibrium. Since both charge carriers and phonons can carry heat, the total thermal conductivity, κ_t, is the sum of the electronic (κ_e) and lattice (κ_l) components

$$\kappa_t = \kappa_e + \kappa_l \quad (4)$$

The primary challenge in optimizing materials for thermoelectric energy conversion is the fact that each of these three material properties (σ, α, and κ_t) are inter-related and do not have the same dependence on carrier density, as shown in Figure 1b. As the carrier density increases, the electrical conductivity increases (beneficial for zT) but the Seebeck coefficient decreases (detrimental to zT). An increase of the charge carrier density also tends to increase the electrical contribution to the thermal conductivity, which tends to reduce zT. This complex interdependence begets three guiding principles for the rational development of thermoelectric materials—(1) the peak value of zT at a given temperature for a given material is found at a particular value/range of carrier density, (2) since each critical material property has its own temperature dependence, the peak value of zT for a given material is also found at a particular temperature, and (3) zT can often be increased by strategies that help to decouple or weaken the interdependence of σ, α, and κ_t.

3. Thermoelectric Properties of SWCNTs

3.1. Electronic Structure of SWCNTs

There are a number of review articles that discuss SWCNT synthesis, basic electronic structure, and electronic structure-based separations of SWCNTs, so we will not cover these topics extensively in this review. For the purposes of this review article, it is primarily important to appreciate that the SWCNT electronic structure can either be semiconducting or metallic, depending on the "roll-up vector" of the SWCNT in question (**Figure 2**). The magnitude and chiral angle (α) of this roll-up vector (with respect to the zig-zag axis) define a set of (n,m) indices that denote unique SWCNTs and can be used to determine the

© 2017 WILEY-VCH Verlag GmbH & Co. KGaA, Weinheim

Pursuant to the DOE Public Access Plan, this document represents the authors' peer-reviewed, accepted manuscript. The published version of the article is available from the relevant publisher.

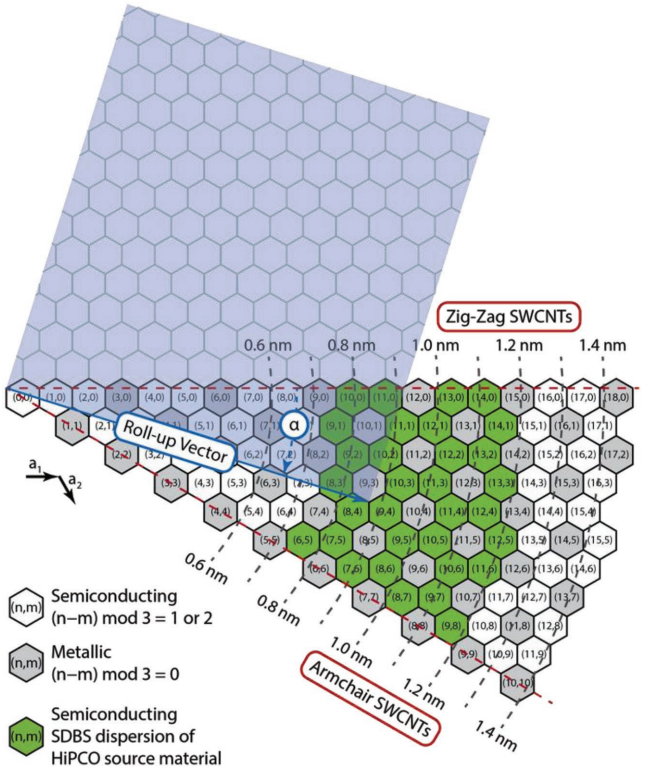

Figure 2. Segment of a graphene sheet showing the chiral indices (*n*,*m*) corresponding to the SWCNT formed by rolling the sheet from (0,0) to (*n*,*m*) along the highlighted roll-up vector to form a cylinder. Rolling up the shaded blue area forms a cylinder corresponding to a segment of the unit cell for the (9,4) SWCNT. The white hexagons identify chiral indices corresponding to semiconducting SWCNTs, the gray hexagons identify chiral indices corresponding to metallic SWCNTs, and the green hexagons identify chiral indices corresponding to the semiconducting SWCNTs present in a typical batch of commercial SWCNTs produced by the HiPCO process.

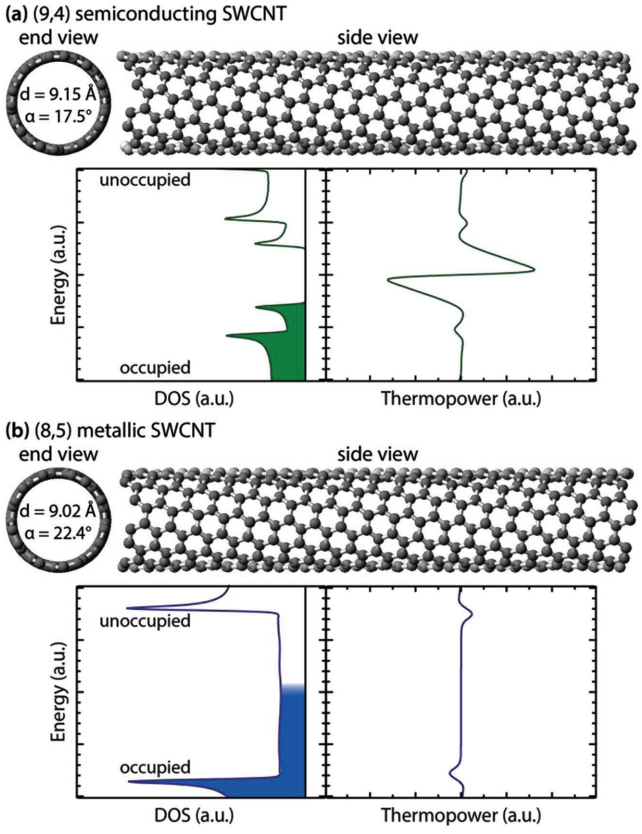

Figure 3. The chemical structure and corresponding electronic properties of the semiconducting (9,4) SWCNT and metallic (8,5) SWCNT, illustrating that subtle changes in the chirality, SWCNT diameter, and chiral angle can produce dramatic differences in the electronic DOS and predicted thermopower.

particular electronic structure of that SWCNT. Statistically, 1/3 of all possible SWCNTs are metallic, while the other 2/3 have semiconducting electronic structure (**Figure 3**). Most (but not all) SWCNT syntheses produce this statistical ratio of semiconducting and metallic SWCNTs along with a range of SWCNT diameters. As such, a number of strategies have been developed to separate as-prepared SWCNT samples on the basis of electronic structure, diameter, and chirality.

Quantum confinement in two dimensions produces sharp singularities in the densities of states for SWCNTs, which are termed van Hove singularities (vHS, Figure 3). The electronic band gap is the energy difference between the first electron and hole vHS. With respect to charge carrier doping, the energy of these vHS also define the first reduction and oxidation potentials, respectively, of a particular s-SWCNT (also referred to as the electron affinity and ionization potential, respectively). The most commonly utilized SWCNTs have diameters in the range of ≈0.7–2.0 nm, with electronic band gaps in the range of ≈1.7–0.6 eV, respectively. The s-SWCNT species (and by extension the overall diameter distribution) present in a particular sample can be readily identified by spectroscopic techniques, such as photoluminescence excitation (PLE) spectroscopy (**Figure 4**), at least for SWCNTs with d < ≈1.7 nm (using an InGaAs detector). In this case, s-SWCNTs within a sample that have been dispersed as isolated nanotubes by surfactants or polymers emit light via radiative excitonic recombination at the optical band gap, which is smaller than the electronic band gap by a quantity known as the exciton binding energy. Almost universally, this same surfactant/polymer dispersion process serves as the starting point for the SWCNT separations and composite fabrications that enable the bulk of the thermoelectric materials discussed in this review.

We will also discuss some TE composites that contain double-walled carbon nanotubes (DWCNTs), which are a subset of what can generally be called multiwalled carbon nanotubes (MWCNTs). DWCNTs are also typically produced as a polydisperse mixture of diameters and electronic structures, with further complications from SWCNT contamination and the four unique permutations of inner@outer wall combinations: semi@semi, metal@metal, semi@metal, and metal@metal.[17] While some progress has been made in separations of DWCNTs by the outer wall structure,[18] production of highly pure samples with defined inner@outer wall combinations has proven difficult due to the strong coupling between the inner and outer walls.

© 2017 WILEY-VCH Verlag GmbH & Co. KGaA, Weinheim

Pursuant to the DOE Public Access Plan, this document represents the authors' peer-reviewed, accepted manuscript. The published version of the article is available from the relevant publisher.

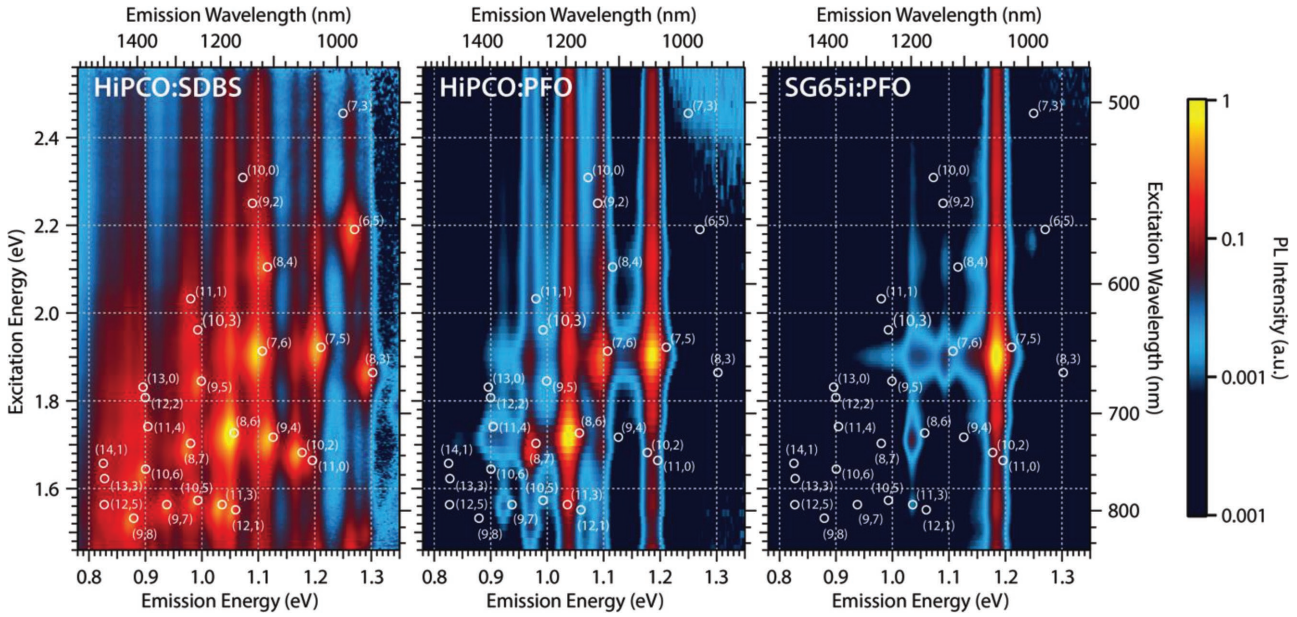

Figure 4. Photoluminescence excitation (PLE) maps for dispersions prepared from (left) HiPCO SWCNTs using the nonselective surfactant SDBS, and (middle) HiPCO SWCNTs and (right) CoMoCAT (SG65i) SWCNTs using the highly selective polymer PFO.

3.2. Effect of SWCNT Electronic Structure on σ and α

The magnitudes of the Seebeck coefficient and electrical conductivity of SWCNTs are intimately tied to electronic structure. In the low-temperature limit, the intrinsic (or ballistic) Seebeck coefficient (α_i) of a material is directly tied to the shape of the density of states near the Fermi energy, through the equation

$$\alpha_i(E_f) = -\frac{\pi}{3}\frac{k_B}{e}k_B T\left[\frac{\partial \ln[N(E)]}{\partial E}\right]_{E=E_f} \quad (5)$$

In Equation (5), E is the energy, E_f is the Fermi energy, k_B is the Boltzmann constant, T is the absolute temperature, and e is the elementary charge. The derivative term in the square brackets of Equation (5) implies that an important contributing factor to a large intrinsic thermopower is high curvature within the density of states ($N(E)$) near the Fermi energy or transport level.

Early (2005 or prior) studies on mixed SWCNT samples containing both m- and s-SWCNTs measured thermopowers in the range of 11–65 μV K^{-1} (**Table 1**),[19] with the exact magnitude depending on the form factor (ropes versus bulk mats), processing method, and the degree of intentional or unintentional doping. All of these samples presumably contained the statistical ratio of semiconducting and metallic SWCNTs (2:1). The average of the Seebeck values reported in these early studies for samples with mixed electronic structure, where no intentional doping was employed (i.e., the samples may be considered to be "adventitiously" doped by O_2 molecules), is 49 ± 12 μV K^{-1}, showing fairly good reproducibility across a wide range of studies.[19a–i]

Qualitatively, a consideration of the density of states for metallic SWCNTs suggests a relatively low thermopower since m-SWCNTs have a nearly constant (i.e., relatively flat) density of states between the widely spaced (energetically) first electron and hole van Hove singularities (Figure 3). This prediction was born out experimentally (**Figure 5**a) when studies on separated SWCNTs demonstrated only modest values of thermopower for highly enriched m-SWCNTs, in the range of 10–20 μV K^{-1}.[20] The same studies found significantly higher Seebeck coefficients for s-SWCNTs, in the range of 80–160 μV K^{-1}, and the thermopower for mixed networks with both s- and m-SWCNTs also systematically increased as the concentration of s-SWCNTs was increased in the network.[20] These studies were able to simulate the dependence of the experimentally measured thermopower on the fraction of s-SWCNT in the network by considering the intertube or interbundle junctions in parallel and/or series conducting pathways.[20]

The thermopower was calculated for a variety of SWCNT species in two recent papers (Figure 5b,c).[16a,21] Avery, et al. used density functional theory to calculate the dependence of α_i on SWCNT diameter, electronic structure, and E_f,[16a] whereas Hung et al. utilized the Boltzmann transport formalism combined with an extended tight-binding model.[21] Avery et al. found that, for similar SWCNT diameters, the peak intrinsic thermopower for s-SWCNTs is nearly an order of magnitude higher than that of m-SWCNTs (Figure 5b). Both studies found that the thermopower for s-SWCNTs dramatically rises as E_f is moved away from the center of the gap, in either a positive (hole doping) or negative (electron doping) direction. In both cases, the maximum thermopower was achieved after only a small shift (≈50–60 meV) of E_f, after which α_i decreased with increasing magnitude of the Fermi level shift. Both studies also found that α_i generally increased with decreasing s-SWCNT diameter, or alternatively increasing s-SWCNT band gap. The study of Hung et al. demonstrates that the family dependence seen in typical Kataura plots was also reproduced in the species-dependent thermopower trend (Figure 5c).[21] It is noteworthy

© 2017 WILEY-VCH Verlag GmbH & Co. KGaA, Weinheim

Pursuant to the DOE Public Access Plan, this document represents the authors' peer-reviewed, accepted manuscript. The published version of the article is available from the relevant publisher.

Q5 **Table 1.** Preparation and thermoelectric properties of unsorted, p-type, carbon nanotube-only samples at room temperature.

SWCNT material[a)]	Preparation	Dopant	Electrical conductivity [S cm^{-1}]	Seebeck coefficient [μV K^{-1}]	Power factor [μV m^{-1} K^{-2}]	Thermal conductivity [W m^{-1} K^{-1}]	zT	Year	Ref.
Pulsed LV	Rope	O_2-doped	–	52	–	–	–	1998	[19a]
			–	65	–	–	–		
Pulsed LV	Mats	O_2-doped	–	39	–	–	–	1998	[19b]
AD			–	45	–	–	–		
Pulsed LV		I_2-doped	–	19	–	–	–		
AD			–	11	–	–	–		
Pulsed LV	Film deposited from dichloroethane	O_2-doped	–	24	–	–	–	2000	[19c]
Carbolex Inc.	Pressed mats	O_2-doped	–	45	–	–	–	2000	[19d]
Pulsed LV or AD	Filter-deposited buckypaper/film deposited from methanol	O_2-doped	–	45	–	–	–	2000	[19e]
Unknown	Filtered buckypaper	Partially O_2-doped	≈600–1000	50	≈150–250	–	–	2002	[19f]
		O_2-doped	–	62	–	≈15	–		
Carbolex Inc.	Film deposited from ethanol	Partially O_2-doped	–	64	–	–	–	2002	[19g]
			–	35	–	–	–		
HiPCO	Filter-deposited buckypaper	O_2-doped	–	60	–	–	–	2003	[19h]
		Nitric acid	–	25	–	–	–		
CVD	Strand of CNT ropes	O_2-doped	–	50	–	–	–	2005	[19i]
		Partially O_2-doped	–	20	–	–	–		
Pulsed LV	Filter-deposited buckypaper	Nitric acid	650	19	23.5	–	–	2005	[19j]
		Sulfuric acid	1100	15.5	26.4	–	–		
HiPCO	Film deposited from oleum	Nitric acid	–	20	–	–	–		
		Sulfuric acid	–	16.5	–	–	–		
"Super-growth" CVD	Filter-deposited buckypaper	O_2-doped	36	49	8.6	0.098	0.027	2013	[29]
"Super-growth" CVD	Filter-deposited buckypaper	O_2-doped	35	26	2.4	2.6	0.0003	2015	[52]
AD	As-purchased buckypaper	Water vapor	40	50	11.2	–	–	2016	[36]
eDIPS	Pressed mats		165	55	50	–	–		
			175	48	40	–	–		
			135	47.5	30.5	–	–		
"Super-growth" CVD	Filter-deposited buckypaper		50	42	8.8	–	–		
eDIPS	Filter-deposited buckypaper	O_2-doped	1510	38	218	9.8	0.0067	2016	[26]
Floating catalyst CVD	As-synthesized buckypaper	O_2-doped	3200	88	2480	51	0.015	2016	[51]
	Laminated sheet from multiple buckypaper films		1370	92	1160	21	0.017		
	Fiber from twisted buckypaper		2220	100	2200	53	0.013		

© 2017 WILEY-VCH Verlag GmbH & Co. KGaA, Weinheim

Pursuant to the DOE Public Access Plan, this document represents the authors' peer-reviewed, accepted manuscript. The published version of the article is available from the relevant publisher.

Table 1. Continued.

SWCNT material[a)]	Preparation	Dopant	Electrical conductivity [S cm^{-1}]	Seebeck coefficient [μV K^{-1}]	Power factor [μV m^{-1} K^{-2}]	Thermal conductivity [W m^{-1} K^{-1}]	zT	Year	Ref.
AD	Filter-deposited buckypaper	Nitric acid	670	35	85	–	–	2016	[53]
eDIPS	Filter-deposited buckypaper	O_2-doped	512	38	73.9	–	–	2016	[28]
Floating catalyst CVD	As-synthesized buckypaper	O_2-doped	3020	78	1840	–	–	2017	[46]
			2230	87	1690	24	0.021		
eDIPS[b)]	Filter-deposited buckypaper	O_2-doped	626	40	102	–	–	2017	[31e]
		Leuco malachite green (MGH) in benzyl alcohol	588	58	200	–	–		
		MGH in benzene	571	51	147	–	–		
		MGH in 1-butanol	488	45	100	–	–		
		MGH in ethanol	436	42	78	–	–		
		MGH in methanol	407	39	61	–	–		
		MGH in acetonitrile	460	26	30	–	–		
		MGH in *N*-methyl pyrrolidone	475	9.3	4.1	–	–		
		MGH in *N*,*N*-dimethyl formamide	483	8.8	3.8	–	–		
Floating catalyst CVD	Aligned yarn	Iron (III) chloride ($FeCl_3$)	7476	57	2387	–	–	2017	[54]

[a)]When the thermoelectric properties corresponding to the peak power factor are not reported directly in the manuscript they are estimated from plots of Seebeck coefficient and electrical conductivity; [b)]This study found that the ability for MGH to dope SWCNT n-type depended on the basicity of the solvent. The solvents in this table did not foster measurable n-type behavior, so the majority of hole carriers likely result from ambient O_2 doping.

that both studies predict very large values for the intrinsic thermopower of s-SWCNTs, in the range of 400 μV K^{-1} for large-diameter (≈1.5 nm) s-SWCNTs and up to 2000 μV K^{-1} for very small diameter (≈0.5 nm) s-SWCNTs).

The effect of electronic structure on electrical conductivity has been studied in much more detail, both theoretically and experimentally. The advent of the density gradient ultracentrifugation separation technique[12a] afforded some key early experimental studies on the influence of electronic structure and doping on m- and s-SWCNT thin-film conductivity.[22] Completely intrinsic s-SWCNT networks have inherently low (and in the most ideal cases, essentially immeasurable) conductivity, since there are few carriers present. In contrast m-SWCNTs can have appreciable electrical conductivity in their intrinsic state, due to the presence of carriers at E_f. However, s-SWCNT networks become incredibly conductive when heavily doped with charge transfer dopants, and in fact are significantly more conductive than heavily doped m-SWCNT networks.[22b,c] Regarding the diameter dependence of the electrical conductivity, since the charge carrier mobility increases with increasing SWCNT diameter, it is expected that the electrical conductivity (at a given carrier density) should increase with increasing SWCNT diameter.[16a]

The considerations above, regarding the effects of SWCNT electronic structure on σ and α, suggest a few initial guiding principles for the optimization of the thermoelectric power factor of SWCNT thin films: (1) Pure s-SWCNT samples can theoretically achieve extremely large magnitudes of α;[16a,20,21] (2) once doped appropriately, pure s-SWCNTs can also exhibit very large magnitudes of σ;[22a–c] and (3) both α and σ are

© 2017 WILEY-VCH Verlag GmbH & Co. KGaA, Weinheim

Pursuant to the DOE Public Access Plan, this document represents the authors' peer-reviewed, accepted manuscript. The published version of the article is available from the relevant publisher.

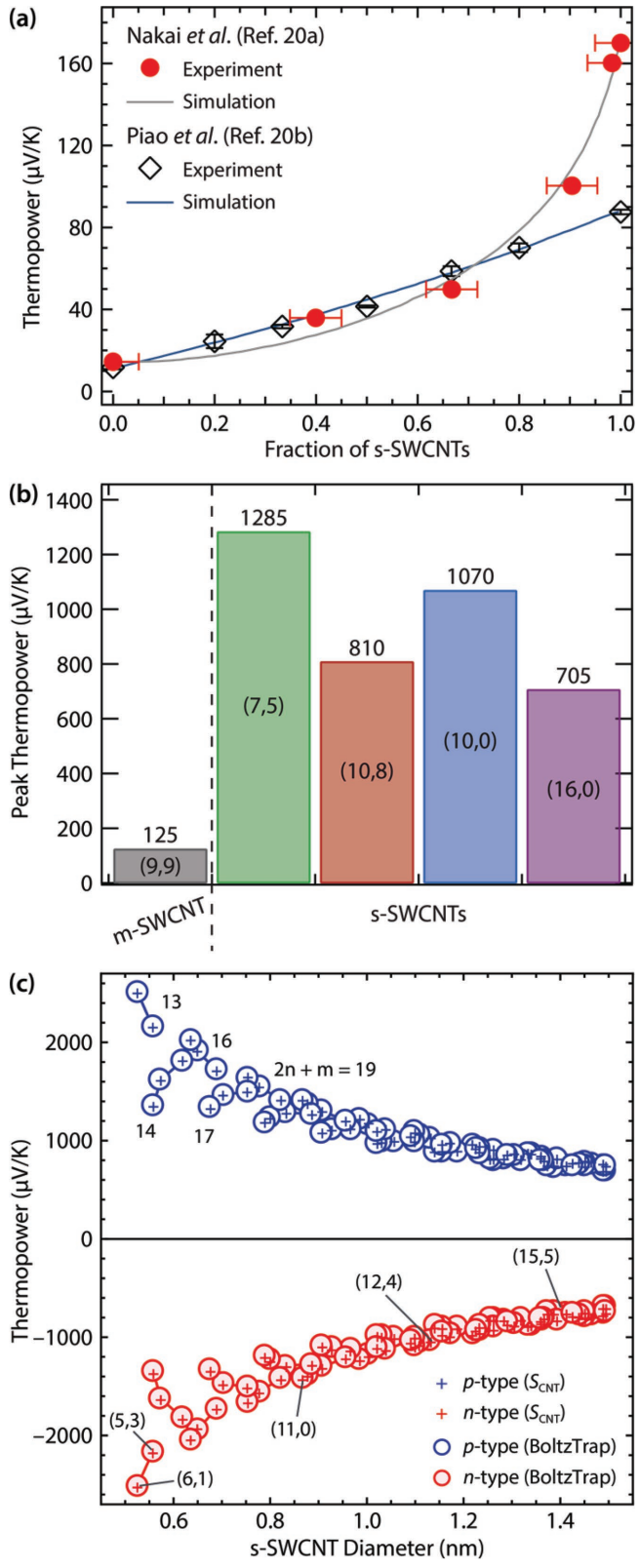

Figure 5. a) Experimentally measured thermopowers for networks composed of different loadings of s-SWCNTs. The solid lines are theoretical models that consider the junctions between SWCNT bundles in serial and/or parallel conducting pathways. Nakai et al.'s data reused with permission.[20a] Copyright 2014, The Japan Society of Applied Physics. Piao et al.'s data reused with permission.[20b] Copyright 2014, American Chemical Society. b) Theoretically predicted peak thermopowers for SWCNTs with the defined chiral indices. Adapted with permission.[16a] Copyright 2016, Nature Publishing Group. c) Theoretically predicted diameter dependence for the peak thermopower for various s-SWCNTs. Reproduced with permission.[21] Copyright 2015, American Physical Society.

highly sensitive to the position of the Fermi energy (controlled by the carrier density) and to the s-SWCNT diameter.[16a,20a,21] These guiding principles set the stage for the detailed study of carrier doping and SWCNT diameter (and hence band gap) as variables for sensitively tuning the SWCNT thermoelectric power factor.

3.3. Effect of SWCNT Doping on σ and α

Since all three parameters comprising zT typically depend on the carrier density in a given semiconductor (Figure 1b), the ideal strategy to probe this dependence would employ methods to sensitively tune the carrier density over a large range while probing α, σ, and κ. This is difficult in many organic and inorganic TE systems, however, due to a variety of factors. In inorganic semiconductors, it is often difficult to find the proper conditions and atomic dopants with appropriate characteristics that enable precise tuning of the carrier density without encountering structural deformations and phase segregation. In typical organic polymers, molecular dopants can be used to tune carrier density via ground state charge transfer interactions that inject holes or electrons into the polymers.[23] However, the addition of these dopants to polymer solutions can create phase segregation and/or completely different morphologies in the subsequently deposited solid-state polymer/blend.[24] In both cases, the expected improvements to conductivity (via increasing the carrier density) can often be counteracted by deleterious structural changes that reduce the electronic coupling between domains and hinder long-range charge carrier transport.

SWCNTs represent a unique system with some clear advantages for using charge transfer dopants to tune the carrier density. First, SWCNT networks tend to have both porosity and very high surface areas, so SWCNT surfaces are typically quite accessible for adsorbing redox molecules (**Figure 6**a–c). Second, the morphology of a SWCNT thin film is essentially "locked in" once it is deposited. In other words, the network can be immersed in a wide variety of solvents and dopant-containing solutions without leading to any changes in morphology. Third, the sensitivity of the SWCNT pi electron system to surface-mediated redox reactions means that no covalent bonds need to be formed to generate large swings in the carrier density injected by physisorbed molecules. These traits imply that SWCNT networks can be doped simply by soaking in solutions of redox molecules, without any appreciable changes to the network morphology (e.g., SWCNT connectivity, bundle size, porosity, etc.) or SWCNT atomic or electronic structure (e.g., no creation of sp^3 defects, no modification of intrinsic band structure, etc.). Such a system stands in marked contrast to most

© 2017 WILEY-VCH Verlag GmbH & Co. KGaA, Weinheim

Pursuant to the DOE Public Access Plan, this document represents the authors' peer-reviewed, accepted manuscript. The published version of the article is available from the relevant publisher.

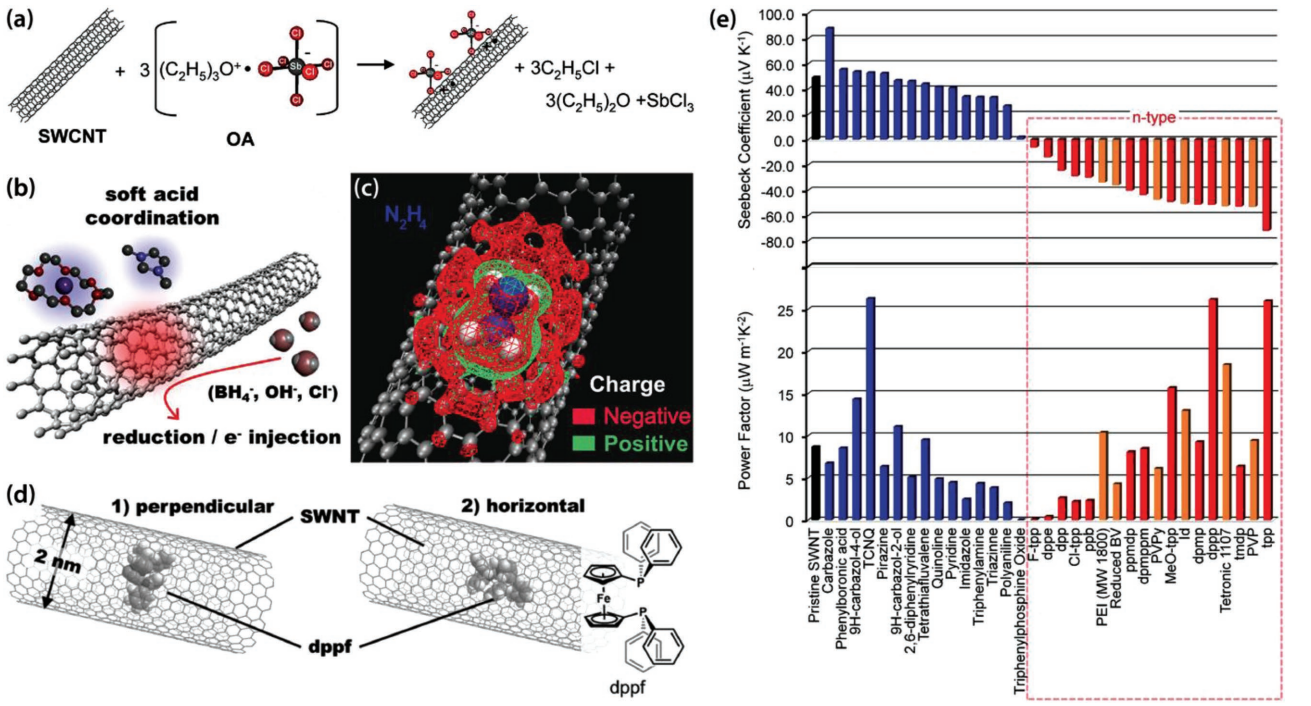

Figure 6. Remote doping for SWCNT thermoelectric materials. a,b) Schematic cartoons illustrating stabilization of injected carrier density by physisorption of counterions onto the SWCNT sidewall. a) Adapted with permission.[25] Copyright 2010, American Chemical Society. b) Adapted with permission.[26] Copyright 2016, Wiley-VCH. c) Schematic cartoon illustrating stabilization of injected carrier density by physisorption of charge-transfer dopants onto the SWCNT sidewall. Adapted with permission.[27] Copyright 2011, American Chemical Society. d) Schematic cartoons illustrating encapsulation of charge-transfer dopants into the SWCNT endohedral volume. Adapted with permission.[28] Copyright 2016, Wiley-VCH. e) Thermopower (top) and thermoelectric power factor (bottom) for p-type and n-type redox doping of unsorted, small bandgap SWCNT buckypapers. Adapted with permission.[29] Copyright 2013, Macmillan Publishers Ltd.

typical organic and inorganic semiconductors utilized for TE energy generation.

A host of redox dopants are available for doping s-SWCNT thin films either p- or n-type. In general, Brønsted or Lewis acids create p-type SWCNT networks upon physisorption,[22a,b,25,30] whereas Brønsted or Lewis bases create n-type SWCNT networks.[26,27,29,31] In general, the primary consideration for a successful p-type redox dopant is to have an electron affinity that is larger than the ionization potential of the SWCNT in question. Conversely, successful n-type redox dopants have ionization potentials that are lower than the electron affinity of the SWCNT in question. One important consideration for TE device stability is the thermal and environmental stability of the physisorbed redox dopants. Early studies demonstrated that adsorbed p-type redox dopants such as HNO_3 and $SOCl_2$ desorbed slowly at room temperature and quickly at elevated temperature, eliminating the hole density in the SWCNT networks.[22a] Chandra et al. addressed this issue by utilizing triethyloxonium hexachloroantimonate (OA; Figure 6a),[25] a one-electron oxidant that had been used extensively on producing oxidized π-conjugated organic molecules.[32] When used on SWCNTs, OA produces p-type networks that are dramatically more stable with respect to time and temperature than typical p-type dopants, such as HNO_3.

As with all organic semiconductors, obtaining stable electron-rich s-SWCNTs is one of the biggest challenges to surmount for SWCNT-based TE devices. n-type dopants tend to be very unstable in air even at room temperature. For example, Mistry et al. and Bult et al. demonstrated that adsorbed amines (Figure 6c) create heavily doped SWCNT networks and graphene thin films in inert environments (i.e., nitrogen glovebox).[27,33] When moved into an ambient environment, the mobile electron density decreases relatively rapidly, which can be attributed, at least in part, to compensation of the injected electrons by adsorbed O_2 or H_2O molecules.[27,33] This compensation reaction can be slowed by encapsulation of the film with a polymeric amine, and can even be partially or fully reversed by returning the film to an inert environment and/or mildly heating to desorb the compensating molecules. Several groups have recently developed new n-type dopants based on a variety of different molecules and polymers. Mai et al. utilized fluorene-*alt*-benzothiadiazole and cyclopenta-[2,1-*b*;3,4-*b*′]-dithiophene-*alt*-benzothiadiazole based conjugated polyelectrolytes with tethered cationic pyridinium units that convert SWCNTs from p-type to n-type.[31c] Nonoguchi et al. utilized alkali earth metal salts, with the injection electron density stabilized either by complexation of the alkali earth metal cation with crown ethers or by an onium cation, to dope mixed SWCNT networks n-type, and observe stable thermopower over 600 h for large diameter (≈2.0 nm) SWCNTs doped with potassium benzo-18-crown-6-ether salts (Figure 6b).[26] Materials prepared with these SWCNT exhibit anisotropic TE properties, zT of 0.1 (crossplane) or zT of 0.017 (in-plane), with air stability for more than 1 month at 100 °C for the largest diameter SWCNTs.[26] The same group utilized a

© 2017 WILEY-VCH Verlag GmbH & Co. KGaA, Weinheim

Pursuant to the DOE Public Access Plan, this document represents the authors' peer-reviewed, accepted manuscript. The published version of the article is available from the relevant publisher.

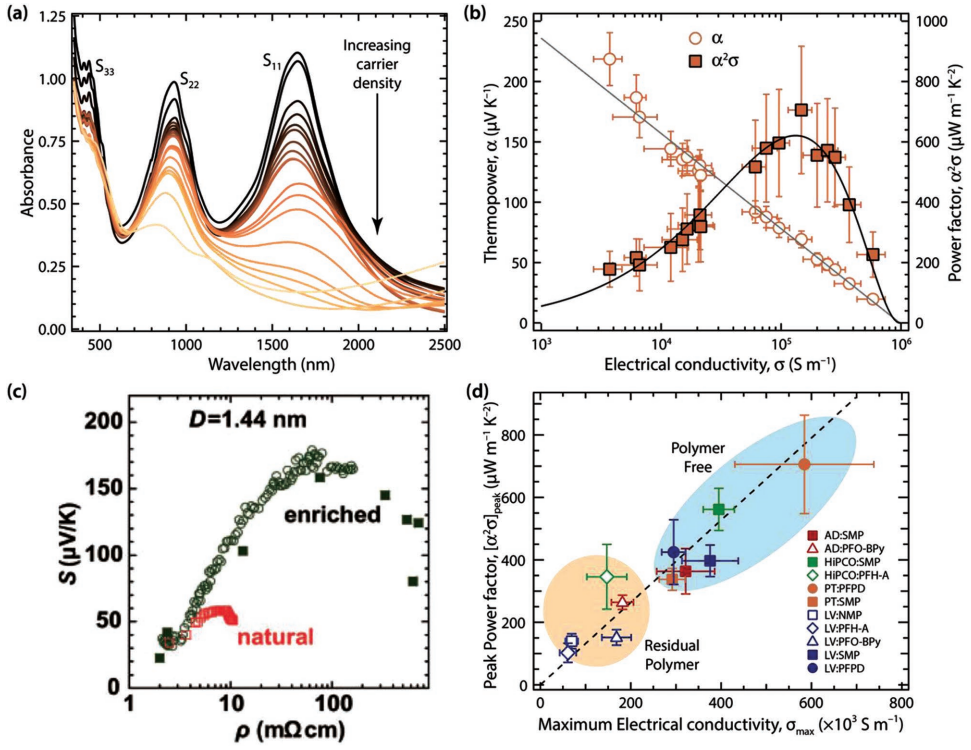

Figure 7. Controlling the carrier density by remote redox doping. a) Bleaching of the excitonic optical transitions by the injection of carrier density from OA into the s-SWCNT networks prepared from the PT:PFPD materials system, and b) the corresponding dependence of the thermopower and TE power factor on electrical conductivity. c) The dependence of the thermopower on electrical resistivity in mixed (natural) SWCNT and enriched s-SWCNT networks doped by nitric acid (HNO_3). Adapted under the terms of the CC BY 4.0 license.[36] Copyright 2016, The Japan Society of Applied Physics. d) Universal enhancement of the peak TE power factor by removal of the selective polymer from the enriched s-SWCNT network, showing also that the peak TE power factor can be correlated to the maximum electrical conductivity in a fully doped network. Reproduced with permission.[34] Copyright 2017, The Royal Society of Chemistry.

variety of amine- and phosphine-based dopants (Figure 6e), and also cite good long-term stability of the thermopower.[29] Several groups have employed the strategy of encapsulating the redox dopant, typically a metallocene compound, within the carbon nanotube endohedral volume (Figure 6d) to stabilize the n-type doped SWCNT network.[28,31b] Films prepared with cobaltocene-doped SWCNT demonstrated a power factor of 70.7 μW m^{-1} K^{-2} and low thermal conductivity (0.15 W m^{-1} K^{-1}), achieving a zT value of 0.14 at ≈300 K.[31b]

It should be noted that most of these dopants have not been extensively applied to highly enriched s-SWCNT networks, so it remains to be seen whether all of these n-type dopants will succeed in combining the high power factors that have been achieved with s-SWCNT networks and the long-term stability that has been demonstrated for mixed SWCNT networks. Recently, MacLeod et al. employed either potassium benzo-18-crown-6-ether salts and/or benzyl viologen to n-type dope enriched polymer-free s-SWCNTs networks, demonstrating equivalent performance to similar p-type doped networks.[34] Interestingly, Geier et al. demonstrated that benzyl viologen-doped n-type thin-film s-SWCNT FETs are unstable in air, reverting back to p-type within minutes.[35] In both studies, encapsulation of the n-type thin films in only 50 nm of Al_2O_3, deposited by atomic layer deposition (ALD), improves the stability dramatically, providing a potential strategy for producing air-stable thin films of n-type s-SWCNTs.[34,35]

Avery et al. utilized a redox doping strategy to sensitively tune the carrier density for SWCNT networks composed of a broad range of s-SWCNT diameters.[16a] They utilized organic solutions with varying concentrations of the one-electron oxidant triethyloxonium hexachloroantimonate (OA, Figure 6a) to dope s-SWCNT networks via physisorption of OA molecules onto the nanotube bundles within the network. The concentration of OA in the doping solution controlled the ultimate magnitude of the hole density (and E_f shift) realized within the s-SWCNT network, which can be tracked qualitatively by measuring the bleaching of the first (S_{11}) and second (S_{22}) excitonic optical transitions in the absorption spectrum (**Figure 7**a). This strategy affords systematic control over the thermopower and conductivity of the doped s-SWCNT network, resulting in optimization of the thermoelectric power factor in polymer-wrapped s-SWCNT networks. As predicted by first-principles calculations,[16a,21] the thermopower of nearly intrinsic (undoped) s-SWCNT networks is very high, in the range of several hundred μV K^{-1}.[16a] As the amount of adsorbed OA increases, the carrier density increases and E_f moves farther away from the middle of the gap, leading to a systematic increase in conductivity and decrease in thermopower (Figure 7b). These trends are universal for SWCNT networks, as shown in Figure 7c for a mixed SWCNT network (semi/metal) and an enriched s-SWCNT network that are each progressively p-type doped with nitric acid.[36] The anti-correlated dependence of σ and α leads to an optimum value for the

© 2017 WILEY-VCH Verlag GmbH & Co. KGaA, Weinheim

Pursuant to the DOE Public Access Plan, this document represents the authors' peer-reviewed, accepted manuscript. The published version of the article is available from the relevant publisher.

power factor ($\alpha^2\sigma$) at relatively high carrier density (Figure 7b), as inferred from the strong bleaching of excitonic optical transitions in the absorption spectrum (Figure 7a) and the high electrical conductivity. For polymer-sorted enriched s-SWCNT networks, Norton-Baker et al. and MacLeod et al have now made detailed comparisons between networks where appreciable amounts of the original sorting polymer remain bound to s-SWCNT surfaces and networks utilizing cleavable polymers where the sorting polymer is completely removed. Both types of networks exhibit a similar dependence of the thermoelectric power factor on the electrical conductivity (Figure 7b), but polymer-free networks achieve a universal enhancement of the optimum power factor when compared to s-SWCNT networks containing residual sorting polymer (Figure 7d).[34,37]

Avery et al. also found that the maximum power factor varied systematically with the s-SWCNT band gap (or diameter) for s-SWCNT films containing residual polyfluorene sorting polymer.[16a] In that study, HiPCO s-SWCNT networks displayed the highest maximum power factor of ≈350 μW m^{-1} K^{-2} (Figure 7d; empty green diamond).[16a] This power factor is competitive with some of the best single-component polymer thin films.[38] An extension of this study to enriched polymer-free s-SWCNTs networks demonstrated that other morphological factors, such as the extent of residual sorting polymer and the size of s-SWCNT bundles formed in the film, also play important roles in determining the ultimate TE power factor.[34,37] In the most recent study by MacLeod et al., s-SWCNTs prepared from larger diameter plasma torch (PT) SWCNTs displayed the highest maximum power factor of ≈700 μW m^{-1} K^{-2}.[34] These high power factor films were prepared with a removable polymer (PFPD) first demonstrated by the Bao group,[39] and thus the resulting thin film was composed of ≈100% s-SWCNTs. Due to the equivalent effective masses of electrons and holes in s-SWCNTs, the n-type power factor for an identically prepared PT:PFPD film doped with potassium benzo-18-crown-6-ether was also ≈700 μW m^{-1} K^{-2}.[34] These studies suggest that further exploration is needed to successfully disentangle the degree to which intrinsic (e.g., s-SWCNT diameter and band gap) and extrinsic (e.g., film morphology, bundle size, etc.) properties affect the ultimate power factor of s-SWCNT networks.

An alternative strategy toward tuning the shift in the Fermi energy (or carrier chemical potential) is to incorporate the SWCNTs into a transistor geometry and use the gate voltage to tune the carrier density within the sample. This approach has been applied to both single s-SWCNT samples (**Figure 8**a)[40] and thin film networks of s-SWCNTs (Figure 8b),[41] which both exhibit broadly similar behavior as a function of the applied gate voltage. The measurements performed on the s-SWCNT networks (Figure 8b) suggest that the optimum thermoelectric power factor is obtained when the gate voltage corresponds to the location of the Fermi level within the second sub-band in the electronic DOS.[41] This observation appears to be qualitatively similar to those for chemical redox doping of enriched s-SWCNT networks, where the peak power factor is observed at very large carrier densities, corresponding to the location of the Fermi level near the second sub-band in the electronic DOS,[16a] suggesting that control of the carrier density around this second sub-band is important to optimize the thermoelectric performance in enriched s-SWCNT samples.

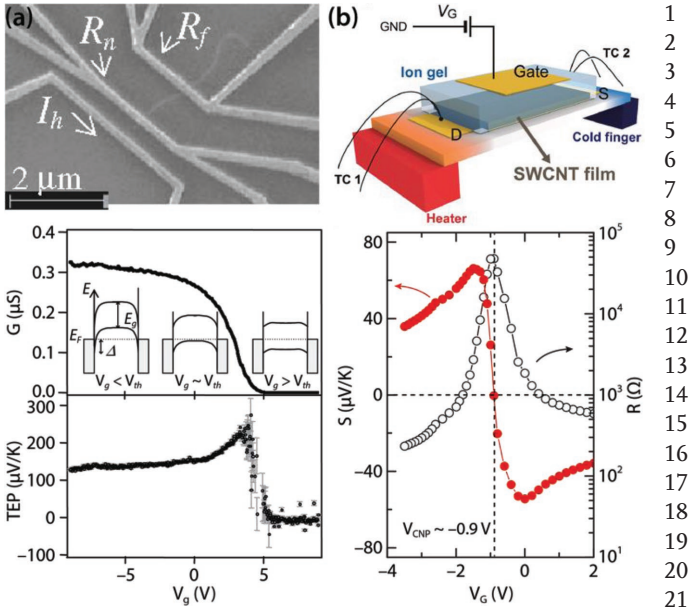

Figure 8. Controlling the position of the Fermi level by electric-field gating in field-effect transistors. a) The upper panel shows a scanning electron micrograph of a typical device used probe the dependence of the conductance, *G*, and thermopower, TEP, on the gate voltage, V_g, in a single s-SWCNT. Reproduced with permission.[40] Copyright 2003, American Physical Society. b) The upper panel shows a schematic for an ion-gated-transistor device used to probe the dependence of the resistance, *R*, and thermopower, *S*, on the gate voltage, V_G, in a s-SWCNT network. Adapted with permission.[41] Copyright 2016, Wiley-VCH.

3.4. Thermal Conductivity of SWCNT

A recent review on the thermal properties of nanostructured carbon materials[42] suggests that, despite the many theoretical[43] and experimental[44] studies on the thermal conductivity of SWCNT, this crucial component of the thermoelectric figure of merit is probably the least understood for this class of materials. This is particularly true for the more complex interconnected SWCNT networks that will ultimately be used in TE devices, because most studies focus on isolated individual SWCNT or bundles.[42] Additionally, most early experimental studies on SWCNT κ studied as-produced SWCNT mats,[44a–c] not the solution-deposited networks that have emerged in recent years for high-performance applications. Another underlying reason is more universal, and is simply related to the inherent difficulties in accurately measuring bulk thermal conductivity, especially for anisotropic conductors. Despite these difficulties, a number of important early studies provide important insights into the thermal conductivity of SWCNT. There are very detailed reviews of both nanoscale thermal transport[45] and the thermal conductivity of nanostructured carbon materials,[42] so the treatment here is concise.

A number of theoretical studies have attempted to understand the dependence of κ on SWCNT diameter,[43d–g] and how this value compares to the value of graphene.[43a,b] Two separate

© 2017 WILEY-VCH Verlag GmbH & Co. KGaA, Weinheim

Pursuant to the DOE Public Access Plan, this document represents the authors' peer-reviewed, accepted manuscript. The published version of the article is available from the relevant publisher.

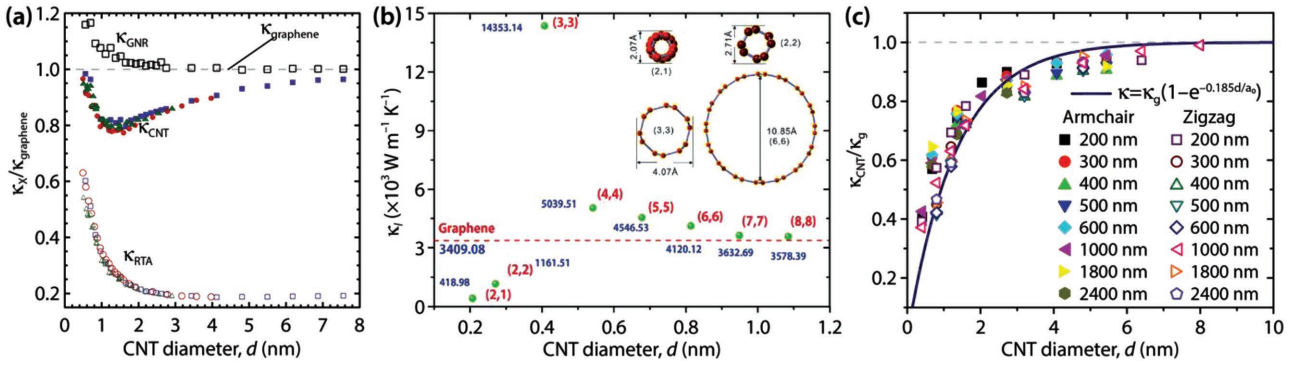

Figure 9. Theoretically predicted diameter dependence for the thermal conductivity for various SWCNTs. a,b) Simulations based on a Boltzmann–Peierls phonon-transport-equation approach, including anharmonic three-phonon scattering. Reproduced with permission.[43e] Copyright 2010, American Physical Society. Adapted under the terms of the CC license.[43g] Copyright 2015, Nature Publishing Group. c) Simulations based on nonequilibrium molecular dynamics. Reproduced with permission.[43f] Copyright 2012, AIP Publishing.

molecular dynamics simulations of isolated (10,10) m-SWCNT predict $\kappa \approx 6600$–9500 W m^{-1} K^{-1} at 300 K, a value similar to that calculated for graphene and resulting from a large phonon mean free path.[43a,b] In general, recent theoretical studies suggest that κ for SWCNT converges to the value found for a graphene sheet as the diameter increases to very large diameters (>5 nm), but the relative value of κ_{SWCNT} and $\kappa_{graphene}$ differ (**Figure 9**). Thomas et al. and Yue et al. predict that the SWCNT thermal conductivity is larger than that of graphene and asymptotically approaches $\kappa_{graphene}$ as SWCNT diameter increases,[43d,g] whereas Lindsay et al. and Cao et al. predict that $\kappa_{SWCNT} < \kappa_{graphene}$ and that κ_{SWCNT} asymptotically increases with increasing diameter.[43e,f]

Hone et al. measured $\kappa \approx 0.7$ W m^{-1} K^{-1} for a low-density bulk mat of SWCNT prepared by laser vaporization.[44b] They used this value to extrapolate to an expected value of $\kappa \approx 1800$–6000 W m^{-1} K^{-1} for a single "rope" or fiber of SWCNT. Hone et al. then measured κ for dense mats of SWCNT that were either random ($\kappa \approx 30$ W m^{-1} K^{-1} at 300 K) or magnetically aligned ($\kappa \approx 220$ W m^{-1} K^{-1}) networks.[44c] More recent studies of SWCNT films prepared by vacuum filtration of aqueous SWCNT dispersions measured similar values of κ to those for dense SWCNT mats ($\kappa > 25$ W m^{-1} K^{-1} at 300 K),[44g,h] but also observed that the measured thermal conductivity is sensitive to the morphology and processing of the SWCNT networks.[44h]

The Wiedemann–Franz (WF) law is commonly used to calculate the expected value for the magnitude of the electronic contribution to the thermal conductivity (κ_e) at temperature T, where L is the so-called Lorenz number

$$\kappa_e = L\sigma T \tag{6}$$

For metals or degenerately doped semiconductors, the value of L is taken to be $L = 2.44 \times 10^{-8}$ W Ω K^{-2}. Hone et al. made the important observation that their extrapolated value of κ for SWCNT fibers was orders of magnitude higher than expected from the WF law, implying that thermal transport in SWCNT is dominated by phonons. This was also confirmed in recent measurements of dense SWCNT films prepared by vacuum filtration, where κ_e was calculated to be less than 1.1 W m^{-1} K^{-1} for SWCNT samples of various compositions.[44h]

3.5. Effect of Electronic Structure and Doping on κ in SWCNT Networks

To date, there have been few systematic experimental studies on the dependence of thermal conductivity on the ratio of m- and s-SWCNT in networks, although some recent studies provide a basis for some comparisons. Lian et al. recently compared the thermal conductivity of vacuum filtered films prepared from enriched metallic and semiconducting dispersions as well as the statistical mixture.[44h] This study indicated that the electronic character had no impact on the measured thermal conductivity, which was primarily determined by the relative lengths of the SWCNT present in the network (longer nanotubes resulting in fewer junction between nanotubes/bundles and more efficient thermal transport).[44h] Nonoguchi et al. measured the in-plane ($\kappa_\parallel$) and cross-plane ($\kappa_\perp$) thermal conductivity of SWCNT networks containing both m- and s-SWCNT, utilizing a periodic heating method and a Xenon flash method, respectively.[26] This study found values ranging from ≈10 to 40 W m^{-1} K^{-1} for $\kappa_\parallel$ and ≈0.12 W m^{-1} K^{-1} for $\kappa_\perp$. In these studies, n-type doping of the networks increased $\kappa_\parallel$ by a factor of 3, relative to as-prepared (p-type) networks, even though the electrical conductivity only increased by ≈30%.[26] For the same two samples (as-prepared and n-type doped), $\kappa_\perp$ remained unchanged after the n-type doping procedure. The same group measured thermal conductivity values of 0.098–0.205 W m^{-1} K^{-1} for mixed SWCNT networks that were either lightly p-type (as-prepared) or doped n-type with amine- or phosphine-based molecules or polymers.[29] Although it was not specified whether this value corresponded to $\kappa_\parallel$ or $\kappa_\perp$, the commercial hot-wire apparatus (designed for solids, liquids, and powders) utilized for their measurement presumably provided $\kappa_\perp$. While the authors used this value to calculate zT, the other two parameters (σ and α) were measured in-plane.

Duzynska et al. utilized a Raman heating method to determine a value of $\kappa_\parallel \approx 26$ W m^{-1} K^{-1} at 300 K for highly enriched s-SWCNT networks with diameters between 1.2 and 1.7 nm,[44g] but did not report a value for the sample's electrical conductivity. Avery et al. and Norton-Baker et al. have measured $\kappa_\parallel$ for networks of s-SWCNT with slightly smaller average diameters of $\langle d \rangle \approx 1.3$ nm,[16a,37] using a suspended platform technique where

© 2017 WILEY-VCH Verlag GmbH & Co. KGaA, Weinheim

Pursuant to the DOE Public Access Plan, this document represents the authors' peer-reviewed, accepted manuscript. The published version of the article is available from the relevant publisher.

thin films are deposited onto a micromachined Si–N platform with ultralow background thermal conductance. These studies found a value of $K_{\|}$ for undoped s-SWCNT networks prepared by laser vaporization ≈17 W m^{-1} K^{-1} at 300 K (**Figure 10**a).[16a] As the electrical conductivity of this intrinsic semiconducting film was immeasurable ($\sigma \approx 0$ S m^{-1}), $\kappa_e \approx 0$ W m^{-1} K^{-1} (Equation (5)) and $\kappa_t = \kappa_l \approx 17$ W m^{-1} K^{-1} (Equation (4)). These experimental measurements of the thermal conductivity in intrinsic and undoped pure semiconducting SWCNTs[16a] provide a crucial confirmation that the thermal conductivity of SWCNT is heavily dominated by phonons. The thermal conductivity of the s-SWCNT networks studied by Avery et al. is dramatically lowered to the range of 3–4 W m^{-1} K^{-1} upon p-type doping with the OA redox molecule, whereas σ increases by several orders of magnitude (Figure 10a).[16a,37] This effect suggests that (1) the thermal conductivity is largely decoupled from the electrical conductivity in SWCNT, and (2) the dopant molecules may lower the thermal conductivity by affecting the phonon mean free path.

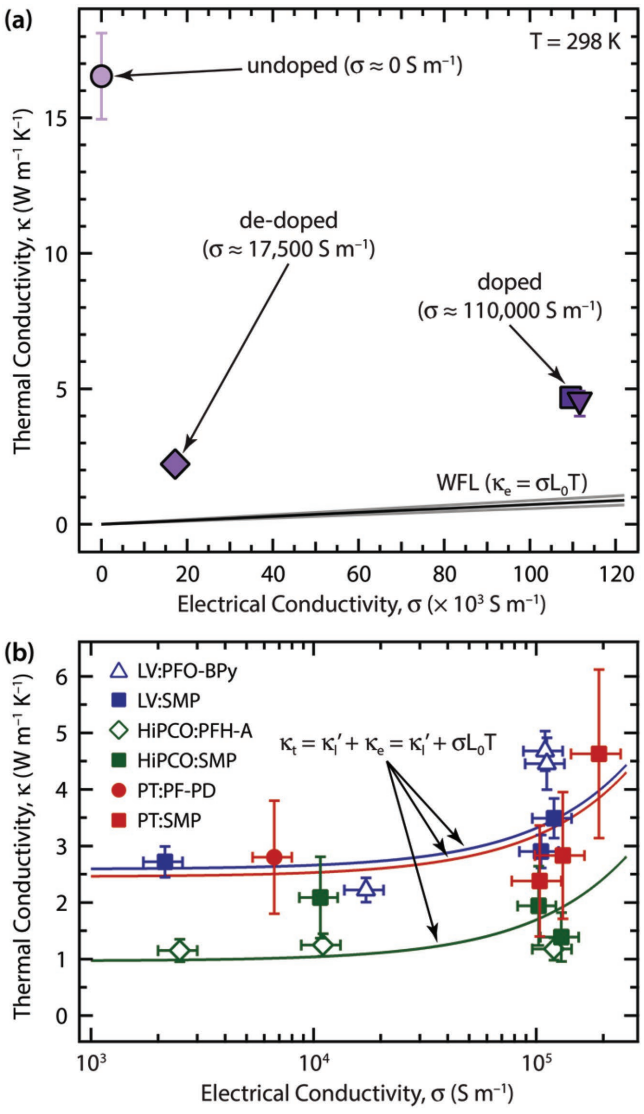

Figure 10. a) Reduction in thermal conductivity for a s-SWCNT network upon p-type doping with a molecular charge-transfer dopant. Adapted with permission.[16a] Copyright 2016, Nature Publishing Group. b) Dependence of the total thermal conductivity on electrical conductivity for p-type-doped s-SWCNT networks with varying diameter. Reproduced with permission.[34] Copyright 2017, The Royal Society of Chemistry.

Zhou et al. measured thermal conductivity of mixed SWCNT networks, containing 1/3 m- and 2/3 s-SWCNT, prepared by a floating catalyst CVD method, using the self-heating technique.[46] They obtained a thermal conductivity of 24 W m^{-1} K^{-1} for as-prepared (undoped, lightly p-type) networks and a value of 18 W m^{-1} K^{-1} for n-type networks. They attributed the reduction in thermal conductivity to the introduction of phonon scattering from the polyethylenimine (PEI) polymer used to dope the networks.[46]

Experimental studies on the diameter, or band gap, dependence of κ_{SWCNT} are rare. Fujii et al. measured κ for individually suspended MWCNTs in vacuum, obtaining $\kappa \approx 2000$ W m^{-1} K^{-1} for a 9.8 nm diameter MWCNT.[44d] A recent study by MacLeod et al. found that κ measured for a thin film of s-SWCNT, with average diameter of 1.1 nm, was about 50%—$\kappa \approx 1.3$ W m^{-1} K^{-1}—of the value measured for s-SWCNT with average diameter of 1.3 nm—$\kappa \approx 2.9$ W m^{-1} K^{-1} (Figure 10b).[34]

While these initial studies provide some interesting comparisons, there is still not enough experimental data in the literature to draw broad conclusions on the effect of band gap, electronic structure, and charge carrier doping on the thermal conductivity of SWCNT networks. It is still unclear whether many of the differences observed between groups and across different material sets are due primarily to the intrinsic properties of the SWCNT themselves, differences in the measurement techniques utilized to measure κ, or morphological properties of the networks that are not directly related to SWCNT electronic structures. Additionally, several studies have now demonstrated that molecules adsorbed on the exterior,[16a,46] or more recently in the endohedral volume,[47] of SWCNTs can significantly reduce κ. A robust theoretical understanding of these phenomena is lacking, and would be valuable for guiding the rational incorporation of molecular, nanocrystalline, or polymeric additives that can reduce SWCNT κ while maintaining or enhancing σ and α. Thus, these areas of research appear to be ripe for further exploration.

3.6. Temperature Dependence of α, σ, and κ

As for any thermoelectric material, it is important to understand the temperature dependence of α, σ, and κ, in order to determine the optimal operational temperature range and to accurately predict the expected power density as a function of operating temperature.[48] At a more fundamental level, temperature-dependent transport measurements also provide a window into the transport mechanisms at play in a particular material system, enabling further materials engineering and optimization. For brevity, this review will not delve deeply into transport mechanisms for organic semiconductors or SWCNTs, but some recent reviews provide detailed treatments of this topic.[4c,49] Even so, it is useful to point to a few general trends in temperature-dependent transport in SWCNTs.

© 2017 WILEY-VCH Verlag GmbH & Co. KGaA, Weinheim

Pursuant to the DOE Public Access Plan, this document represents the authors' peer-reviewed, accepted manuscript. The published version of the article is available from the relevant publisher.

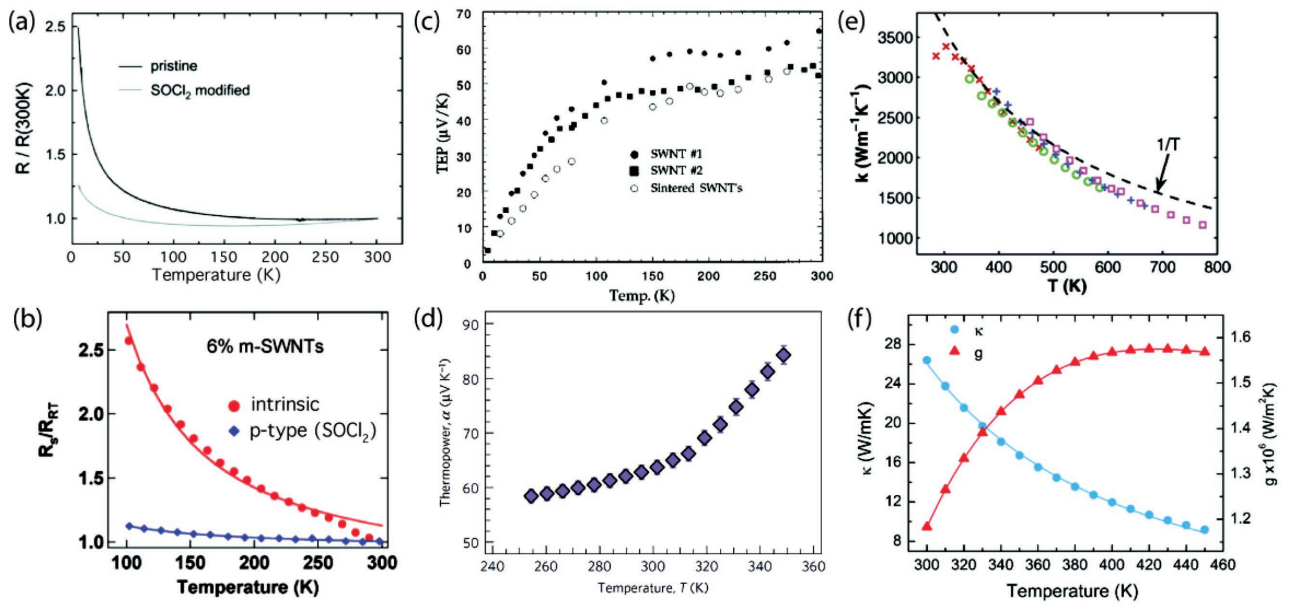

Figure 11. Literature examples for the temperature dependence of critical TE properties for single nanotubes, mixed networks, or enriched networks. Temperature-dependent resistivity for a) mixed SWCNT networks and b) enriched s-SWCNT networks that are either undoped (pristine/intrinsic) or p-type-doped with $SOCl_2$. a) Adapted with permission.[30a] Copyright 2005, American Chemical Society. b) Adapted with permission.[22b] Copyright 2008, American Chemical Society. Temperature-dependent thermopower for c) individual SWCNTs or d) enriched s-SWCNT networks. c) Reproduced with permission.[19a] Copyright 2017, American Physical Society. d) Adapted with permission.[16a] Copyright 2016, Nature Publishing Group. Temperature-dependent thermal conductivity for e) individual SWCNTs or f) enriched s-SWCNT networks (the red diamonds plot the interfacial thermal conductance (g) between the s-SWCNT film and the SiO_2 substrate). e) Reproduced with permission.[44f] Copyright 2006, American Chemical Society. f) Reproduced with permission.[44g] Copyright 2015, AIP Publishing.

With regard to electrical conductivity, it is most important to note that SWCNT films are best represented as a disordered and percolated network of highly conductive wires. Within a single nanotube, electron and hole mobilities are typically very high, whereas the junctions between SWCNTs typically have appreciable resistance. The markedly higher junction resistance gives rise to a positive temperature coefficient for the electrical conductivity (negative temperature coefficient for resistivity) of SWCNT mats, where increasing the temperature provides the thermal energy necessary to surmount the barriers at tube-tube junctions (**Figure 11**a,b). This behavior is often modeled within a framework of fluctuation-induced tunneling or variable range hopping.[22a,b,50] Many early studies report a transition to a negative temperature coefficient for conductivity above a transition temperature, indicating phonon-limited transport at higher temperatures that is more representative of metals.[50b] As other studies have noted, this transition to "metallic" conductivity may be convoluted with the temperature-induced desorption of the molecules (oxygen or intentionally added, thermally labile dopants) that impart the p-type character of these films.[22a,b] Doping SWCNTs with excess charge carriers "flattens out" the increase of conductivity with temperature, suggesting that the dopants ameliorate to some degree the barriers that charge carriers encounter at tube-tube junctions (Figure 11a,b).[22a,b]

For most doped organic semiconductors, the Seebeck coefficient increases with increasing temperature, with the dependence varying from linear (degenerately doped and/or relatively ordered) to sublinear (lightly doped and/or relatively disordered).[4c,49a] Reports of temperature-dependent thermopower in SWCNT networks demonstrate that the Seebeck coefficient increases with increasing temperature, both below and above room temperature (Figure 11c,d).[16a,19a,b,20a,50b] This behavior appears to hold for individual SWCNTs and networks comprised of metallic, semiconducting, and mixed SWCNTs at a variety of doping levels.

Temperature-dependent thermal conductivity has been studied for a number of SWCNT systems. Below room temperature, the thermal conductivity of single tubes has been observed to increase with rising temperature.[44b] Above room temperature, κ was observed to decrease with rising temperature for a single tube, generally consistent with Umklapp phonon–phonon scattering (Figure 11e).[44f] For s-SWCNT networks, κ is observed to decrease (Figure 11f) or remain relatively constant with increasing temperature.[16a,44g]

While much work remains to be done in using temperature-dependent transport to uncover transport mechanisms relevant to thermoelectric energy harvesting in SWCNT networks, the results summarized here are encouraging. Notably, for s-SWCNT networks, the electrical conductivity and thermopower both tend to increase with increasing temperature, whereas the thermal conductivity tends to decrease. These trends imply that zT should continue to increase above room temperature. Indeed, Avery et al. recently observed that zT for doped s-SWCNT networks was ≈2.5 times higher at 350 K than at 300 K.[16a] Performance at elevated temperatures (with associated studies of thermally stable doping/encapsulation strategies) should be a fruitful research direction for realizing the true potential of SWCNT-based materials and devices.

© 2017 WILEY-VCH Verlag GmbH & Co. KGaA, Weinheim

Pursuant to the DOE Public Access Plan, this document represents the authors' peer-reviewed, accepted manuscript. The published version of the article is available from the relevant publisher.

3.7. Current Performance Metrics of SWCNT-Only Thermoelectrics

Tables 1–3 and **Figure 12** summarize the TE performance metrics reported for p-type SWCNTs (single tubes/bundles and networks) and SWCNT-based thin films where the dominant transport phase is the SWCNTs. In general, the SWCNT samples that are sorted by electronic structure to produce enriched s-SWCNTs give higher thermopower at a given conductivity, which then directly translates to improved power factor for a given conductivity (Figure 12c). Notable outliers are outlined with a blue oval in each panel. Interestingly, each of these outliers arise from a group that utilizes a floating-catalyst CVD method to directly synthesize SWCNT buckypapers that contain the statistical ratio of metallic and semiconducting SWCNTs (Figure 12d,e). Interestingly, these reports obtain values of conductivity and thermopower that are significantly larger than any previous reports on mixed SWCNT networks. As this synthesis method produces SWCNT networks that are utilized directly without any processing, such as sonication, the SWCNTs should be significantly longer than typical solution-processed SWCNTs, which explains the high conductivity values. It is not immediately clear why the thermopower values for these same buckypapers should be nearly double the maximum values that other groups have measured for mixed SWCNTs, as the Seebeck coefficient is affected primarily by electronic structure and is not directly related to SWCNT length. In any event, it would be beneficial to perform side-by-side comparisons of solution-processed films to these "directly synthesized" buckypapers to confirm these large TE power factors and uncover the mechanisms underlying these differences. Importantly, power factor values exceeding 1–2 mW m^{-1} K^{-2} begin to compete with traditional telluride-based inorganic TE materials.

4. Carbon Nanotube-Based Thermoelectric Composites

Organic semiconducting polymers have attracted attention as thermoelectric materials due to their low cost, mechanical flexibility, environmental friendliness, and facile processing into complex forms.[38a,55] Additionally, the inherently low thermal conductivity in polymers (often about one order of magnitude lower than conventional inorganics) serves to further improve TE performance. Despite these advantages, insufficient electrical conductivity and low Seebeck coefficient have prevented conducting polymers from gaining significant traction in TE devices. The power factor for most viable polymers

Table 2. Preparation and thermoelectric properties of unsorted, n-type, carbon-nanotube-only samples at room temperature.

SWCNT material[a)]	Preparation	Dopant	Electrical conductivity [S cm^{-1}]	Seebeck coefficient [μV K^{-1}]	Power Factor [μV m^{-1} K^{-2}]	Thermal conductivity [W m^{-1} K^{-1}]	zT	Year	Ref.
"Supergrowth" CVD	Filter-deposited buckypaper	1,3-Bis(diphenyl-phosphino) propane (dppp)	98	−52	26.5	0.174	0.046	2013	[29]
			49.8	−73	26.5	0.103	0.077		
Meijo-SO	Filter-deposited buckypaper	Cobaltocene	430	−40.4	70.7	0.15	0.14	2015	[31b]
eDIPS	Filter-deposited buckypaper	KOH + 18-crown-6-ether	2050	−33	223	39	0.0017	2016	[26]
eDIPS	Filter-deposited buckypaper	1,1′-Bis(diphenylphosphino) ferrocene	716	−38	103.4	–	–	2016	[28]
Floating catalyst CVD	As-synthesized buckypaper	Polyethyleneimine (PEI)	3630	−64	1490	–	–	2017	[46]
			1780	−82	1200	18	0.020		
eDIPS[b)]	Filter-deposited buckypaper	MGH in *N*,*N*-dimethylacetimide	557	−8.7	4.2	–	–	2017	[31e]
		MGH in dimethyl sulfoxide	582	−19	22	–	–		
		MGH in 1,3-dimethyl-2-imidazolidinone	505	−25	31	–	–		
		MGH in 1-formylpiperidine	593	−52	163	–	–		
		MGH in *N*-cyclohexyl-2-pyrrolidone	1097	−43	200	–	–		
eDIPS	Filter-deposited buckypaper	*o*-MeO-DMBI	620	−43	115	24.4	0.0017	2017	[31d]
Floating catalyst CVD	Aligned yarn	PEI	7850	−56	2456	–	–	2017	[54]

[a)]When the thermoelectric properties corresponding to the peak power factor are not reported directly in the manuscript they are estimated from plots of Seebeck coefficient and electrical conductivity; [b)]This study found that the ability for MGH to dope SWCNTs n-type depended on the basicity of the solvent. The solvents in this table enabled measurable n-type behavior.

© 2017 WILEY-VCH Verlag GmbH & Co. KGaA, Weinheim

Pursuant to the DOE Public Access Plan, this document represents the authors' peer-reviewed, accepted manuscript. The published version of the article is available from the relevant publisher.

Table 3. Preparation and thermoelectric properties of enriched carbon nanotube samples at room temperature.

SWCNT material[a)]	Preparation	Enrichment	Dopant	Electrical conductivity [S cm^{-1}]	Seebeck coefficient [μV K^{-1}]	Power factor [μV m^{-1} K^{-2}]	Thermal conductivity [W m^{-1} K^{-1}]	zT	Year	Ref.
AD	Filter-deposited buckypaper	Semiconducting	O_2-doped	13	150	33	–	–	2014	[20a]
		Semiconducting	Nitric acid	180	78	108	–	–		
		Natural		52	36	6.7	–	–		
		Metallic		200	14	3.9	–	–		
Nanointegris	Filter-deposited buckypaper	Semiconducting	O_2-doped	270	88	210	–	–	2014	[20b]
		Metallic	O_2-doped	300	13	5.1	–	–		
AD	As-purchased buckypaper	Semiconducting	Nitric acid	110	110	134	–	–	2016	[36]
CoMoCAT (7,5)	Spray-coated polymer:SWCNT film	Semiconducting	Triethyloxonium hexachloroantimonate (OA)	158	84	112	–	–	2016	[16a]
HiPCO				415	91	346	–	–		
Pulsed LV				255	77	152	2.2	0.021		
Tuball				1685	18	57	–	–		
Pulsed LV	Spray-coated polymer-free SWCNT film	Semiconducting	Triethyloxonium hexachloroantimonate (OA)	1270	56	398	3.0	0.04	2016	[37]
AD	Spray-coated polymer-free SWCNT film	Semiconducting	Triethyloxonium hexachloroantimonate (OA)	512	84	363	–	–	2017	[34]
Pulsed LV										
HiPCO				1140	70	562	1.4	0.12		
Plasma Torch				1475	69	706	2.8	0.08		
			Benzyl viologen (BV)	1190	−78.5	730	–	–		

[a)]When the thermoelectric properties corresponding to the peak power factor are not reported directly in the manuscript they are estimated from plots of Seebeck coefficient and electrical conductivity; [b)]

is in the range of 10^{-4} to 10^2 μW m^{-1} K^{-2}, which is far below state-of-the-art inorganic TE materials.[56] While there have been some recent reports of high power factors through various doping strategies,[38] photooxidative instability of these polymers remains a significant challenge.

Although the thermoelectric properties of most individual polymers are still far away from the best inorganic materials, nanocomposites containing carbon nanofillers have provided an effective means to improve the power factor of polymeric materials (resulting from the combination of properties of the individual components).[4a,57] Among the various carbon nanoparticles (e.g., nanotubes (CNTs), graphene, carbon black, etc.), CNTs are the most studied due to their high electrical conductivity and Seebeck coefficient that dramatically improve polymer TE behavior. High nanotube thermal conductivity, reported to be as high as several thousand W m^{-1} K^{-1} for isolated individual CNTs (Figure 11), can be mediated by surface coverage of polymers with low thermal conductivity (<0.7 W m^{-1} K^{-1}).[44e,58] In the case of CNT-filled composites, the associated polymers can be insulating or conductive. This section focuses on the recent progress with these nanocomposites using both types of matrices.

4.1. Nanocomposites Prepared with Insulating Polymers

Incorporation of CNTs into ceramics has been shown to produce a dramatic improvement in electrical conductivity and a significant decrease in thermal conductivity, suggesting potential for its use as a promising thermoelectric composite.[59] Despite their potential, only a few studies have been conducted because carbon nanotube/ceramic nanocomposite exhibit low thermoelectric properties (e.g., 0.001 at room temperature < zT < 0.02 at 850 K in SWCNT/3Y-TZP composite), coupled with low electrical conductivity relative to other thermoelectric composites.[60]

One of the key issues facing thermoelectric polymer nanocomposites is controlling the dispersion of CNTs within the

© 2017 WILEY-VCH Verlag GmbH & Co. KGaA, Weinheim

Pursuant to the DOE Public Access Plan, this document represents the authors' peer-reviewed, accepted manuscript. The published version of the article is available from the relevant publisher.

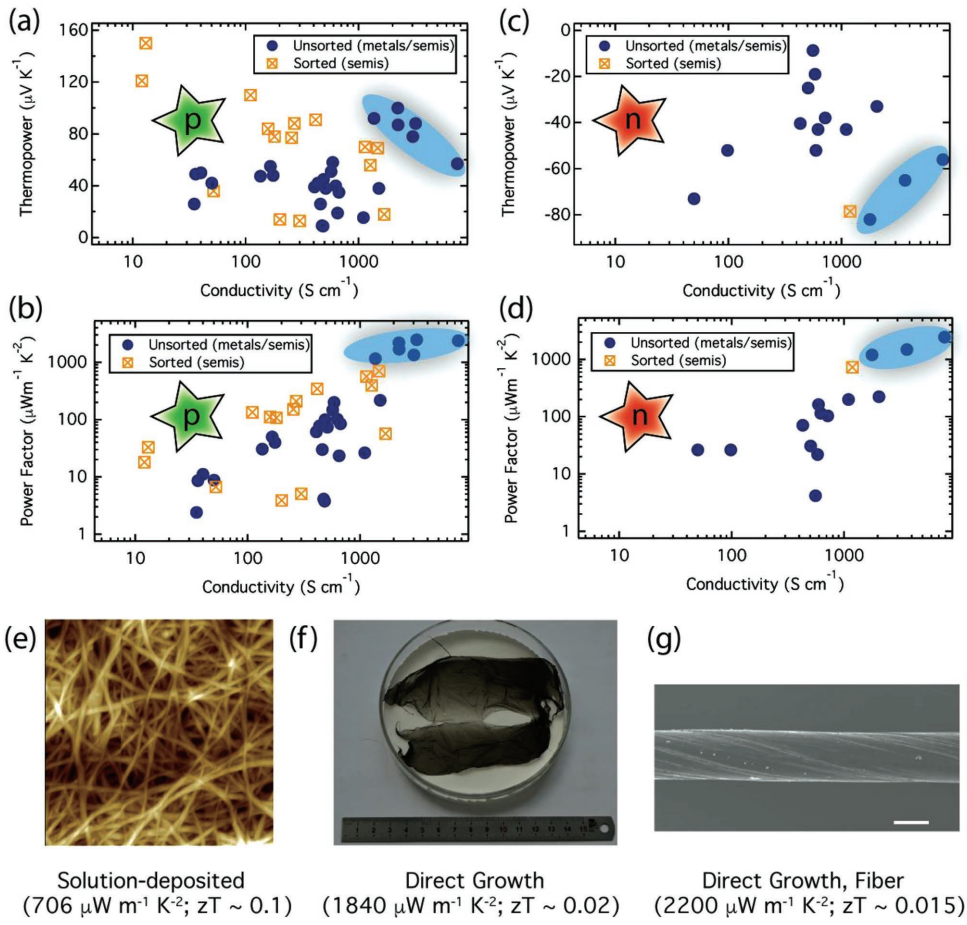

Figure 12. Literature survey of the thermopower (a) p-type and c) n-type) and power factor (b) p-type and d) n-type) of SWCNT-only (or SWCNT-dominated) thin films, as a function of electrical conductivity. All of the data points are taken at the maximum power factor, if the reports provide multiple doping levels. The blue ovals in each panel highlight SWCNT networks or yarns that are synthesized by a floating catalyst CVD method and are directly utilized without any ultrasonic processing. e–g) Images of some of the highest performance p-type SWCNT-only thermoelectrics reported to date, with associated power factor and zT values. e) 750 × 750 nm atomic force microscopy image of solution-deposited s-SWCNT network. Reproduced with permission.[34] Copyright 2017, The Royal Society of Chemistry. f) Photograph of directly grown (floating catalyst CVD) buckypaper. Adapted with permission.[46] Copyright 2017, Nature Publishing Group. g) SEM image of SWCNT fiber, twisted from directly grown (floating catalyst CVD) buckypaper. Reproduced with permission.[51] Copyright 2016, Wiley-VCH.

polymer matrix. Nanotube aggregation due to high surface energy and strong van der Waals attractive forces between CNTs in the polymer matrix can result in low electrical conductivity and Seebeck coefficient.[61] While much work has been dedicated to improving dispersion through covalent surface modification (e.g., chemical functionalization using strong acids), these treatments can create defects on the sidewalls and reduce conductivity due to the disruption of the extended π conjugation in CNT.[62] On the other hand, noncovalent stabilization of CNTs can eliminate oxidation or damage to the sp^2 character.[63] Water-soluble polymers work well as dispersants because they provide hydrophobic interactions between the polymer backbone and the CNT surface, and render the polymer/CNT complex miscible in water due to the presence of numerous ionic or polar groups. Noncovalent, physical adsorption of polymers onto the hydrophobic nanotube surfaces effectively changes the tubes from hydrophilic to hydrophobic. In contrast to rod-like conjugated polymers, coiled insulating polymers can serve as a flexible and robust matrix. In terms of TE nanocomposites prepared with insulating polymers, significant work has been performed only with polymer emulsions and with nitrogen-rich polymers that impart n-type character to the nanotubes,[57] as discussed in the following sections.

4.1.1. Segregated-Network Nanocomposites

The first demonstration of a nanotube-filled composite with true thermoelectric behavior (i.e., zT > 0.001) was achieved by Yu et al.[64] In their work, an aqueous poly(vinyl acetate) (PVAc) emulsion (a stable suspension of solid, spherical polymer particles) was used as the matrix. CNTs stabilized in aqueous gum Arabic (GA) were combined with the PVAc and dried. The relatively large PVAc particles (100 nm to 1 μm) created excluded volume that pushed the smaller nanotubes into the interstitial space between them, resulting in a segregated-network (**Figure 13**a,b). With reduced space available for the nanotubes, a strong electrical network was formed at relatively low

© 2017 WILEY-VCH Verlag GmbH & Co. KGaA, Weinheim

Pursuant to the DOE Public Access Plan, this document represents the authors' peer-reviewed, accepted manuscript. The published version of the article is available from the relevant publisher.

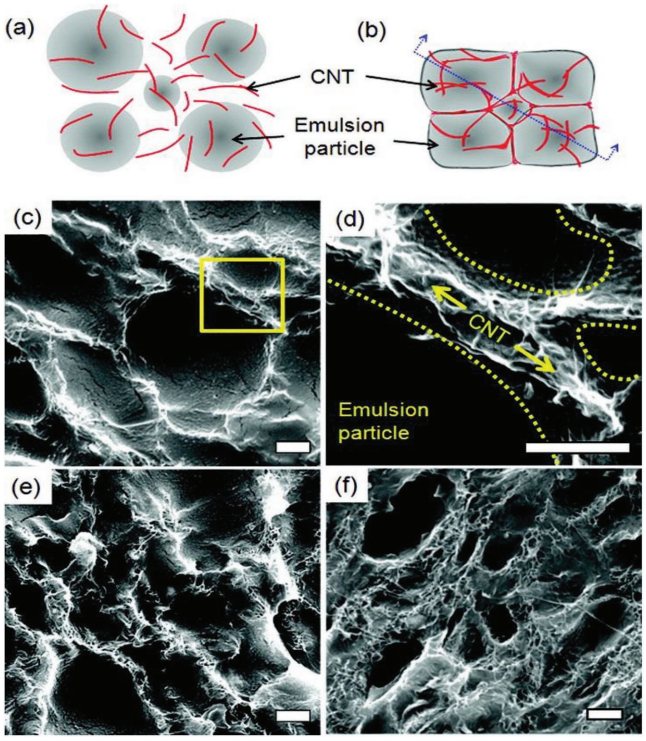

Figure 13. a) Schematic of CNTs suspended in an aqueous emulsion. Gray spheres and red lines represent emulsion particles and CNTs, respectively. b) Schematic of the emulsion-based composite after drying. The CNT form a 3D network along the surfaces of the spherical emulsion particles. SEM images of the cross-sections of 5, 5, 10, and 20 wt% CNT-filled composites are respectively shown in panels (c)–(f) after the composites were freeze-fractured (for instance, along the dotted line in (b)). The high-magnification SEM shown in (d) is a portion of the sample in (c) indicated by a yellow solid square. CNT (indicated by arrows) are wrapped around the emulsion particles (indicated by yellow dotted lines) rather than homogenously mixed. Denser CNTs were observed for higher concentration composites. The scale bars indicate 1 μm. Reproduced with permission.[64] Copyright 2008, American Chemical Society.

concentration compared to randomly dispersed composites.[65] SEM images of the CNT/PVAc composites show remnants of emulsion particles and chain-like CNT bundles (Figure 13c–f). With a CNT concentration of 20 wt%, these composites exhibit an electrical conductivity of 48 S cm^{-1}, thermal conductivity of 0.34 W m^{-1} K^{-1}, and a thermoelectric figure of merit (zT) greater than 0.006 at room temperature. These properties are attributed to the fact that the electrical conductivity was significantly improved by creating a CNT network, while the Seebeck coefficient and thermal conductivity remained insensitive to the nanotube concentration due to the existence of the junctions that significantly impede thermal transport.[64]

The transport phenomena in segregated network composites made with a polymer emulsion (or latex) are strongly dependent on filler properties, concentration, and interactions between fillers.[66] Surfactants needed to stabilize the hydrophobic carbon nanotubes in water also influence electrical and thermal transport behaviors because they can create interfacial barriers that scatter charge carriers and/or phonons. Gum arabic was used to disperse SWCNT in water prior to combination with a PVAc emulsion. The influence of stabilizing agent on the transport properties of the dry latex-based polymer nanocomposites was examined by varying the SWCNT:GA ratio.[64] The electrical conductivity of the composite increases up to 900 S m^{-1} as the SWCNT:GA ratio increases from 1:3 to 10:1, while thermal conductivity and Seebeck coefficient remain nearly constant (near 0.25 W m^{-1} K^{-1} and 40 μV K^{-1}, respectively). This thermally disconnected and electrically connected behavior in CNT-filled latex composites suggests that phonon and electron transport are significantly affected by tube/tube junctions, and the carrier transport across the junctions can be controlled by properly adjusting the stabilizer concentration.

Thermoelectric behavior of these segregated network composites was improved by using a semiconductor stabilizer for the CNTs. Moriarty et al. prepared nanocomposites with DWCNT and MWCNT, stabilized with sodium deoxycholate (DOC) or meso-tetra(4-carboxyphenyl) porphyrin (TCPP).[67] DOC has been used as an effective stabilizing agent for CNTs,[68] while porphyrin derivatives are known to interact, stabilize, and exfoliate CNT in water due to their conjugated structure that promotes π–π overlap.[69] The electrical conductivity of the TCPP-stabilized MWCNT composite was slightly reduced relative to that of the DOC-stabilized composite. Replacing MWCNTs with DWCNTs in the TCPP composite improved the electrical conductivity by a factor of five relative to DOC-stabilized, which is due to a facile electron transfer between the conjugated TCPP and DWCNTs. The Seebeck coefficient of MWCNT-based composites increased from 8 to 28 μV K^{-1} when the stabilizer was changed from DOC to TCPP. DWCNT-filled PVAc composites also showed an increase in Seebeck coefficient from 71 to 78 μV K^{-1} with TCPP stabilization. This dramatic increase in Seebeck coefficient in TCPP-stabilized composites can be ascribed to either a lower carrier concentration or larger effective mass of the charge carriers relative to DOC.[3a] The calculated power factor of the DWCNT-filled composites increases from 7.53 to 42.8 μW m^{-1} K^{-2} when DOC is replaced by TCPP. These values are two orders of magnitude greater than the MWCNT-filled composite.

4.1.2. Solution and Melt-Processed Nanocomposites

In addition to insulating PVAc-based composites, polymers such as Nafion, polystyrene (PS), polycarbonate (PC), polypropylene (PP), and polyurethane (PU) have been used for the fabrication of organic nanocomposite films due to their good affinity with CNTs.[70] For example, Choi et al. studied the effect of various types of nanotubes on the thermoelectric properties of a CNT/Nafion composite.[70a] Three different types of CNTs including SWCNTs, few-walled carbon nanotubes (FWCNTs), and MWCNTs, were effectively dispersed in a water-soluble Nafion. CNT/Nafion nanocomposite films fabricated by the doctor blade method show that both the electrical conductivity and Seebeck coefficient increase with the concentration, irrespective of the type of CNT. The highest electrical conductivity is 13 S cm^{-1} in the MWCNT/Nafion composite containing 30 wt% nanotubes. While the electrical conductivity in these composites depends on the type of CNT, the Seebeck coefficient is relatively insensitive to the nanotube type. This indicates that high energy charge carriers can participate in the transport

© 2017 WILEY-VCH Verlag GmbH & Co. KGaA, Weinheim

Pursuant to the DOE Public Access Plan, this document represents the authors' peer-reviewed, accepted manuscript. The published version of the article is available from the relevant publisher.

process because the Seebeck coefficient is related to the transport of energetic charges, while the electrical conductivity is related to the transport of all mobile charges.[70d] The FWCNT/Nafion films exhibited the highest power factor of 1 μW m^{-1} K^{-2} among all of the CNT/Nafion composites studied.

Thin flexible insulating polymer-based composites were also prepared by solvent casting with a viscous dispersion of SWCNTs in a polycarbonate matrix. The incorporation of SWCNTs in PC profoundly modified the electrical properties of the composite in proportion with the SWCNT concentration. Addition of 1 wt% SWCNTs increased the electrical conductivity of the composites by 16 orders of magnitude, while the Seebeck coefficient decreased slightly, within the range of 60–70 μV K^{-1} as a function of SWCNT loading. The maximum power factor was 3.2 μW m^{-1} K^{-2} at 25 wt% SWCNTs. The TE properties of PC/CNT composites were further improved by employing a cyclic butylene terephthalate (CBT) oligomer as an additive.[70e] Tzounis et al. studied the influence of CBT on the processability and thermoelectric properties of PC/MWCNT nanocomposites. The CBT additive improves the MWCNT dispersion within the polymer matrix, resulting in a power factor of 7.6 μW m^{-1} K^{-2} and zT of 7.94×10^{-9} at room temperature.

CNT bundles in polystyrene were reported to have good thermoelectric behavior by Suemori et al. In these composites, SWCNT bundles were directly dispersed within the PS matrix by a planetary ball milling-based dispersion technique.[70b] The SWCNT/PS composite shows excellent flexibility with a very low density (1.58 g cm^{-2}), which is roughly 5 × lower than that of traditional inorganic TE materials (i.e., 7.8 g cm^{-2} in Bi_2Te_3). This composite system exhibits a power factor of 413 μW m^{-1} K^{-2}.

For wearable thermoelectric textile coating applications, Wu et al. developed a water-processable TE composite in which poly(3,4-ethylenedioxythiophene) (PEDOT):poly(styrene sulfonate) (PSS) stabilized MWCNTs are incorporated into a viscous polymer matrix of nonionic waterborne polyurethane (WPU).[70f] With 20 wt% MWCNTs and a 1:4 ratio of MWCNTs to PEDOT:PSS, the electrical conductivity and Seebeck coefficient achieve 138 S cm^{-1} and 10 μV K^{-1}, respectively, resulting in a power factor of 1.41 μW m^{-1} K^{-2}. The fabricated WPU/MWCNT-PEDOT:PSS composite was successfully coated on commercial cotton and polyester yarns (**Figure 14**a). The electrical resistance of both polyester and cotton yarns decreased with increased dipping cycles (Figure 14b). Polyester yarn showed lower resistance than cotton yarns due to the more uniform and smooth surface of the polyester yarn(Figure 14c,d). This work demonstrates that a WPU-based composite with satisfactory TE performance and the coating technology to textile yarns could be promising for flexible and wearable thermoelectric devices.

4.1.3. Nanocomposites Prepared with Electron Donating Stabilizers

The most efficient thermoelectric devices require p-type and n-type elements to be organized in series.[71] The thermoelectric performance of organic p-type composites has become very competitive in recent years,[72] but the development of

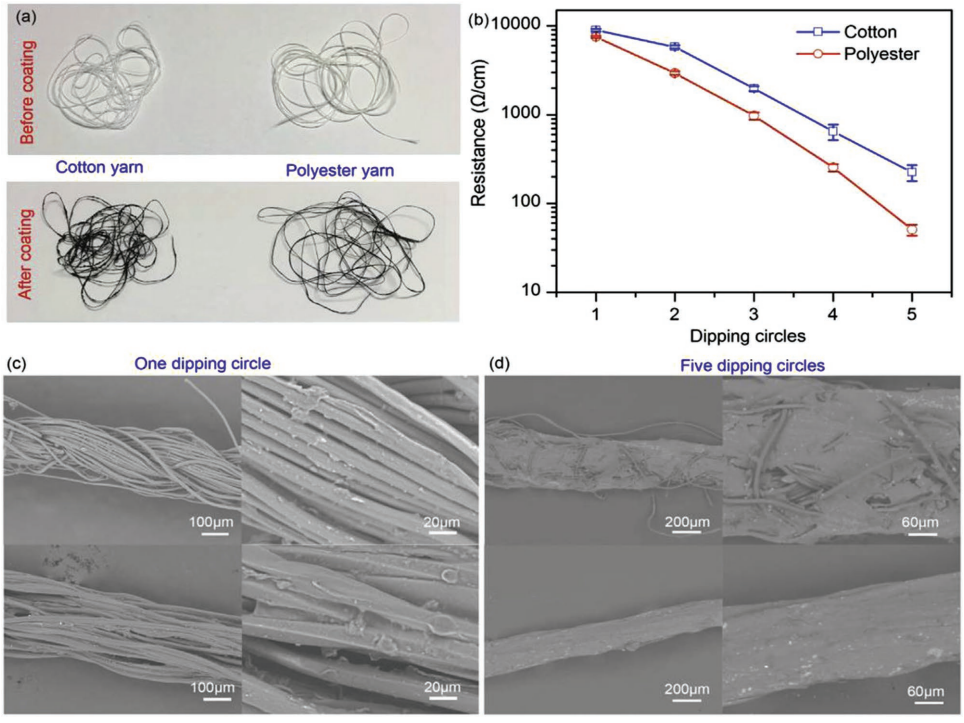

Figure 14. a) Images of cotton and polyester yarns before and after coating with thermoelectric. b) Electrical resistance of cotton and yarns with increased dipping cycles. c,d) SEM photographs of cotton (above) and polyester (below) yarns coated for one and five times respectively. Reproduced with permission.[70f] Copyright 2016, Elsevier.

© 2017 WILEY-VCH Verlag GmbH & Co. KGaA, Weinheim

Pursuant to the DOE Public Access Plan, this document represents the authors' peer-reviewed, accepted manuscript. The published version of the article is available from the relevant publisher.

their n-type counterparts has been more challenging. Several approaches have been used to produce air stable n-type organic materials. For example, Sun et al. reported powder-pressed n-type thermoelectric films, assembled with conducting poly(K_x(Ni-1,1,2,2-ethenetetrathiolate)s) (poly(Ni-ett)s), that achieve a stable high power factor of 66 μW m^{-1} K^{-2} and zT of 0.2.[23d] Unfortunately, these polymers are neither soluble nor fusible, which significantly limits their processability. As discussed above, CNTs are typically p-type in the absence of chemical manipulation, and CNTs doped n-type with molecular redox dopants are susceptible to "dedoping" by oxygen in ambient conditions, such that the Seebeck coefficient becomes positive over time.[19c,73]

Another method to prepare n-type TE nanocomposites involves noncovalent functionalization of carbon nanotubes with electron-rich polymers. The physical adsorption of PEI onto CNTs converts them from p-type to n-type due to the amine-rich polymer donating electrons to the nanotubes.[74] The amine groups in PEI contain electron lone pairs, acting as donors that shift the Fermi energy to upward relative to its initial energy state, resulting in n-type behavior. Ryu et al. employed PEI functionalization of CNT in air, achieving a large n-type Seebeck coefficient (−58 μV K^{-1}) without vacuum or a controlled environment.[75] The thermoelectric performance of CNT-filled polymer composites was improved by dispersing nanotubes in sodium dodecylbenzenesulfonate (SDBS) prior to the physical adsorption of PEI.[76] SDBS is a good surfactant to facilitate nanotube dispersion, forming a smooth coating layer. The SWCNT/PEI composites exhibit air-stable n-type characteristics, with electrical conductivity as high as 15 S cm^{-1} and Seebeck coefficient as large as −100 μV K^{-1}. Better CNT dispersion with greater SDBS concentration improves thermoelectric performance due to greater physical contact with PEI and more effective doping.

Doping carbon nanotubes with polyethylenimine in conjunction with sodium borohydride ($NaBH_4$) reduction has been shown further increase n-type behavior,[77] since $NaBH_4$ reduction increases the electrical conductivity of CNTs.[22a,78] Immersion of nanotubes with p-type Seebeck coefficient of 22 μV K^{-1} into $NaBH_4$ solution for 48 h converts S to −24 μV K^{-1} at room temperature (**Figure 15**a,b). The Seebeck coefficient became more negative (i.e., n-type) with longer doping time. A Seebeck coefficient of −57 μVK^{-1} was obtained by PEI doping. The combination of PEI and $NaBH_4$ doping results in Seebeck as large as −80 μV K^{-1}, with better conductivity than using individual dopants. Storage of the doped film in a glove box maintained the n-type properties, but air exposure caused these characteristics to deteriorate rapidly over 3 d, as shown in Figure 15c,d. Lamination of the doped samples with a polyester film slowed the degradation in air, preserving the n-type characteristics over 25 d. This simple lamination could be a viable approach to prevent the deterioration of n-type characteristics in a variety of doped systems.

Luo et al. investigated the thermoelectric properties of n-type composites fabricated with a solvent-free melt mixing technique, which is environmentally friendly and can be easily scaled.[79] PP was melt mixed with SWCNTs to generate an electrical network inside the insulating polymer matrix.

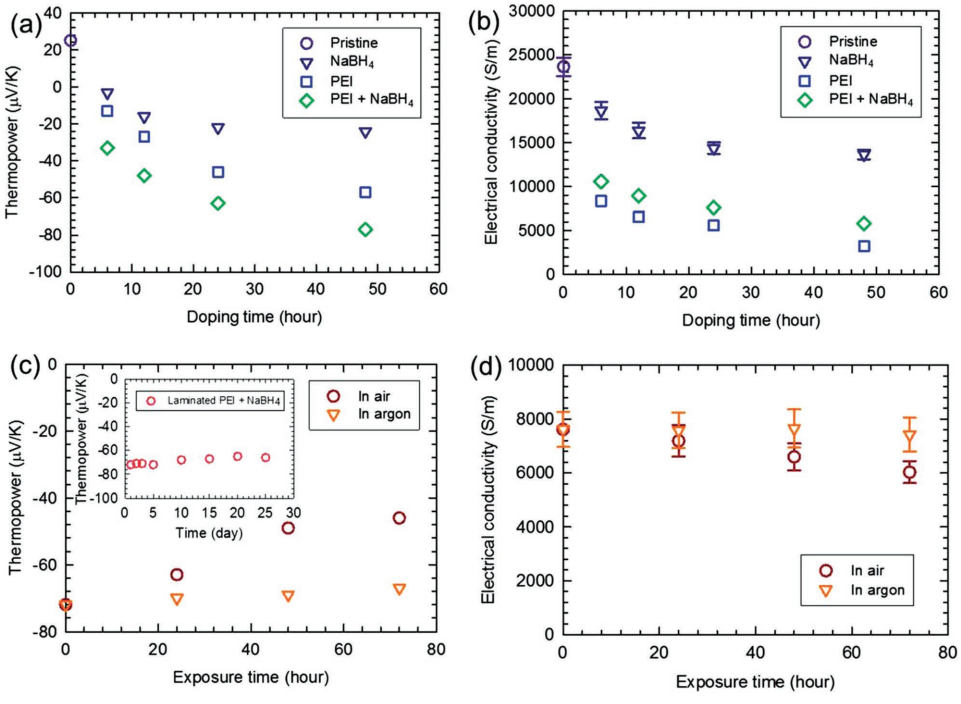

Figure 15. a) Thermopower and b) electrical conductivity before and after doping with $NaBH_4$, PEI, and both together, on filtered membrane samples. The samples doped with both PEI and $NaBH_4$ were made by uniformly immersing pristine samples in 1 M $NaBH_4$ for 24 h after PEI doping for varying time periods. c,d) The air stability of the samples doped with both PEI and $NaBH_4$ after they were exposed to air or argon environments. The samples were doped with PEI for 48 h and soaked in an aqueous 1 M $NaBH_4$ solution for 24 h. After lamination, the stability is shown in the inset of (c). All tests were performed at room temperature. Reproduced with permission.[77] Copyright 2012, The Royal Society of Chemistry.

© 2017 WILEY-VCH Verlag GmbH & Co. KGaA, Weinheim

Pursuant to the DOE Public Access Plan, this document represents the authors' peer-reviewed, accepted manuscript. The published version of the article is available from the relevant publisher.

CuO was added to the PP/SWCNT composites to further increase the electrical conductivity. Finally, the addition of polyethylene glycol switched these p-type composites to n-type with a Seebeck coefficient of −56.6 μV K^{-1}. The composites remain n-type after exposure to air for 8 months, with little change in electrical conductivity. The n-type power factor is 7.8×10^{-2} μW m^{-1} K^{-2}, which is greater than the p-type counterpart (2.3×10^{-2} μW m^{-1} K^{-2}). This is the first demonstration of switching p-type polymer composites to n-type using melt mixing and is a relatively simple approach.

4.2. Nanocomposites Prepared with Intrinsically Conductive Polymers

Composites prepared with nonconductive polymers typically result in low thermoelectric performance due to the insulating effect of the matrix surrounding the nanotubes. In contrast, conjugated polymers themselves behave as TE materials due to availability of charge carriers and efficient transport through π-orbitals.[49a] The behavior of conjugated polymer-based composites can be tailored without adversely impacting the desirable electronic properties of CNTs. Conducting polymers such as polyaniline (PANI), polypyrrole (PPy), poly(3-hexylthiophene) (P3HT), PEDOT, polyacetylene, PC, and their derivatives have recently attracted attention for use as TE materials due to their relatively low cost, abundant electron energy bands (through modulation), high energy density, and low thermal conductivity.[38a,55b,c] The chemical structure of these conducting polymers, along with the insulating polymers discussed in Section 2.1, are shown in **Table 4**. A summary of carbon nanotube-filled polymer composite preparation and TE properties is provided in **Table 5**. This section highlights advances in conducting polymer-based CNT composites.

4.2.1. Polyaniline-Based Composites

PANI has been the most studied polymer for thermoelectric energy generation due to its relatively easy preparation, control of electrical conductivity, good environmental stability, and unique doping/dedoping process.[55a,80] Hydrochloric acid (HCl)-doped PANI exhibits electrical conductivity and zT values that initially increase, but then decline, with more doping.[81] Thermal conductivity is insensitive to the doping conditions, achieving zT_{max} of 2.67×10^{-4} at 423 K with an HCl-doping concentration of 1.0 M. A multilayer film, composed of electrically insulating emeraldine base layers and electrically conducting (±)-10-camphorsulfonic acid (CSA)-doped emeraldine salt layers, was reported to have a zT of 1.1×10^{-2} at 423K, which was a factor of six greater at 300 K relative to a bulk film of CAS-doped PANI.[82] When stretched, PANI films doped by CSA exhibit a zT_{max} of 2.9×10^{-2} (4.4×10^{-3} for the unstretched counterpart).[83] The improvement of both the electrical conductivity and Seebeck coefficient in stretched PANI films is attributed to increased charge carrier mobility caused by the extended coil-like conformation of PANI.

Although reported zT values of PANI-based composites are below 0.02, approximately two orders of magnitude less than those of state-of-the-art inorganic thermoelectric materials, significant improvements have been reported with incorporation of carbon nanotubes.[84] Yao et al. prepared SWCNT/PANI nanocomposites through in situ polymerization.[55a] PANI was observed to grow on the surface of SWCNTs, forming an ordered chain structure during the SWCNT-directed polymerization process, as shown in **Figure 16**. During polymerization, the arrangement of the PANI chains improves due to strong donor–acceptor electron interactions and π–π interactions between PANI and SWCNT. In Figure 16, a bundle of SWCNT are tightly wrapped by PANI and some parts of individual nanotubes are naked (as shown by the arrows), implying strong

Table 4. Chemical structures of polymers used to prepare thermoelectric composites.

Polymers	Abbreviation	Polymer structure	Polymers	Abbreviation	Polymer structure
Poly(vinyl acetate)	PVAc	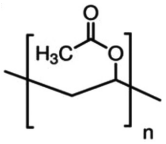	Polypyrrole	PPy	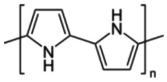
Polyethylenimine	PEI	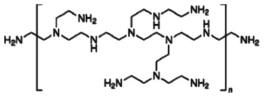	Polythiophene	PTh	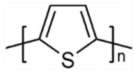
Polypropylene	PP	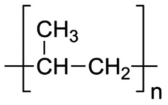	Poly(3,4-ethylene-dioxythiophene)	PEDOT	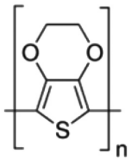
Polyaniline leucoemeraldine ($x = 1$, $y = 0$) emeraldine($x = y = 0.5$) [ermograniline($x = 0$, $y = 1$)	PANI	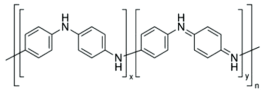	Polycarbazole	PC	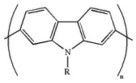

© 2017 WILEY-VCH Verlag GmbH & Co. KGaA, Weinheim

Pursuant to the DOE Public Access Plan, this document represents the authors' peer-reviewed, accepted manuscript. The published version of the article is available from the relevant publisher.

Table 5. Preparation and thermoelectric properties of carbon-nanotube-filled polymer nanocomposites.

Materials	Preparation method	Electrical conductivity [S cm^{-1}]	Seebeck coefficient [μV K^{-1}]	Power factor [μW m^{-1} K^{-2}]	Thermal conductivity [W m^{-1} K^{-1}]	zT	Ref.
PVAc/DWCNT/TCPP	Polymer emulsion	48	80	30.7	0.34	0.006	[64]
PVAc/SWCNT		9	40	1.4	≈0.25	0.0015 (300k)	[88]
PVAc/SWCNT		71	78	42.8	0.2–0.4		[67]
Nafion/FWCNT	Simple mixing	12.5	27	1	–	–	[70a]
PVP	–	5×10^{-4}	–9.5	5×10^{-6}	–	–	[118]
PEI	–	5.5×10^{-4}	–5.5	2×10^{-6}	–	–	
SWCNT	Doped with KOH	69	–63	27.00	0.124	0.07	[26]
PEI/SWCNT/PEI	Polymer emulsion	15	–100	15	–	–	[76]
PEI/SWCNT/$NaBH_4$	Simple mixing	20	–80	12.8	–	–	[77]
PP/SWCNT/CuO	Simple mixing	0.17	36.8	2.3×10^{-2}	–	–	[79]
PANI	–	≈10^{-7} to 320	≈16–225	–	≈0.02–0.542	1.1×10^{-2} (423K)	[84a]
PANI/SWCNT	In situ polymerization	125	40	20	–	–	[55a]
PANI/SWCNT/Te		345	54	101	0.3	–	[92]
PANI/MWCNT		14.1	79.8	8.98	0.27	0.01 (298K)	[114b]
PANI/MWCNT		50	28	5	0.4–0.5	–	[80]
PANI/SWCNT	Casting suspension	769	65	176	0.43	0.12	[56a]
PANI/SWCNT	In situ polymerization + solution processing	1440	38	217	0.2–0.5	–	[84b]
PANI/MWCNT	In situ polymerization + electrospinning	17.1	10	0.17	–	–	[87]
PANI/SWCNT	Electrochemical deposition	31.53	45.4	6.5	–	–	[89a]
PANI/MWCNT	Cryogenic grinding + spark plasma sintering	159	25	0.1	0.18–0.79	7.6×10^{-5} (300K)	[91]
PANI/DWCNT	Simple mixing	610	61	220	–	–	[114c]
PEDOT:PSS	Dope with DMSO	880	65	400	0.52	0.42 (300 K)	[38b]
PEDOT:PSS/SWCNT/GA	Polymer emulsion	400	25	25	0.2–0.4	–	[96]
PEDOT:PSS/SWCNT/PVAc		1350	41	160	0.2–0.4	–	[97]
PEDOT:PSS/SWCNT		4000	19	140	0.53	0.03 (300K)	[58b]
PEDOT:PSS/DWCNT/TCPP		960	70	500	–	–	[58a]
PEDOT:PSS/SWCNT	Spin casting	241	38.9	21.1	–	–	[101]
PEDOT:PSS/graphene/MWCNT	In situ polymerization	689	23.2	37.08	0.36	0.031 (300K)	[104]
PEDOT:PSS/DWCNT	EG post-treatment	780	42	151	–	–	[105]
PPy	–	4.6	9.4	0.04	–	–	[56c]
PPy/MWCNT	In situ polymerization	32	25	2.1	–	–	[108]
PPy/SWCNT	Chemical oxidative polymerization	300	26.5	21.7	–	–	[109]
P3HT	–	320	269	62.4	–	–	[94b]

© 2017 WILEY-VCH Verlag GmbH & Co. KGaA, Weinheim

Pursuant to the DOE Public Access Plan, this document represents the authors' peer-reviewed, accepted manuscript. The published version of the article is available from the relevant publisher.

Table 5. Continued.

Materials	Preparation method	Electrical conductivity [S cm^{-1}]	Seebeck coefficient [μV K^{-1}]	Power factor [μW m^{-1} K^{-2}]	Thermal conductivity [W m^{-1} K^{-1}]	zT	Ref.
P3HT/MWCNT	Oxidative polymerization	0.11	11.3	1.56×10^{-3}	–	–	[84a]
P3HT/SWCNT	Wire-bar-coating	510	40	105	–	–	[111a]
P3HT/MWCNT	Solution mixing	27.5	27	2	–	8.71×10^{-4} (393K)	[111b]
P3HT/SWCNT	Doped with $FeCl_3$	1000	–	95	–	–	[112]
P3HT/SWCNT	Spin-coating	2760	31	267	–	–	[104]
PAH/PSS/MWCNT	LbL assembly	–	35	–	–	–	[116]
PANI/graphene/PANI/DWCNT		1080	130	1825	–	–	[117]
PANI/graphene/PANI/DWCNT-PEDOT:PSS		1885	120	2710	–	–	[16b]
PEI-DWCNT/PVP-graphene		300	80	190	–	–	[121]

binding between CNTs and PANI. The chain packing of PANI was also ordered due to the template effect of 1D nanostructured CNTs. This ordered structure results in increased carrier mobility. Both electrical conductivity and Seebeck coefficient of these composites improves with increasing SWCNT content, achieving a maximum power factor of 20 μW m^{-1} K^{-2} and the zT value of 0.004 at room temperature.

The same research group reported significantly improved thermoelectric transport properties of SWCNT/PANI hybrid films prepared by casting a suspension containing well-dispersed SWCNTs and CSA-doped PANI.[56a] They hypothesized that the remarkably higher TE properties, relative to those of either individual component, could be ascribed to two key factors: (1) conformational change of PANI from a compacted coil to an expanded coil and associated delocalization of polarons by the chemical interactions between PANI and m-cresol solvent and (2) chain-ordering due to the π–π interaction between PANI and CNTs.[85] Chemical interactions, such as hydrogen bonding and ionic interaction, between m-cresol and PANI can overcome the van der Waals interactions within the PANI molecules, resulting in the conformational changes of PANI molecules (from a compacted and random arrangement to an expanded coil), as shown in **Figure 17**.[86] This expanded molecular conformation of PANI has more area for interaction with the surface of SWCNTs, strengthening the growth of PANI molecules along the nanotube surface by strong overlap area of π–π orbitals, which increases the degree of molecular ordering of PANI.[55a,87] This nanocomposite exhibits electrical conductivity and Seebeck coefficient up to 769 S cm^{-1} and 65 μV K^{-1}, respectively, producing a power factor of 176 μW m^{-1} K^{-2}. It is believed that this SWCNT/PANI nanocomposite contains many nanotube-nanotube and PANI-nanotube interfaces, which may scatter phonons and depress the lattice thermal conductivity. zT is 0.12 for a composite with 64% SWCNTs at room temperature.

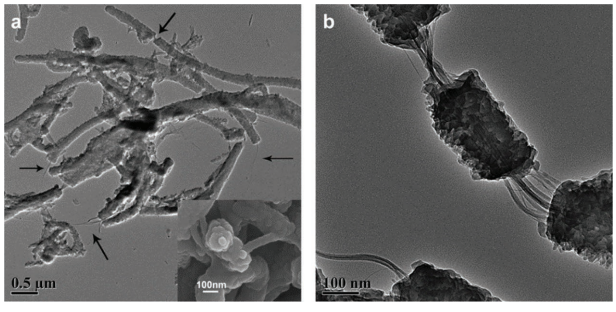

Figure 16. a,b) TEM images of SWCNT/PANI composites with 25 wt% SWCNTs. Inset of (a) is the SEM top view of the nanocable. Reprinted with permission.[55a] Copyright 2010, American Chemical Society.

Wang et al. further improved the TE properties of SWCNT/PANI composite films with improved ordering of the PANI molecular chains through a combination of in situ polymerization and solution processing.[84b] The in situ polymerization improved the dispersion of the SWCNTs in the composites and created strong π–π interactions with PANI.[56a] The improved ordering of the PANI increased the carrier mobility and thereby simultaneously improved electrical conductivity and Seebeck coefficient. The maximum power factor of the composite films reached 217 μW m^{-1} K^{-2} at room temperature. The thermal conductivity was as low as 0.44 W m^{-1} K^{-1} for a composite with 65 wt% SWCNTs. This low thermal conductivity was attributed to numerous nanointerfaces in the composite films and large differences in the vibrational spectra of the PANI and SWCNT that impedes phonon transport.[55b]

A combination of in situ polymerization and electrospinning was reported to improve the thermoelectric behavior of MWCNT/PANI composites by highly orienting the arrangement of polymer chains.[87] While the directly mixed MWCNT/PANI nanofibers had randomly oriented polymer chains and an isotropic structure, the combination of in situ polymerization and electrospinning created anisotropic uniaxial orientation, as shown in **Figure 18**. The highly ordered PANI backbone increases the number of effectively delocalized polarons due to the reduction of π–π conjugation defects (i.e., ring twists) in the polymer backbone. This in turn lowers the hopping barrier,

© 2017 WILEY-VCH Verlag GmbH & Co. KGaA, Weinheim

Pursuant to the DOE Public Access Plan, this document represents the authors' peer-reviewed, accepted manuscript. The published version of the article is available from the relevant publisher.

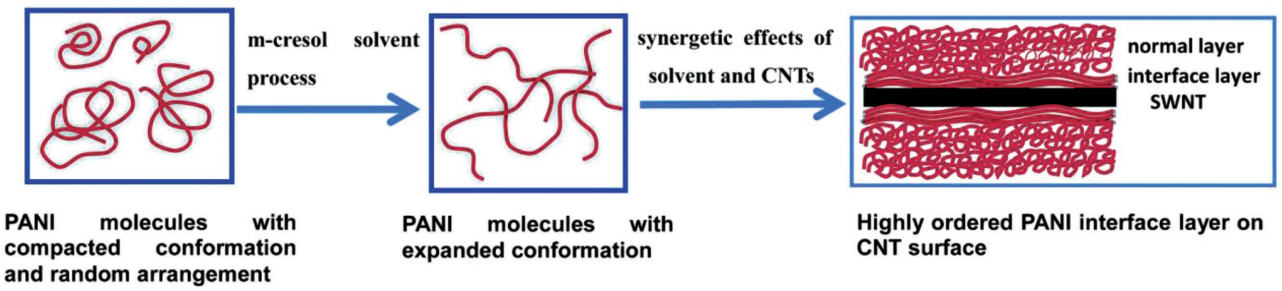

Figure 17. Schematic representations of the formation of an ordered PANI interface layer induced by the synergistic effects of the solvent process and the π–π interaction between PANI and SWCNT. Reproduced with permission.[56a] Copyright 2014, The Royal Society of Chemistry.

increases the carrier mobility, and improves both the electrical conductivity and Seebeck coefficient.[55a,88] The PANI-coated MWCNT composites align along the injection direction during the electrospinning process, which results in highly anisotropic thermoelectric properties with more than two times improvement of the maximum power factor (0.17 μW m^{-1} K^{-2}) in the direction of orientation.

Flexible SWCNT/PANI composite films were prepared via an in situ electrochemical polymerization process that is capable of adjusting the morphology and microstructure of the PANI composites, such as controlling the thickness of the PANI coated layer and the orientation of chains along the axis of nanotubes through subtle modulation of the electrolyte component and electric current.[89] The resulting composites formed 3D networks in which PANI acts as conductive glue that assembles the SWCNT into a conductive network. The polycrystalline PANI coated layer induced size-dependent electron energy filtering by scattering some of the charge carriers along the CNTs, which improves the Seebeck coefficient and reduces the electrical conductivity.[80,90]

Zhang et al. demonstrated a simple and facile method for fabricating MWCNT/PANI nanocomposites in which nanotubes and PANI were homogeneously mixed by cryogenic grinding (CG) without a dispersant and then consolidated via spark plasma sintering.[91] CG refined the grain size of PANI and truncated the MWCNTs, leading to good dispersion. The resulting films exhibit increased electrical conductivity with greater MWCNT content, with a maximum power factor of 1.73 μW m^{-1} K^{-2}.

Another strategy to greater composite power factor was studied by Wang et al., who used poly(styrenesulfonic acid)-doped PANI as the polymer matrix and SWCNTs and Te nanorods as filler.[92] The ternary PANI/SWCNT/Te nanocomposite films exhibit high Seebeck coefficient due to energy filtering at two different interfaces (PANI/SWCNT and PANI/Te) without much loss of electrical conductivity. As a result, the

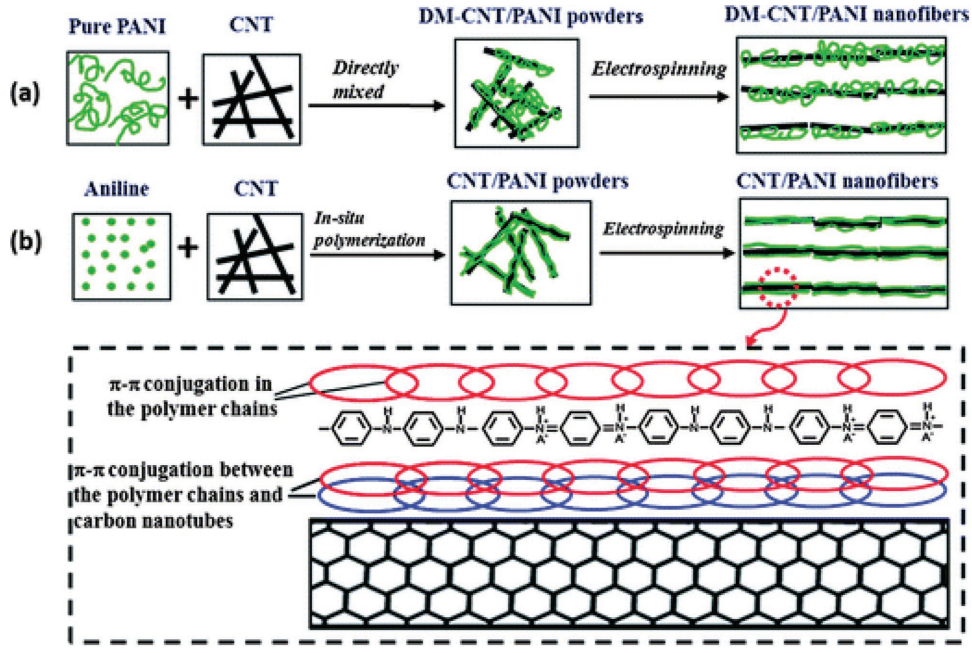

Figure 18. Schematic representations of the formation mechanism of a) DM-CNT/PANI and b) CNT/PANI nanofibers. The enlargement at the bottom shows the highly ordered arrangement of the PANI backbone chains on the surface of the CNT. Reproduced with permission.[87] Copyright 2012, The Royal Society of Chemistry.

© 2017 WILEY-VCH Verlag GmbH & Co. KGaA, Weinheim

Pursuant to the DOE Public Access Plan, this document represents the authors' peer-reviewed, accepted manuscript. The published version of the article is available from the relevant publisher.

maximum power factor for the composites is 101 μW m^{-1} K^{-2}. The two unique interfaces, with controlled interfacial energy barriers, seem to act as an energy filter that allows charge carriers with higher energy to preferentially cross the energy barrier at the interface, while low charge carriers are deterred.[55b,80]

4.2.2. Poly(3,4-Ethylenedioxythiophene)-Based Composites

PEDOT has attracted significant attention because of its high electrical conductivity, optical transparency, environmental stability, good flexibility, processability, and ease of doping.[93] PEDOT films have been used in organic solar cells, light emitting diodes, and organic field-effect transistors. The thermoelectric properties of PEDOT can be improved with chemical or electrochemical doping and/or dedoping.[57] Of the various forms of PEDOT available, doping with PSS is the most studied because of its water-solubility, low cost, excellent stability, good mechanical properties, and commercial availability.[38b,94] With appropriate treatment, the power factor for PEDOT-based polymers can exceed 400 μW m^{-1} K^{-2}.[94a,95]

Various PEDOT:PSS-based nanocomposites have been prepared to gain the best individual traits from the polymer (i.e., low thermal conductivity and solution processibility) and carbon nanotubes (i.e., electrical conductivity and Seebeck coefficient). The first study of the thermoelectric behavior of a CNT/PEDOT:PSS composite was reported by Kim et al.[96] Segregated network composites were prepared by drying a water-based polymer emulsion containing CNTs stabilized by PEDOT:PSS. The PEDOT:PSS existed as colloidal particles that decorated the surface of the nanotubes and bridged tube–tube junctions, which helped charge carriers to travel more efficiently through the composite. These composites have an electrical conductivity as high as 400 S cm^{-1} with 35 wt% SWCNTs and the Seebeck coefficient remains relatively constant as nanotube loading increases. This decoupling of Seebeck coefficient and conductivity differs from conventional TE bulk materials, whose properties are strongly correlated. It is believed that thermally disconnected and electrically connected contact junctions between nanotubes exist in these composites.[96,97] Thermal conductivity remains as low as 0.3 W m^{-1} K^{-1} due to the suppression of thermal transport across the tube-tube junctions caused by the dissimilar bonding and mismatches in vibrational spectra between CNTs and PEDOT:PSS. The composite containing 35 wt% SWCNTs and 35 wt% PEDOT:PSS, with the balance being vinyl acetate–ethylene copolymer, exhibits a zT of 0.02 at room temperature.[97]

Moriarty et al. investigated the behavior of SWCNT/PEDOT:PSS nanocomposites prepared by liquid-phase exfoliation, in which SWCNTs were stabilized by PEDOT:PSS in an aqueous solution.[58b] Electrically conductive junctions are formed between the two materials when the aqueous solution is dried, as shown in **Figure 19**a. These junctions depend on the interparticle distance, contact potential barriers, and stabilizers used to exfoliate the CNTs.[67,96–98] Electrical conductivity increases linearly from 20 to 95 wt% SWCNT in these films (Figure 19b), reaching 4000 S cm^{-1} with 95 wt% SWCNT. This is among the highest values ever reported for electrical conductivity in an organic composite.[96,98,99] Barriers between

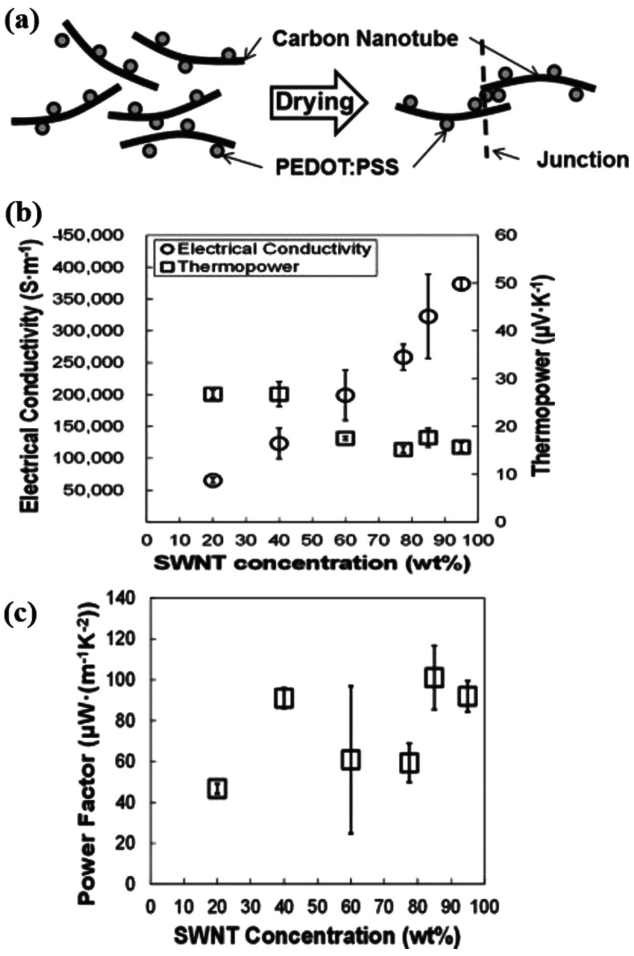

Figure 19. a) Schematic of CNTs coated by PEDOT:PSS particles in their exfoliated state that form an electrically conductive junctions upon drying. b) Electrical conductivity, thermopower, and c) power factor of SWCNT/PEDOT:PSS films as a function of nanotube concentration. Reproduced with permission.[58b] Copyright 2013, John Wiley & Sons.

SWCNTs and PEDOT:PSS interfaces preferentially allow high-energy carriers to pass across the tube junctions, while the transport of low-energy charge carriers is hindered. This results in an increase of mean carrier energy that effectively decouples electrical conductivity and Seebeck coefficient. Thin films composed of 5 wt% SWCNTs and 95 wt% PEDOT:PSS exhibit a power factor of 140 μW m^{-1} K^{-2} (Figure 19c).

The first report of a simultaneous increase in both electrical conductivity and Seebeck coefficient in an organic nanocomposite occurred for CNTs stabilized with both PEDOT:PSS and TCPP.[58a] TCPP is a semiconductor that has been shown to stabilize CNT through π–π overlap, increasing the Seebeck coefficient of segregated network composites.[67,100] The electrical conductivity of MWCNT/PEDOT:PSS/TCPP-filled composites can be as high as 95 S cm^{-1}, while the Seebeck coefficient and thermal conductivity remain relatively unaffected by the CNT concentration (**Figure 20**a,b). This dual-stabilizer system creates a larger energy barrier for low energy electrons.[58a] Replacing MWCNTs with DWCNTs in the same composite system increases the electrical conductivity to 960 S cm^{-1} and nearly doubles the Seebeck coefficient (≈70 μV K^{-1}), achieving

© 2017 WILEY-VCH Verlag GmbH & Co. KGaA, Weinheim

Pursuant to the DOE Public Access Plan, this document represents the authors' peer-reviewed, accepted manuscript. The published version of the article is available from the relevant publisher.

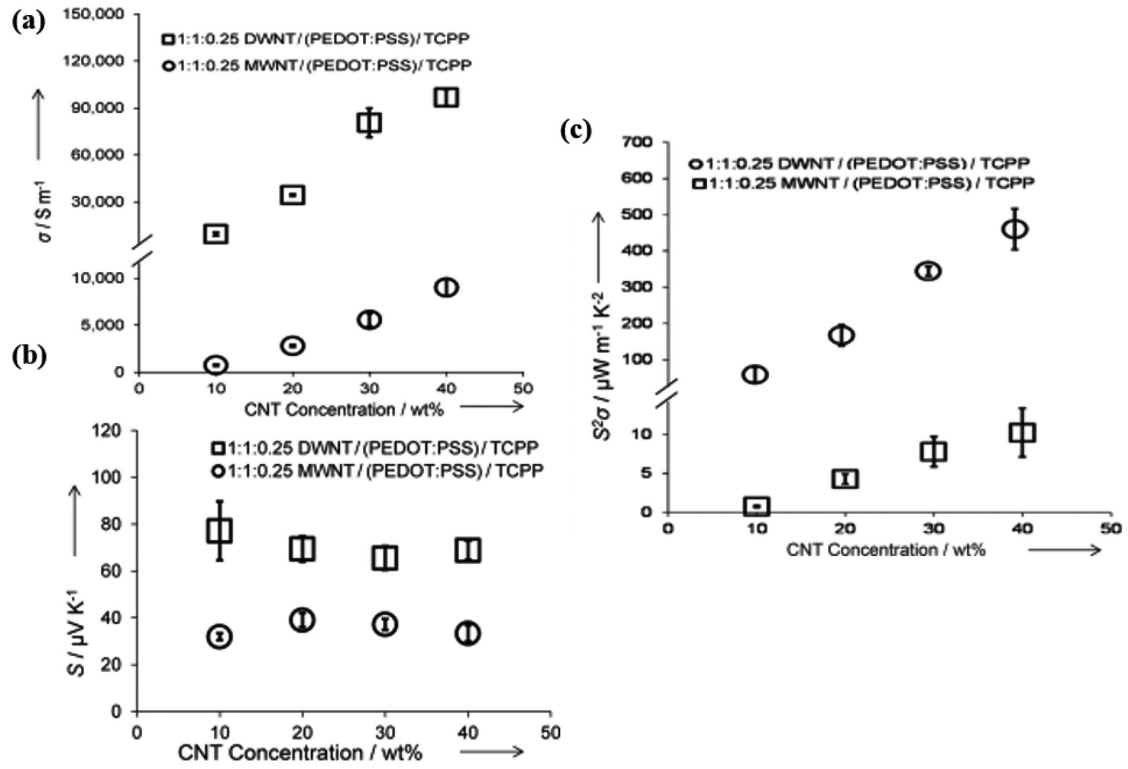

Figure 20. a) In-plane electrical conductivity and b) Seebeck coefficient as a function of CNT concentration and type. c) Composite power factor measured as a function of both CNT concentration and type. Reproduced with permission.[58a] Copyright 2013, John Wiley & Sons.

a power factor of approximately 500 μW m^{-1} K^{-2} at room temperature (Figure 20c). This large increase from DWCNTs is believed to be due to their highly conductive π-conjugated pathways that remain undisturbed through the inner tube during functionalization.[58a]

Layered SWCNT/PEDOT:PSS composites, prepared by a two-step spin casting process, were also shown to exhibit improved thermoelectric properties relative to control PEDOT:PSS.[101] A two-layer SWCNT/PEDOT:PSS film has electrical conductivity of 241 S cm^{-1} and Seebeck coefficient of 38.9 μV K^{-1}, achieving a power factor of 21.1 μW m^{-1} K^{-2}, which is four orders of magnitude greater than the pure PEDOT:PSS control sample analyzed in the same study (≈10^{-2} μW m^{-1} K^{-2}).[102] It is proposed that the improved properties in these layered nanocomposites are due to the bonding disruption of SO_3H group with the insulating PSS chains, after the addition of SWCNTs and the use of quantum confinement and interface effects in the layered nanostructure.[90,103]

Yoo et al. investigated how the combination of 1D MWCNT and 2D graphene platelets, stabilized with PEDOT:PSS, influences the thermoelectric properties of composites.[104] MWCNT/graphene/PEDOT:PSS composites were fabricated by in situ polymerization of 3,4-ethlyenedioxythiophene monomer in water in the presence of MWCNT and graphene, dispersed by PSS. This composite has an electrical conductivity and Seebeck coefficient of 689 S cm^{-1} and 23.2 μV K^{-1}, respectively. The power factor of 21.1 μW m^{-1} K^{-2} is much higher than that of a pristine PEDOT:PSS control sample and binary composites of PEDOT:PSS/graphene or PEDOT:PSS/CNT. This behavior is attributed to the synergistic effects of multidimensional electrical bridges and electronic coupling between PEDOT:PSS and the carbon nanoparticles. The PEDOT:PSS and low-dimensional carbon materials have strong electronic interactions that result in better long-range bridging between conductive domains.

Post-treatment of CNT/PEDOT:PSS nanocomposites by ethylene glycol (EG) exhibit improved TE properties.[105] Immersion of as-prepared DWCNT/PEDOT:PSS films into EG for 1h followed by annealing at 140 °C for 10 min effectively removes noncomplexed PSS chains. Ethylene glycol treatment has been previously used to improve the electrical conductivity of PEDOT:PSS films.[106] The average inter-DWCNT bundle distance in the nanocomposite films decreases with EG treatment, so the electrical conductivity and power factor increase significantly, up to ≈800 S cm^{-1} and 151.34 μW m^{-1} K^{-2}, respectively.

4.2.3. Other Conjugated Polymer-Based Composites

PPy is relatively low cost, easy to process, and exhibits reasonable environmental stability.[107] Wang et al. prepared MWCNT/PPy composites using an in situ polymerization method, using p-toluenesulfonic acid as a dopant and iron chloride as an oxidant.[108] The thermoelectric properties of MWCNT/PPy composite powder were measured after cold pressing. The electrical conductivity increases with MWCNT content, reaching 72 S cm^{-1} at a MWCNT loading of 15 wt%. This conductivity is much higher than that of a pure PPy control sample

© 2017 WILEY-VCH Verlag GmbH & Co. KGaA, Weinheim

Pursuant to the DOE Public Access Plan, this document represents the authors' peer-reviewed, accepted manuscript. The published version of the article is available from the relevant publisher.

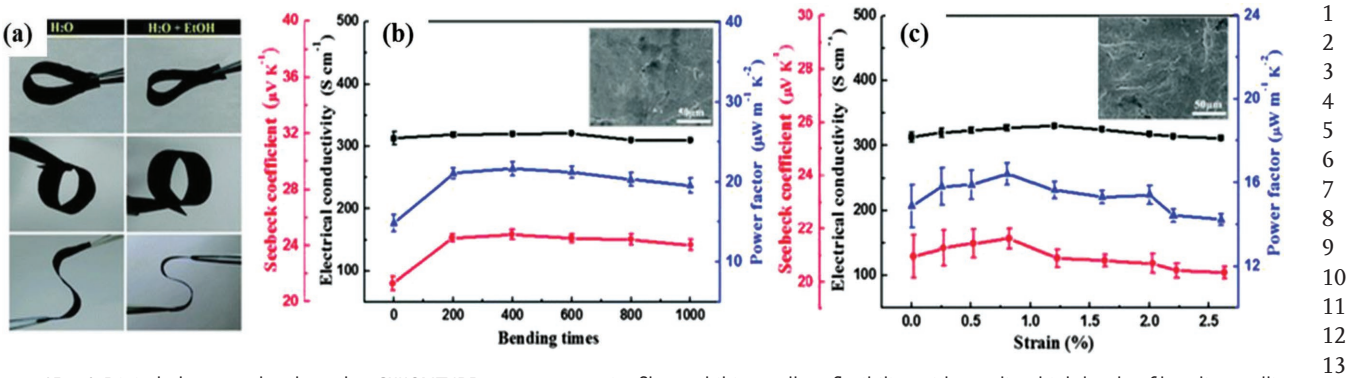

Figure 21. a) Digital photographs show that SWCNT/PPy nanocomposite films exhibit excellent flexibility, withstanding high levels of bending, rolling, and twisting. b) Thermoelectric performance for a composite with 40 wt% SWCNT before and after bending. c) Dependence of mechanical stretching on the thermoelectric performance of the composite. Insets are the FESEM images showing no cracks after b) bending for 1000 times, c) stretching 2.6%. Reproduced with permission.[56c] Copyright 2016, The Royal Society of Chemistry.

(2.2 S cm^{-1}) due to high nanotube conductivity and more ordered crystalline alignment of PPy. The composite power factor reached 2.07 μW m^{-1} K^{-2}, at a MWCNT content of 20%, which was 26 times as large as that of the neat PPy control.

More recently, SWCNT/PPy composites with a unique layered morphology were investigated by Liang et al.[109] In this work, free-standing composite films were prepared via a chemical oxidative polymerization and subsequent dispersion in either SDBS or cetyltrimethyl ammonium bromide solution. A suspension of PPy nanowires was produced and mixed with SWCNT, followed by vacuum filtration. The layered morphology, composed of densely packed SWCNT nanosheets sandwiched by PPy nanowires with a diameter of 55–75 nm, improves thermoelectric performance with increasing SWCNT content. The composites prepared with SDBS, display the best behavior, indicating that the dispersion medium plays an important role in the composite properties. The power factor of the composites with 60 wt% SWCNTs is 21.7 μW m^{-1} K^{-2}, which is four orders of magnitude greater than that of the neat PPy nanowires (0.02 μW m^{-1} K^{-2}) and the largest value reported for PPy-based nanocomposites.

The same group demonstrated large-area, flexible, and stretchable polymer/CNT composite films with stable thermoelectric performance (**Figure 21**a).[56c,110] The relatively high power factor (20 μW m^{-1} K^{-2}) is attributed to the smooth and uniform surface wrapping of PPy on the SWCNT (Figure 21b). More interestingly, the TE properties remain stable with repeated bending (as many as 1000 times). The composite also maintains its properties under a strain level of 2.6% (Figure 21c). This excellent mechanical stability is the result of strong interfacial interactions and surface wrapping that leads to effective stress transfer in the films.[56c]

P3HT, a derivative of polythiophene, has also been studied for its thermoelectric behavior in combination with nanotubes. P3HT exhibits higher solubility in common organic solvents, relative to most conjugated polymers, and has a highly tunable molecular structure, making it suitable for spin-coating, blade-coating, spray-printing, and ball milling.[111] The strong π-stacking between P3HT and CNTs causes the polymer to crystallize on the nanotube surface, which increases electrical conductivity from 1.7×10^{-5} S cm^{-1} (for P3HT alone) to ≈24 and 275 S cm^{-1} for MWCNT/P3HT and SWCNT/P3HT composites, respectively.[112] The more semiconducting character of the SWCNT-based composites produces a higher Seebeck coefficient (≈32 μV K^{-1}) compared to MWCNT/P3HT films (≈12 μV K^{-1}). Doping these composites with $FeCl_3$ nitromethane solution significantly increases electrical conductivity and raises power factor to 95 ± 12 μW m^{-1} K^{-2}.

SWCNT/P3HT composites were prepared by dispersing SWCNTs in a mixture of *o*-dichlorobenzene and P3HT, followed by coating onto a glass substrate to obtain large-area uniform films.[104] An $FeCl_3$/nitromethane solution was spun onto these as-prepared SWCNT/P3HT hybrid films to produce a power factor of 267 μW m^{-1} K^{-2}. The undoped composite and the composite doped by conventional immersion have power factors of 44.4 μW m^{-1} K^{-2} and 103 μW m^{-1} K^{-2}, respectively. Considering the electrical conductivity of SWCNTs show little sensitivity to doping, the authors suggest that the dramatic improvement of SWCNT/P3HT hybrid films doped by spin-coating originates from doping of the P3HT matrix. Further improvements in these films were realized by using a spray-printing method.[113] Spray-printed CNT/P3HT films exhibit a power factor of 325 μW m^{-1} K^{-2} at room temperature, which is the highest values reported for P3HT-based organic nanocomposites.

4.2.4. Layer-by-Layer Deposited Films

Great progress has been made with CNT-based nanocomposites using physical mixing, spin-coating, drop-casting, spray-coating, one-pot fabrication, creation of porous core/shell nanocomposites, and polymer emulsions, as described above.[104,112–114] In most cases, homogenous dispersion of carbon nanofillers in a polymer matrix, which is required to achieve high power factor nanocomposites, is challenging using these methods. Template-directed in situ polymerization can produce well-dispersed polymer/organic nanocomposites, but the thermoelectric performance is far below that of inorganic materials.[115] Polymer wrapping of CNTs by means of layer-by-layer (LbL) deposition offers the ability to easily adjust nanotube distance, density, and film thickness, which alters the Seebeck coefficient.[116] In a recent study, homogeneous films of polymer-coated CNT were prepared by first dispersing CNT in

© 2017 WILEY-VCH Verlag GmbH & Co. KGaA, Weinheim

Pursuant to the DOE Public Access Plan, this document represents the authors' peer-reviewed, accepted manuscript. The published version of the article is available from the relevant publisher.

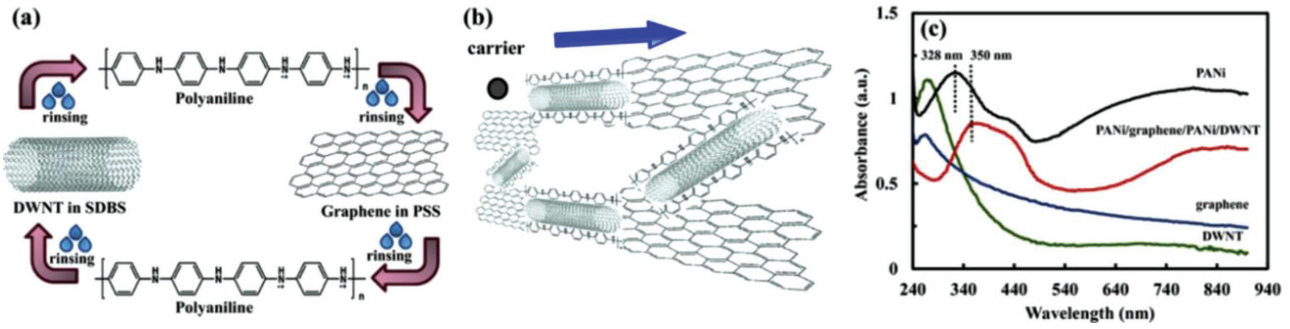

Figure 22. a) Schematic representation of the layer-by-layer (LbL) assembly procedure and b) carrier transport in the PANI/graphene/PANI/DWCNT multilayers. c) UV–vis spectra of aqueous DWCNTs, graphene, and PANI solutions and a four PANI/graphene/PANI/DWCNT quadlayer film. Reproduced with permission.[117] Copyright 2015, Wiley-VCH.

a positively charged poly(allylamine hydrochloride) (PAH) solution, followed by assembly with an aqueous solution of negatively charged PSS.[116] The desired polymer thickness around each nanotube, and therefore tube–tube distance in the film, was dictated by the number of PAH/PSS bilayers deposited onto the CNT layer. The Seebeck coefficient of the PAH/PSS/CNT nanocomposites increases with the number of polymer layers (15–20% per layer at room temperature) without compromising the electrical properties of the nanotubes. Unfortunately, the resistivity of the composites also increases with the number of polymer layers surrounding the CNTs.

Cho et al. prepared nanocomposite thin films with PANI, graphene, and DWCNTs using LbL assembly, as shown in **Figure 22**a.[117] A 470 nm thick film, comprised of 40 PANI/graphene/PANI/DWCNT "quad-layers", exhibits electrical conductivity of 1080 S cm^{-1} and a Seebeck coefficient of 130 μV K^{-1}, resulting in a remarkable power factor of 1825 μW m^{-1} K^{-2}. The exceptional thermoelectric behavior of these thin films is attributed to the continuous 3D PANI-wrapped DWCNTs and graphene network. PANI-covered DWCNTs bridge adjacent graphene nanoplatelets along their surfaces (Figure 22b) and this hybrid network provides synergistic improvement of the electrical conductivity. As more layers are deposited, these nanocomposite thin films become more electrically conductive because the density of the interconnections in the layers increases. UV–vis analysis revealed that the benzenoid peak of PANI at 328 nm in solution is red-shifted by 22 nm on the surface of DWCNTs in the deposited film (Figure 22c), indicating structural rearrangement of the polymer from random (ring twisting) to an extended chain conformation. This extension of conjugation (or extended chain conformation) caused by the strong π–π interaction of PANI oriented along the DWCNTs allows for better electron flow in the DWCNT network, improved carrier mobility, and ultimately an increase in both electrical conductivity and Seebeck coefficient through adjustment of the hopping barrier.[55a,118]

More recently, multilayer nanocomposite thin films with PEDOT:PSS stabilizing graphene and DWCNTs were reported.[16b] The earlier LbL-deposited films used insulating stabilizers for the carbon nanoparticles, instead of the highly conductive PEDOT:PSS stabilizer, which has good thermoelectric performance on its own.[111b,117] A 1 μm thick film exhibits a power factor of 2710 μW m^{-1} K^{-2}, which is the highest ever reported for a completely organic material and among the highest for any material at room temperature. By substituting intrinsically conductive PEDOT:PSS for insulating surfactants like PSS and SDBS that were used to disperse graphene and DWCNTs, respectively, the electrical conductivity increases by 70% (due to the reduction in contact resistance), while the Seebeck coefficient decreases by only 10%. The resulting power factor increases by 50 % relative to the previous work.[117] The high power factors of these PANI/graphene-PEDOT:PSS/PANI/DWCNT-PEDOT:PSS multilayers are attributed to two factors: (1) the strong interfacial π–π interactions within the film and (2) the 3D interconnected structure, consisting of well-dispersed graphene platelets connected by DWCNT-PANI and -PEDOT:PSS.

A clear synergy occurs when the PANI/graphene-PEDOT:PSS and PANI/DWCNT-PEDOT:PSS bilayer systems are combined into a quad-layer system which has a more continuous interconnected network. It is noteworthy that both electrical conductivity and Seebeck coefficient of this system increase simultaneously with the number of layers deposited. In typical bulk inorganic materials, the TE properties are strongly correlated, making this simultaneous increase extremely difficult to realize.[90,119] These decoupled properties are believed to be due to a carrier energy-filtering effect that is created by numerous interfaces between each component in the layers. It is likely that the carriers with higher energy preferentially participate in the transport, while lower energy carriers are deterred at the junctions (i.e., energy-dependent carrier scattering).[120] Energy filtering is confirmed by Hall Effect measurements in which mobility more than doubles with increasing layers, while carrier concentration remains nearly constant. This is the cause of the increase in Seebeck coefficient without suppressing electrical conductivity.

The LbL assembly technique was also used to fabricate high power factor n-type organic nanocomposites by alternately depositing DWCNTs, stabilized by PEI, and graphene stabilized by polyvinylpyrrolidone (PVP).[121] Electrostatic repulsions provided by wrapping of the DWCNTs with cationic PEI creates a stable colloidal dispersion in water, while graphene is exfoliated by steric and/or depletion stabilization by nonionic PVP.[122] The DWCNT-PEI/graphene-PVP assembly is driven by π–π interactions and van der Waals forces between DWCNT, graphene, and the polymers. Electrical conductivity increases with the number

© 2017 WILEY-VCH Verlag GmbH & Co. KGaA, Weinheim

Pursuant to the DOE Public Access Plan, this document represents the authors' peer-reviewed, accepted manuscript. The published version of the article is available from the relevant publisher.

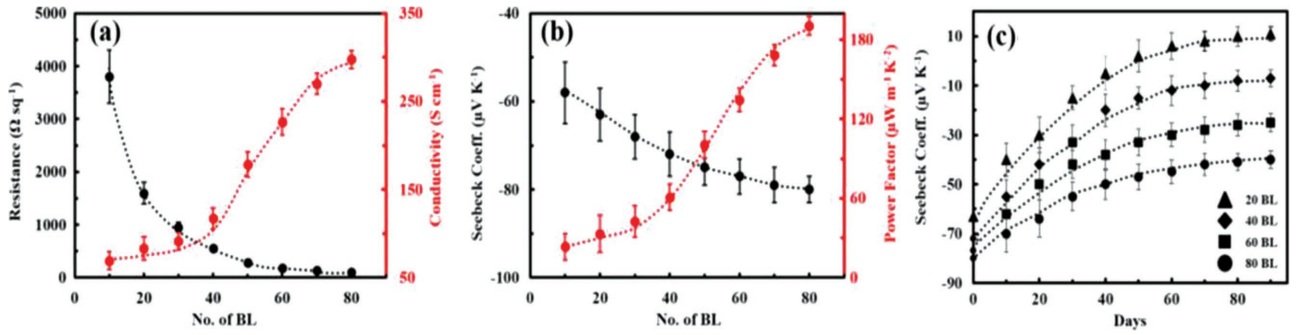

Figure 23. a) Sheet resistance and electrical conductivity, and b) Seebeck coefficient and power factor of DWCNT-PEI/graphene-PVP assemblies as a function of bilayers deposited on a PET substrate. c) Air-stability of Seebeck coefficient under ambient conditions. Reproduced with permission.[121] Copyright 2016, Elsevier.

of layers deposited (**Figure 23**a), which suggests improved electrical connection between the nanotubes and graphene. The conductivity levels off at 80 bilayers, indicating the 3D network of graphene and DWCNT is maintained.[123] These thin films exhibit a modest increase in Seebeck coefficient with thickness, achieving –80 μV K^{-1} at 80 bilayers (Figure 23b). In addition to helping to stabilize the carbon nanoparticles, both PEI and PVP act as electron donors that cause graphene and DWCNT charge carriers to change from holes to electrons.[124] This is the first ever investigation of an n-type thermoelectric LbL-assembled film. An 80-bilayer DWCNT-PEI/graphene-PVP film (≈320 nm thick) exhibits a remarkable power factor of –190 μW m^{-1} K^{-2} at room temperature (one of the highest values ever reported for a completely organic n-type material). Furthermore, unlike most organic n-type materials, this nanocomposite is relatively air-stable (Figure 23c), which is attributed to the gas barrier imparted by the highly aligned and exfoliated graphene layers that presumably creates tortuosity for molecular diffusion.[125]

5. Nanotube-Based Thermoelectric Devices

Thermoelectric generators (TEG) are solid-state devices that do not require moving components, offering a unique power generation system. A TE module consisting of legs of alternating p-type and n-type materials is connected electrically in series and thermally in parallel. This leg-type configuration is typical for energy generation because it minimizes any parasitic losses due to electrical resistance and facilitates the transfer of heat to the system. The efficiency of a generator is given by

$$\eta = \frac{P}{Q} \tag{7}$$

where Q is the amount of heat provided and P is the power generated by the device. The effectiveness of materials used in a device is determined by their efficiency, which is related to the Carnot efficiency by[3a]

$$\eta = \frac{\Delta T}{T_h} \cdot \frac{\sqrt{1+ZT}-1}{\sqrt{1+ZT}+\frac{T_c}{T_h}} \tag{8}$$

where ΔT is the temperature difference, T_h and T_c are the hot and cold temperatures, respectively. As mentioned earlier, we use uppercase ZT here to denote the device figure of merit, rather than the intrinsic material figure of merit (zT), following a previously employed convention.[3a] It should be noted that TEG efficiency can still be estimated from the material properties by assuming that both n-type and p-type legs exhibit equivalent material performance. The best inorganic TE materials have achieved a zT of 2.6 ± 0.3 at 923K, corresponding to a maximum efficiency of 20–25%. This efficiency is not competitive with traditional mechanical power generators.[126] New materials with zT of 3 or higher, operating between 300 and 773 K, are sought to provide the desired Carnot efficiency of 50%, which would make thermoelectric power generation commercially viable for more than niche applications.[127]

Although inorganic thermoelectric devices have exhibited high power output and power density relative to organics, certain drawbacks such as brittleness, poor processibility, high cost, and toxicity have made it difficult for them to find widespread use. Furthermore, their high ZT (>1) is typically achieved at temperatures above 600 K and often drops below 0.5 at room temperature (corresponding to a power factor < 400 μW m^{-1} K^{-2}). In other words, many inorganic TE materials can generate a greater amount of voltage only at elevated temperature. These inorganic generators have mostly been used for waste-heat recovery in relatively high temperature (>400K) ranges, such as automotive exhaust and industrial processes, due to this greater efficiency at elevated temperature.[128] Carbon nanotube-based TE devices are better suited for harvesting low-grade heat (e.g., transportation exhaust or human body heat in the 300–400K range. The use of organic thermoelectric materials for efficient harvesting of waste heat in a low temperature range (300–400 K) has attracted attention due to advantages such as cost effectiveness, ease of fabrication, and ability to use in a wide range of applications. In particular, with recent progress on flexible and stretchable electronic devices, there is great demand to use flexible TE generators on nonplanar surfaces. Recycling the heat dissipated by the human body could potentially charge the batteries of small electronic devices simply by embedding a flexible organic thermoelectric device into an article of clothing. Body heat could be used to charge batteries in a cell phone or run low-power devices (health sensors, hearing aids, etc.) using wearable power generators.

© 2017 WILEY-VCH Verlag GmbH & Co. KGaA, Weinheim

Pursuant to the DOE Public Access Plan, this document represents the authors' peer-reviewed, accepted manuscript. The published version of the article is available from the relevant publisher.

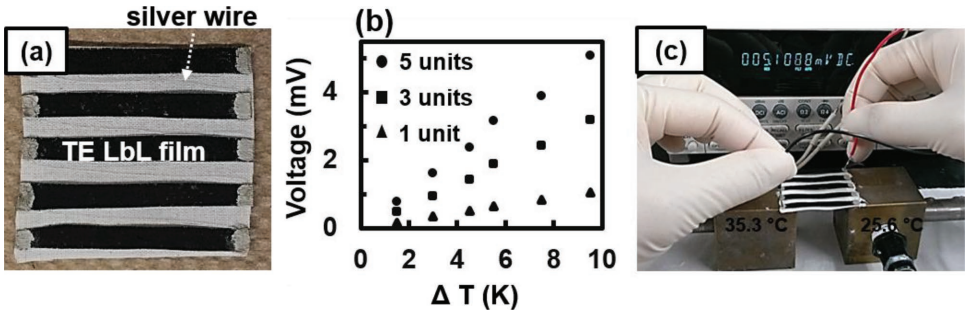

Figure 24. a) Images of cotton-based 80 quadlayer thermoelectric generator modules connected with silver ink and wires. b) TE voltage generated by the cotton-based devices as a function of ΔT. c) Generated voltage measured at an ambient temperature of 25.6 °C. With a ΔT of 9.7 K, the device generates 5.10 mV. Reproduced with permission.[16b] Copyright 2016, Wiley-VCH.

Solution processable, portable organic TE devices have been successfully introduced through a variety of methods such as inkjet printing, spray-printing, roll-to-roll printing, and photolithography patterning.[113,129] Hong et al. were the first to demonstrate a spray-printed flexible organic TEG comprised solely of p-type CNT/P3HT nanocomposite patterns on a polyimide substrate.[113] The generator was fabricated with 41 p-type lines with a width of 1 mm and a length of 15 mm, connected in series by dispenser-printed silver electrode lines. With a temperature difference of 10K, this device produces 32.7 nW of power. Cho et al. used p-type PANI/graphene/PANI/DWCNT multilayer films directly deposited on cotton fabric (**Figure 24**a).[16b] The voltage generated by coated fabric increases in a linear relationship with the temperature gradient and the number of strips placed in series (Figure 24b). A 5-strip module produces ≈5 mV with a ΔT of 9.5 K (Figure 24c). This demonstration provides a real opportunity for powering portable electronics with clothing that converts body heat to useful electricity.

Dörling et al. demonstrated photoinduced switching of p-type to n-type composites and fabricated a flexible TEG from solution using a single processing step.[129c] Upon UV irradiation, an initially p-type composite comprised of P3HT and nitrogen-doped MWCNTs became n-type. This work greatly simplifies the production of thermoelectric generators. A toroidal geometry of these modules was prepared by connecting p-type and UV-irradiated n-type legs with silver paste, folding into a spiral with adjacent couples (electrically in series) and finally joining to form a torus (**Figure 25**a–e). When one side of this module with 15 double legs was attached to a glass filled with ice water, it generated a voltage of 5 mV, demonstrating the possibility for application as a thermoelectric wristband (Figure 25f,g).

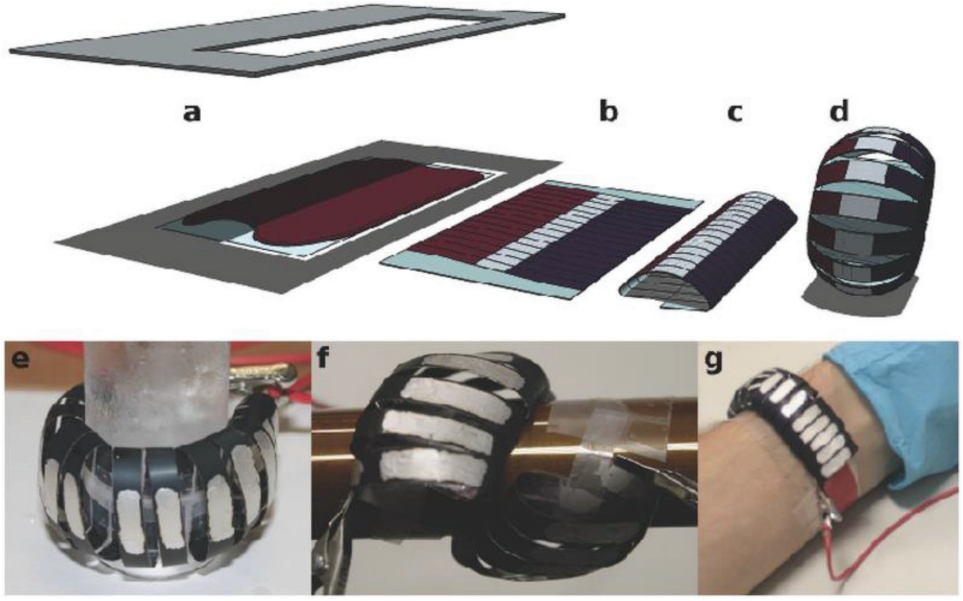

Figure 25. Proposed fabrication and application of a thermoelectric device geometry. a) A large area is coated from a single solution and patterned by UV irradiation. b) If desired, additional contacts (on what will be the outer side) are deposited. c) A flexible PET substrate is employed to easily connect the couples electrically in series by depositing contacts at what will be the inner side of the torus. d) The final toroidal device geometry. Possible application geometries in the form of e) a single torus, f) an extended spiral, and g) a wristband. The width of a single leg is 5 mm. Reproduced with permission.[129c] Copyright 2016, Wiley-VCH.

© 2017 WILEY-VCH Verlag GmbH & Co. KGaA, Weinheim

Pursuant to the DOE Public Access Plan, this document represents the authors' peer-reviewed, accepted manuscript. The published version of the article is available from the relevant publisher.

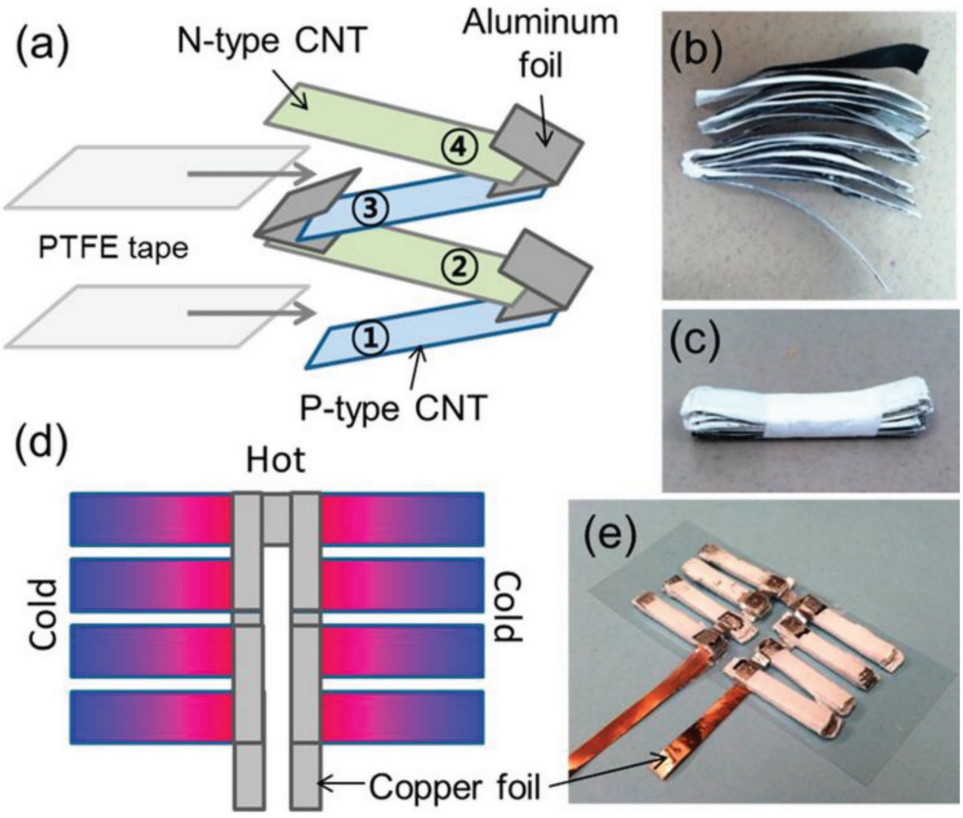

Figure 26. a) Assembly of p- and n-type carbon nanotube films. b) One module (stack) consists of 9 p-type and 9 n-type films. c) The stack is bound by a PTFE tape. d) A device design that maximizes thermoelectric voltage generation and e) a thermoelectric device consisting of 144 films (72 p-type and 72 n-type). Reproduced with permission.[131] Copyright 2014, American Chemical Society.

Hewitt et al.[130] and Kim et al.[131] have both demonstrated flexible and lightweight CNT-based organic TEGs based on a "z-scheme" folded device that capitalizes upon the in-plane transport of CNTs. In the study of Kim et al., the Seebeck coefficient and electrical conductivity are 97 μV K^{-1} and 110 S cm^{-1}, respectively, for the p-type composite. Air-exposed CNT were reduced using PEI and diethylenetriamine, with subsequent $NaBH_4$ treatment, in order to transform to n-type. The n-type electrical conductivity and Seebeck coefficient are 52 S cm^{-1} and –86 μV K^{-1}, respectively, resulting in a power factor of 38 μW m^{-1} K^{-2}. Based on the optimized p- and n-type CNT films, TE modules were alternately connected in series with insulating films of polytetrafluoroethylene inserted in between (**Figure 26**a,b). This stacked structure (called a module) was connected in series by copper foil (Figure 26c–e). The TE modules containing 72 p-type and 72 n-type CNT films produces an open circuit voltage of 9.6 mV (465 mV with temperature gradient of 49 K) and a power output of 1.8 μW with a temperature gradient of 32 K.

Zhou et al. recently utilized a similar *z*-scheme folded architecture to produce TEG devices with their SWCNT buckypapers grown directly by a floating catalyst CVD method (**Figure 27**a–d).[46] PEI was used as an n-type dopant, and the native p-type SWCNT paper was masked in even intervals to generate the alternating n- and p-type legs. Due to the relatively high power factor of these direct-grown films, the modules consisting of 3 p-n pairs produces a voltage of ≈3 mV at a ΔT of 8 K and ≈10 mV at a ΔT of 27.5 K (Figure 27e,f). With a temperature difference of 27.5 K, the device produces ≈2.5 μW of power, which is a power density of ≈16 mW m^{-2}. More recently, Choi et al. reported carbon nanotube yarn (CNTY)-based TE materials with a highly aligned structure that exhibits impressive power factors of 2387 and 2456 μW m^{-1} K^{-2} through p- and n-doping, respectively.[54] A light and flexible generator, fabricated with 60 pairs of p- and n-type CNTY, generates a maximum power density of 697 μW g^{-1} with temperature differential of 40 K. The growing number of impressive device studies shows great potential for flexible and wearable power-conversion devices, such as wireless communication and power management circuits.

6. Conclusions

In recent years, carbon nanotubes have emerged as highly promising materials for thermoelectric energy harvesting. High power factors have now been demonstrated for several unique SWCNT-based systems, both for p- and n-type materials, demonstrating the ability to produce powers that match or exceed the best reported semiconducting polymer systems. While carbon nanotubes in and of themselves are capable of being used as thermoelectric generators, CNT-enabled composites provide additional

© 2017 WILEY-VCH Verlag GmbH & Co. KGaA, Weinheim

Pursuant to the DOE Public Access Plan, this document represents the authors' peer-reviewed, accepted manuscript. The published version of the article is available from the relevant publisher.

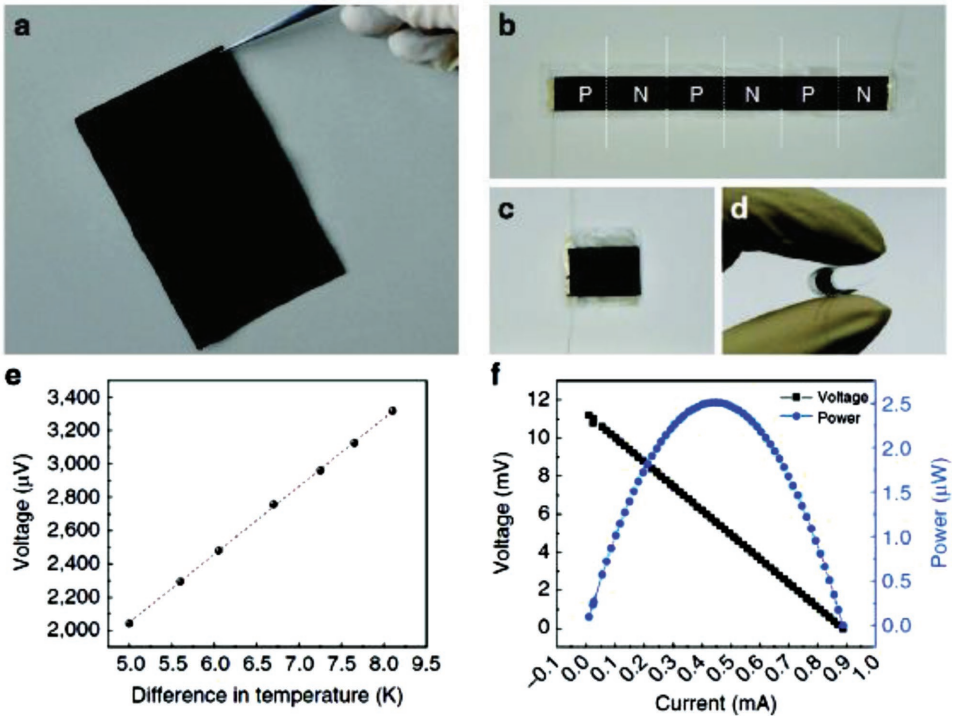

Figure 27. Optical photograph of a) large-area, thick CNT film prepared by superposing multilayer continuously produced CNT films and densified by ethanol, b) a CNT stripe composed of three pairs of continuous p–n couples, c) a compact TE module with dimensions of 16 mm × 10 mm × 0.15 mm that is d) flexible by design. e) Voltage produced by the module for different steady-temperature difference between two ends of the module. f) The voltage–current curve and power–current curve of the module for a hot-side temperature of 330 K and ΔT of 27.5 K. Adapted with permission.[46] Copyright 2017, Nature Publishing Group.

opportunities to engineer critical interfaces toward even higher performance. As shown in this review, both neat SWCNT fabrics and nanotube/polymer composites are already achieving power factors that rival commercial-grade bismuth telluride, demonstrating the potential for nanotube-based materials to compete with and ultimately displace inorganic semiconductors. Despite the tremendous progress made in the last decade, there remains ample room for improvement in the areas of doping, functionalization and stabilization of CNTs in both neat SWCNT-based materials and nanotube-based composites. There is good reason to expect significant advances in the thermoelectric power factor and $zT > 1$ in the coming decade as more researchers enter this exciting sub-field of thermoelectric materials. Improved energy generation efficiency in these materials will naturally lead to widespread use in mobile devices and clothing capable of powering various devices from body heat.

Acknowledgements

J.L.B. and A.J.F. gratefully acknowledge financial support from NREL's Laboratory Directed Research and Development (LDRD) program. J.C.G. and C.C. gratefully acknowledge financial support from the U.S. Air Force Office of Scientific Research (Grant No. FA9550-13-1-0085).

Conflict of Interest

The authors declare no conflict of interest.

Keywords

carbon nanotubes, composite materials, energy harvesting, organic electronics, thermoelectrics

Received: August 3, 2017
Revised: September 24, 2017
Published online:

[1] *International Energy Outlook 2016, Office of Energy Analysis*, U.S. Energy Information Administration, Washington, DC **2016**.
[2] Lawrence Livermore National Laboratory, Estimated U.S. Energy Consumption in 2016, https://flowcharts.llnl.gov/content/assets/docs/2016_United-States_Energy.pdf (accessed: July 2017).
[3] a) G. J. Snyder, E. S. Toberer, *Nat. Mater.* **2008**, *7*, 105; b) J. P. Heremans, M. S. Dresselhaus, L. E. Bell, D. T. Morelli, *Nat. Nanotechnol.* **2013**, *8*, 471.
[4] a) M. He, F. Qiu, Z. Lin, *Energy Environ. Sci.* **2013**, *6*, 1352; b) R. Kroon, D. A. Mengistie, D. Kiefer, J. Hynynen, J. D. Ryan, L. Yu, C. Müller, *Chem. Soc. Rev.* **2016**, *45*, 6147; c) B. Russ, A. Glaudell, J. J. Urban, M. L. Chabinyc, R. A. Segalman, *Nat. Rev. Mater.* **2016**, *1*, 16050; d) M. Orrill, S. LeBlanc, *J. Appl. Polym. Sci.* **2017**, *134*, 44256; e) L. M. Cowen, J. Atoyo, M. J. Carnie, D. Baran, B. C. Schroeder, *ECS J. Solid State Sci. Technol.* **2017**, *6*, N3080.
[5] a) L. D. Hicks, M. S. Dresselhaus, *Phys. Rev. B* **1993**, *47*, 12727; b) L. D. Hicks, M. S. Dresselhaus, *Phys. Rev. B* **1993**, *47*, 16631.
[6] a) D. S. Bethune, C. H. Klang, M. S. de Vries, G. Gorman, R. Savoy, J. Vazquez, R. Beyers, *Nature* **1993**, *363*, 605; b) S. Iijima, T. Ichihashi, *Nature* **1993**, *363*, 603.

© 2017 WILEY-VCH Verlag GmbH & Co. KGaA, Weinheim

Pursuant to the DOE Public Access Plan, this document represents the authors' peer-reviewed, accepted manuscript. The published version of the article is available from the relevant publisher.

[7] a) R. Saito, M. Fujita, G. Dresselhaus, M. S. Dresselhaus, *Phys. Rev. B* **1992**, *46*, 1804; b) J. W. Mintmire, B. I. Dunlap, C. T. White, *Phys. Rev. Lett.* **1992**, *68*, 631; c) N. Hamada, S.-i. Sawada, A. Oshiyama, *Phys. Rev. Lett.* **1992**, *68*, 1579.

[8] a) L. C. Venema, J. W. Janssen, M. R. Buitelaar, J. W. G. Wildöer, S. G. Lemay, L. P. Kouwenhoven, C. Dekker, *Phys. Rev. B* **2000**, *62*, 5238; b) A. Jorio, R. Saito, J. H. Hafner, C. M. Lieber, M. Hunter, T. McClure, G. Dresselhaus, M. S. Dresselhaus, *Phys. Rev. Lett.* **2001**, *86*, 1118.

[9] a) J. W. G. Wilder, L. C. Venema, A. G. Rinzler, R. E. Smalley, C. Dekker, *Nature* **1998**, *391*, 59; b) T. W. Odom, J.-L. Huang, P. Kim, C. M. Lieber, *Nature* **1998**, *391*, 62; c) M. J. O'Connell, S. M. Bachilo, C. B. Huffman, V. C. Moore, M. S. Strano, E. H. Haroz, K. L. Rialon, P. J. Boul, W. H. Noon, C. Kittrell, J. Ma, R. H. Hauge, R. B. Weisman, R. E. Smalley, *Science* **2002**, *297*, 593.

[10] a) S. J. Tans, A. R. M. Verschueren, C. Dekker, *Nature* **1998**, *393*, 49; b) A. Javey, J. Guo, Q. Wang, M. Lundstrom, H. Dai, *Nature* **2003**, *424*, 654.

[11] R. B. Weisman, S. M. Bachilo, *Nano Lett.* **2003**, *3*, 1235.

[12] a) M. S. Arnold, A. a. Green, J. F. Hulvat, S. I. Stupp, M. C. Hersam, *Nat. Nanotechnol.* **2006**, *1*, 60; b) X. Tu, S. Manohar, A. Jagota, M. Zheng, *Nature* **2009**, *460*, 250; c) H. Liu, D. Nishide, T. Tanaka, H. Kataura, *Nat. Commun.* **2011**, *2*, 309; d) A. Nish, J.-Y. Hwang, J. Doig, R. J. Nicholas, *Nat. Nanotechnol.* **2007**, *2*, 640; e) K. S. Mistry, B. A. Larsen, J. L. Blackburn, *ACS Nano* **2013**, *7*, 2231.

[13] a) A. D. Franklin, *Science* **2015**, *349*; b) G. J. Brady, A. J. Way, N. S. Safron, H. T. Evensen, P. Gopalan, M. S. Arnold, *Sci. Adv.* **2016**, *2*.

[14] a) S. Diao, G. Hong, A. L. Antaris, J. L. Blackburn, K. Cheng, Z. Cheng, H. Dai, *Nano Res.* **2015**, *8*, 3027; b) S. Diao, J. L. Blackburn, G. Hong, A. L. Antaris, J. Chang, J. Z. Wu, B. Zhang, K. Cheng, C. J. Kuo, H. Dai, *Angew. Chem.* **2015**, *127*, 14971.

[15] a) M. S. Arnold, J. L. Blackburn, J. J. Crochet, S. K. Doorn, J. G. Duque, A. Mohite, H. Telg, *Phys. Chem. Chem. Phys.* **2013**, *15*, 14896; b) S. N. Habisreutinger, R. J. Nicholas, H. J. Snaith, *Adv. Energy Mater.* **2017**, *7*, 1601839; c) J. L. Blackburn, *ACS Energy Lett.* **2017**, *2*, 1598.

[16] a) A. D. Avery, B. H. Zhou, J. Lee, E.-S. Lee, E. M. Miller, R. Ihly, D. Wesenberg, K. S. Mistry, S. L. Guillot, B. L. Zink, Y.-H. Kim, J. L. Blackburn, A. J. Ferguson, *Nat. Energy* **2016**, *1*, 16033; b) C. Cho, K. L. Wallace, P. Tzeng, J. H. Hsu, C. Yu, J. C. Grunlan, *Adv. Energy Mater.* **2016**.

[17] K. E. Moore, D. D. Tune, B. S. Flavel, *Adv. Mater.* **2015**, *27*, 3105.

[18] K. E. Moore, M. Pfohl, D. D. Tune, F. Hennrich, S. Dehm, V. S. K. Chakradhanula, C. Kübel, R. Krupke, B. S. Flavel, *ACS Nano* **2015**, *9*, 3849.

[19] a) J. Hone, I. Ellwood, M. Muno, A. Mizel, M. L. Cohen, A. Zettl, A. G. Rinzler, R. E. Smalley, *Phys. Rev. Lett.* **1998**, *80*, 1042; b) L. Grigorian, K. A. Williams, S. Fang, G. U. Sumanasekera, A. L. Loper, E. C. Dickey, S. J. Pennycook, P. C. Eklund, *Phys. Rev. Lett.* **1998**, *80*, 5560; c) P. G. Collins, K. Bradley, M. Ishigami, A. Zettl, *Science* **2000**, *287*, 1801; d) G. U. Sumanasekera, C. K. W. Adu, S. Fang, P. C. Eklund, *Phys. Rev. Lett.* **2000**, *85*, 1096; e) K. Bradley, S.-H. Jhi, P. G. Collins, J. Hone, M. L. Cohen, S. G. Louie, A. Zettl, *Phys. Rev. Lett.* **2000**, *85*, 4361; f) J. Vavro, M. C. Llaguno, B. C. Satishkumar, D. E. Luzzi, J. E. Fischer, *Appl. Phys. Lett.* **2002**, *80*, 1450; g) H. E. Romero, G. U. Sumanasekera, G. D. Mahan, P. C. Eklund, *Phys. Rev. B* **2002**, *65*; h) J. Vavro, M. C. Llaguno, J. E. Fischer, S. Ramesh, R. K. Saini, L. M. Ericson, V. A. Davis, R. H. Hauge, M. Pasquali, R. E. Smalley, *Phys. Rev. Lett.* **2003**, *90*, 065503; i) W. J. Kong, L. Lu, H. W. Zhu, B. Q. Wei, D. H. Wu, *J. Phys.: Condens. Matter* **2005**, *17*, 1923; j) W. Zhou, J. Vavro, N. M. Nemes, J. E. Fischer, F. Borondics, K. Kamarás, D. B. Tanner, *Phys. Rev. B* **2005**, *71*, 205423.

[20] a) Y. Nakai, K. Honda, K. Yanagi, H. Kataura, T. Kato, T. Yamamoto, Y. Maniwa, *Appl. Phys. Express* **2014**, *7*, 025103; b) M. Piao, M.-K. Joo, J. Na, Y.-J. Kim, M. Mouis, G. Ghibaudo, S. Roth, W.-Y. Kim, H.-K. Jang, G. P. Kennedy, U. Dettlaff-Weglikowska, G.-T. Kim, *J. Phys. Chem. C* **2014**, *118*, 26454.

[21] N. T. Hung, A. R. T. Nugraha, E. H. Hasdeo, M. S. Dresselhaus, R. Saito, *Phys. Rev. B* **2015**, *92*, 165426.

[22] a) T. M. Barnes, J. L. Blackburn, J. van de Lagemaat, T. J. Coutts, M. J. Heben, *ACS Nano* **2008**, *2*, 1968; b) J. L. Blackburn, T. M. Barnes, M. C. Beard, Y.-H. Kim, R. C. Tenent, T. J. McDonald, B. To, T. J. Coutts, M. J. Heben, *ACS Nano* **2008**, *2*, 1266; c) R. K. Jackson, A. Munro, K. Nebesny, N. Armstrong, S. Graham, *ACS Nano* **2010**, *4*, 1377; d) A. A. Green, M. C. Hersam, *Nano Lett.* **2008**, *8*, 1417.

[23] a) B. Russ, M. J. Robb, F. G. Brunetti, P. L. Miller, E. E. Perry, S. N. Patel, V. Ho, W. B. Chang, J. J. Urban, M. L. Chabinyc, C. J. Hawker, R. A. Segalman, *Adv. Mater.* **2014**, *26*, 3473; b) R. A. Schlitz, F. G. Brunetti, A. M. Glaudell, P. L. Miller, M. A. Brady, C. J. Takacs, C. J. Hawker, M. L. Chabinyc, *Adv. Mater.* **2014**, *26*, 2825; c) K. Shi, F. Zhang, C.-A. Di, T.-W. Yan, Y. Zou, X. Zhou, D. Zhu, J.-Y. Wang, J. Pei, *J. Am. Chem. Soc.* **2015**, *137*, 6979; d) Y. Sun, P. Sheng, C. Di, F. Jiao, W. Xu, D. Qiu, D. Zhu, *Adv. Mater.* **2012**, *24*, 932.

[24] a) A. M. Glaudell, J. E. Cochran, S. N. Patel, M. L. Chabinyc, *Adv. Energy Mater.* **2015**, *5*, 1401072; b) S. N. Patel, A. M. Glaudell, D. Kiefer, M. L. Chabinyc, *ACS Macro Lett.* **2016**, *5*, 268.

[25] B. Chandra, A. Afzali, N. Khare, M. M. El-Ashry, G. S. Tulevski, *Chem. Mater.* **2010**, *22*, 5179.

[26] Y. Nonoguchi, M. Nakano, T. Murayama, H. Hagino, S. Hama, K. Miyazaki, R. Matsubara, M. Nakamura, T. Kawai, *Adv. Funct. Mater.* **2016**, *26*, 3021.

[27] K. S. Mistry, B. A. Larsen, J. D. Bergeson, T. M. Barnes, G. Teeter, C. Engtrakul, J. L. Blackburn, *ACS Nano* **2011**, *5*, 3714.

[28] Y. Nonoguchi, Y. Iihara, K. Ohashi, T. Murayama, T. Kawai, *Chem. Asian J.* **2016**, *11*, 2423.

[29] Y. Nonoguchi, K. Ohashi, R. Kanazawa, K. Ashiba, K. Hata, T. Nakagawa, C. Adachi, T. Tanase, T. Kawai, *Sci. Rep.* **2013**, *3*, 3344.

[30] a) U. Dettlaff-Weglikowska, V. Skákalová, R. Graupner, S. H. Jhang, B. H. Kim, H. J. Lee, L. Ley, Y. W. Park, S. Berber, D. Tománek, S. Roth, *J. Am. Chem. Soc.* **2005**, *127*, 5125; b) M. Nakano, T. Nakashima, T. Kawai, Y. Nonoguchi, *Small* **2017**, *13*, 1700804.

[31] a) H. Wang, P. Wei, Y. Li, J. Han, H. R. Lee, B. D. Naab, N. Liu, C. Wang, E. Adijanto, B. C. K. Tee, S. Morishita, Q. Li, Y. Gao, Y. Cui, Z. Bao, *Proc. Natl. Acad. Sci. USA* **2014**, *111*, 4776; b) T. Fukumaru, T. Fujigaya, N. Nakashima, *Sci. Rep.* **2015**, *5*, 7951; c) C.-K. Mai, B. Russ, S. L. Fronk, N. Hu, M. B. Chan-Park, J. J. Urban, R. A. Segalman, M. L. Chabinyc, G. C. Bazan, *Energy Environ. Sci.* **2015**, *8*, 2341; d) Y. Nakashima, N. Nakashima, T. Fujigaya, *Synth. Met.* **2017**, *225*, 76; e) Y. Nonoguchi, S. Sudo, A. Tani, T. Murayama, Y. Nishiyama, R. M. Uda, T. Kawai, *Chem. Commun.* **2017**, https://doi.org./10.1039/C7CC04295G.

[32] R. Rathore, A. S. Kumar, S. V. Lindeman, J. K. Kochi, *J. Org. Chem.* **1998**, *63*, 5847.

[33] J. B. Bult, R. Crisp, C. L. Perkins, J. L. Blackburn, *ACS Nano* **2013**, *7*, 7251.

[34] B. A. MacLeod, N. J. Stanton, I. E. Gould, D. Wesenberg, R. Ihly, Z. R. Owczarczyk, K. E. Hurst, C. S. Fewox, C. N. Folmar, K. Holman Hughes, B. L. Zink, J. L. Blackburn, A. J. Ferguson, *Energy Environ. Sci.* **2017**, https://doi.org./10.1039/C7EE01130J.

[35] M. L. Geier, J. J. McMorrow, W. Xu, J. Zhu, C. H. Kim, T. J. Marks, M. C. Hersam, *Nat. Nanotechnol.* **2015**, *10*, 944.

© 2017 WILEY-VCH Verlag GmbH & Co. KGaA, Weinheim

Pursuant to the DOE Public Access Plan, this document represents the authors' peer-reviewed, accepted manuscript. The published version of the article is available from the relevant publisher.

[36] D. Hayashi, T. Ueda, Y. Nakai, H. Kyakuno, Y. Miyata, T. Yamamoto, T. Saito, K. Hata, Y. Maniwa, *Appl. Phys. Express* **2016**, *9*, 025102.
[37] B. Norton-Baker, R. Ihly, I. E. Gould, A. D. Avery, Z. R. Owczarczyk, A. J. Ferguson, J. L. Blackburn, *ACS Energy Lett.* **2016**, *1*, 1212.
[38] a) O. Bubnova, Z. U. Khan, A. Malti, S. Braun, M. Fahlman, M. Berggren, X. Crispin, *Nat. Mater.* **2011**, *10*, 429; b) G.-H. Kim, L. Shao, K. Zhang, K. P. Pipe, *Nat. Mater.* **2013**, *12*, 719.
[39] T. Lei, X. Chen, G. Pitner, H. S. P. Wong, Z. Bao, *J. Am. Chem. Soc.* **2016**, *138*, 802.
[40] J. P. Small, K. M. Perez, P. Kim, *Phys. Rev. Lett.* **2003**, *91*, 256801.
[41] S. Shimizu, T. Iizuka, K. Kanahashi, J. Pu, K. Yanagi, T. Takenobu, Y. Iwasa, *Small* **2016**, *12*, 3388.
[42] A. A. Balandin, *Nat. Mater.* **2011**, *10*, 569.
[43] a) S. Berber, Y.-K. Kwon, D. Tománek, *Phys. Rev. Lett.* **2000**, *84*, 4613; b) J. Che, T. Çagin, W. A. Goddard III, *Nanotechnology* **2000**, *11*, 65; c) X.-S. Yang, *Modelling Simul. Mater. Sci. Eng.* **2005**, *13*, 893; d) J. A. Thomas, R. M. Iutzi, A. J. H. McGaughey, *Phys. Rev. B* **2010**, *81*, 045413; e) L. Lindsay, D. A. Broido, N. Mingo, *Phys. Rev. B* **2010**, *82*, 161402; f) A. Cao, J. Qu, *J. Appl. Phys.* **2012**, *112*, 013503; g) S.-Y. Yue, T. Ouyang, M. Hu, *Sci. Rep.* **2015**, *5*, 15440.
[44] a) J. Hone, M. Whitney, C. Piskoti, A. Zettl, *Phys. Rev. B* **1999**, *59*, R2514; b) J. Hone, M. Whitney, A. Zettl, *Synth. Met.* **1999**, *103*, 2498; c) J. Hone, M. C. Llaguno, N. M. Nemes, A. T. Johnson, J. E. Fischer, D. A. Walters, M. J. Casavant, J. Schmidt, R. E. Smalley, *Appl. Phys. Lett.* **2000**, *77*, 666; d) M. Fujii, X. Zhang, H. Xie, H. Ago, K. Takahashi, T. Ikuta, H. Abe, T. Shimizu, *Phys. Rev. Lett.* **2005**, *95*, 065502; e) C. Yu, L. Shi, Z. Yao, D. Li, A. Majumdar, *Nano Lett.* **2005**, *5*, 1842; f) E. Pop, D. Mann, Q. Wang, K. Goodson, H. Dai, *Nano Lett.* **2006**, *6*, 96; g) A. Duzynska, A. Taube, K. P. Korona, J. Judek, M. Zdrojek, *Appl. Phys. Lett.* **2015**, *106*, 183108; h) F. Lian, J. P. Llinas, Z. Li, D. Estrada, E. Pop, *Appl. Phys. Lett.* **2016**, *108*, 103101.
[45] D. G. Cahill, W. K. Ford, K. E. Goodson, G. D. Mahan, A. Majumdar, H. J. Maris, R. Merlin, S. R. Phillpot, *J. Appl. Phys.* **2002**, *93*, 793.
[46] W. Zhou, Q. Fan, Q. Zhang, L. Cai, K. Li, X. Gu, F. Yang, N. Zhang, Y. Wang, H. Liu, W. Zhou, S. Xie, *Nat. Commun.* **2017**, *8*, 14886.
[47] T. Kodama, M. Ohnishi, W. Park, T. Shiga, J. Park, T. Shimada, H. Shinohara, J. Shiomi, K. E. Goodson, *Nat. Mater.* **2017**, *16*, 892.
[48] H. S. Kim, W. Liu, Z. Ren, *Energy Environ. Sci.* **2017**, *10*, 69.
[49] a) O. Bubnova, X. Crispin, *Energy Environ. Sci.* **2012**, *5*, 9345; b) V. Coropceanu, J. Cornil, D. A. da Silva Filho, Y. Olivier, R. Silbey, J.-L. Brédas, *Chem. Rev.* **2007**, *107*, 926.
[50] a) T. Stedman, K. Wei, G. S. Nolas, L. M. Woods, *Phys. Chem. Chem. Phys.* **2015**, *17*, 27883; b) B. Kaiser, Y. W. Park, G. T. Kim, E. S. Choi, G. Düsberg, S. Roth, *Synth. Met.* **1999**, *103*, 2547.
[51] W. Zhou, Q. Fan, Q. Zhang, K. Li, L. Cai, X. Gu, F. Yang, N. Zhang, Z. Xiao, H. Chen, S. Xiao, Y. Wang, H. Liu, W. Zhou, S. Xie, *Small* **2016**, *12*, 3407.
[52] Y. Nonoguchi, K. Hata, T. Kawai, *ChemPlusChem* **2015**, *80*, 1158.
[53] D. Hayashi, Y. Nakai, H. Kyakuno, T. Yamamoto, Y. Miyata, K. Yanagi, Y. Maniwa, *Appl. Phys. Express* **2016**, *9*, 125103.
[54] J. Choi, Y. Jung, S. J. Yang, J. Y. Oh, J. Oh, K. Jo, J. G. Son, S. E. Moon, C. R. Park, H. Kim, *ACS Nano* **2017**, *11*, 7608.
[55] a) Q. Yao, L. Chen, W. Zhang, S. Liufu, X. Chen, *ACS Nano* **2010**, *4*, 2445; b) K. C. See, J. P. Feser, C. E. Chen, A. Majumdar, J. J. Urban, R. A. Segalman, *Nano Lett.* **2010**, *10*, 4664; c) M. Culebras, B. Uriol, C. M. Gómez, A. Cantarero, *Phys. Chem. Chem. Phys.* **2015**, *17*, 15140.
[56] a) Q. Yao, Q. Wang, L. Wang, L. Chen, *Energy Environ. Sci.* **2014**, *7*, 3801; b) N. Dubey, M. Leclerc, *J. Polym. Sci., Part B: Polym. Phys.* **2011**, *49*, 467; c) L. Liang, C. Gao, G. Chen, C.-Y. Guo, *J. Mater. Chem. C* **2016**, *4*, 526.
[57] Y. Chen, Y. Zhao, Z. Liang, *Energy Environ. Sci.* **2015**, *8*, 401.
[58] a) G. P. Moriarty, K. Briggs, B. Stevens, C. Yu, J. C. Grunlan, *Energy Technol.* **2013**, *1*, 265; b) G. P. Moriarty, S. De, P. J. King, U. Khan, M. Via, J. A. King, J. N. Coleman, J. C. Grunlan, *J. Polym. Sci., Part B: Polym. Phys.* **2013**, *51*, 119.
[59] a) J. A. Arsecularatne, L. C. Zhang, *Recent Pat. Nanotechnol.* **2007**, *1*, 176; b) M. T. S. Chani, K. S. Karimov, A. M. Asiri, N. Ahmed, M. M. Bashir, S. B. Khan, M. A. Rub, N. Azum, *PLOS One* **2014**, *9*, e95287.
[60] a) G.-D. Zhan, A. Mukherjee, *Rev. Adv. Mater. Sci.* **2005**, *10*, 185; b) G.-D. Zhan, J. D. Kuntz, A. K. Mukherjee, P. Zhu, K. Koumoto, *Scr. Mater.* **2006**, *54*, 77.
[61] M. Nakano, Y. Nonoguchi, T. Nakashima, K. Hata, T. Kawai, *RSC Adv.* **2016**, *6*, 2489.
[62] a) C. A. Dyke, J. M. Tour, *J. Phys. Chem. A* **2004**, *108*, 11151; b) M. J. Green, N. Behabtu, M. Pasquali, W. W. Adams, *Polymer* **2009**, *50*, 4979; c) N. G. Sahoo, S. Rana, J. W. Cho, L. Li, S. H. Chan, *Prog. Polym. Sci.* **2010**, *35*, 837.
[63] a) P. M. Ajayan, J. M. Tour, *Nature* **2007**, *447*, 1066; b) T. Fujigaya, N. Nakashima, *Sci. Technol. Adv. Mater.* **2015**, *16*, 024802; c) J. Zou, S. I. Khondaker, Q. Huo, L. Zhai, *Adv. Funct. Mater.* **2009**, *19*, 479.
[64] C. Yu, Y. S. Kim, D. Kim, J. C. Grunlan, *Nano Lett.* **2008**, *8*, 4428.
[65] J. C. Grunlan, A. R. Mehrabi, M. V. Bannon, J. L. Bahr, *Adv. Mater.* **2004**, *16*, 150.
[66] a) Y. S. Kim, D. Kim, K. J. Martin, C. Yu, J. C. Grunlan, *Macromol. Mater. Eng.* **2010**, *295*, 431; b) W. Kim, M. Taya, K. Yamada, N. Kamiya, *J. Appl. Phys.* **1998**, *83*, 2593; c) A. Mierczynska, J. Friedrich, H.-E. Maneck, G. Boiteux, J. K. Jeszka, *Cent. Eur. J. Chem.* **2004**, *2*, 363; d) Y. Wang, C. Anderson, *Macromolecules* **1999**, *32*, 6172.
[67] G. P. Moriarty, J. N. Wheeler, C. Yu, J. C. Grunlan, *Carbon* **2012**, *50*, 885.
[68] P. Zhao, E. Einarsson, R. Xiang, Y. Murakami, S. Maruyama, *J. Phys. Chem. C* **2010**, *114*, 4831.
[69] a) J. A. Fagan, J. Y. Huh, J. R. Simpson, J. L. Blackburn, J. M. Holt, B. A. Larsen, A. R. H. Walker, *ACS Nano* **2011**, *5*, 3943; b) J. Chen, C. P. Collier, *J. Phys. Chem. B* **2005**, *109*, 7605.
[70] a) Y. Choi, Y. Kim, S.-G. Park, Y.-G. Kim, B. J. Sung, S.-Y. Jang, W. Kim, *Org. Electron.* **2011**, *12*, 2120; b) K. Suemori, S. Hoshino, T. Kamata, *Appl. Phys. Lett.* **2013**, *103*, 153902; c) M. Piao, G. Kim, G. P. Kennedy, S. Roth, U. Dettlaff-Weglikowska, *Phys. Status Solidi B* **2013**, *250*, 1468; d) L. Tzounis, T. Gärtner, M. Liebscher, P. Pötschke, M. Stamm, B. Voit, G. Heinrich, *Polymer* **2014**, *55*, 5381; e) J. Luo, B. Krause, P. Pötschke, *AIMS Mater. Sci.* **2016**, *3*, 1107; f) Q. Wu, J. Hu, *Composites, Part B* **2016**, *107*, 59.
[71] Q. Zhang, Y. Sun, W. Xu, D. Zhu, *Adv. Mater.* **2014**, *26*, 6829.
[72] M. Culebras, C. M. Gómez, A. Cantarero, *Materials* **2014**, *7*, 6701.
[73] C. Wan, X. Gu, F. Dang, T. Itoh, Y. Wang, H. Sasaki, M. Kondo, K. Koga, K. Yabuki, G. J. Snyder, *Nat. Mater.* **2015**, *14*, 622.
[74] a) E. P. Dillon, C. A. Crouse, A. R. Barron, *ACS Nano* **2008**, *2*, 156; b) K.-S. Liao, J. Wang, D. Früchtl, N. J. Alley, E. Andreoli, E. P. Dillon, A. R. Barron, H. Kim, H. J. Byrne, W. J. Blau, *Chem. Phys. Lett.* **2010**, *489*, 207.
[75] Y. Ryu, D. Freeman, C. Yu, *Carbon* **2011**, *49*, 4745.
[76] D. D. Freeman, K. Choi, C. Yu, *PLOS One* **2012**, *7*, e47822.
[77] C. Yu, A. Murali, K. Choi, Y. Ryu, *Energy Environ. Sci.* **2012**, *5*, 9481.
[78] H. J. Shin, K. K. Kim, A. Benayad, S. M. Yoon, H. K. Park, I. S. Jung, M. H. Jin, H. K. Jeong, J. M. Kim, J. Y. Choi, *Adv. Funct. Mater.* **2009**, *19*, 1987.
[79] J. Luo, G. Cerretti, B. Krause, L. Zhang, T. Otto, W. Jenschke, M. Ullrich, W. Tremel, B. Voit, P. Pötschke, *Polymer* **2017**, *108*, 513.
[80] C. Meng, C. Liu, S. Fan, *Adv. Mater.* **2010**, *22*, 535.
[81] J. Li, X. Tang, H. Li, Y. Yan, Q. Zhang, *Synth. Met.* **2010**, *160*, 1153.
[82] N. Toshima, *Macromol. Symp.* **2002**, *186*, 81.

© 2017 WILEY-VCH Verlag GmbH & Co. KGaA, Weinheim

Pursuant to the DOE Public Access Plan, this document represents the authors' peer-reviewed, accepted manuscript. The published version of the article is available from the relevant publisher.

[83] H. Yan, T. Ohta, N. Toshima, *Macromol. Mater. Eng.* **2001**, *286*, 139.
[84] a) Y. Du, S. Z. Shen, K. Cai, P. S. Casey, *Prog. Polym. Sci.* **2012**, *37*, 820; b) L. Wang, Q. Yao, J. Xiao, K. Zeng, S. Qu, W. Shi, Q. Wang, L. Chen, *Chem. Asian J.* **2016**, *11*, 1804.
[85] Q. Yao, Q. Wang, L. Wang, Y. Wang, J. Sun, H. Zeng, Z. Jin, X. Huang, L. Chen, *J. Mater. Chem. A* **2014**, *2*, 2634.
[86] A. G. MacDiarmid, A. J. Epstein, *Synth. Met.* **1995**, *69*, 85.
[87] Q. Wang, Q. Yao, J. Chang, L. Chen, *J. Mater. Chem.* **2012**, *22*, 17612.
[88] Y. Sun, S. R. Wilson, D. I. Schuster, *J. Am. Chem. Soc.* **2001**, *123*, 5348.
[89] a) J. Liu, J. Sun, L. Gao, *Nanoscale* **2011**, *3*, 3616; b) Z. Wang, J. Yuan, M. Li, D. Han, Y. Zhang, Y. Shen, L. Niu, A. Ivaska, *J. Electroanal. Chem.* **2007**, *599*, 121.
[90] M. S. Dresselhaus, G. Chen, M. Y. Tang, R. Yang, H. Lee, D. Wang, Z. Ren, J. P. Fleurial, P. Gogna, *Adv. Mater.* **2007**, *19*, 1043.
[91] Q. Zhang, W. Wang, J. Li, J. Zhu, L. Wang, M. Zhu, W. Jiang, *J. Mater. Chem. A* **2013**, *1*, 12109.
[92] L. Wang, Q. Yao, W. Shi, S. Qu, L. Chen, *Mater. Chem. Front.* **2017**.
[93] A. Elschner, S. Kirchmeyer, W. Lövenich, U. Merker, K. Reuter, *PEDOT: Principles and Applications of an Intrinsically Conductive Polymer*, CRC Press, Boca Raton, FL **2010**.
[94] a) T. Park, C. Park, B. Kim, H. Shin, E. Kim, *Energy Environ. Sci.* **2013**, *6*, 788; b) R. Yue, J. Xu, *Synth. Met.* **2012**, *162*, 912; c) H.-Y. Chen, H.-P. Shen, C.-H. Wu, W.-Y. Chiu, W.-C. Chen, H.-J. Tai, *J. Mater. Chem. C* **2013**, *1*, 5351; d) M. Scholdt, H. Do, J. Lang, A. Gall, A. Colsmann, U. Lemmer, J. D. Koenig, M. Winkler, H. Boettner, *J. Electron. Mater.* **2010**, *39*, 1589; e) C. Liu, B. Lu, J. Yan, J. Xu, R. Yue, Z. Zhu, S. Zhou, X. Hu, Z. Zhang, P. Chen, *Synth. Met.* **2010**, *160*, 2481.
[95] K. Zhang, J. Qiu, S. Wang, *Nanoscale* **2016**, *8*, 8033.
[96] D. Kim, Y. Kim, K. Choi, J. C. Grunlan, C. Yu, *ACS Nano* **2009**, *4*, 513.
[97] C. Yu, K. Choi, L. Yin, J. C. Grunlan, *ACS Nano* **2011**, *5*, 7885.
[98] S. De, P. E. Lyons, S. Sorel, E. M. Doherty, P. J. King, W. J. Blau, P. N. Nirmalraj, J. J. Boland, V. Scardaci, J. Joimel, *ACS Nano* **2009**, *3*, 714.
[99] R. J. Smith, P. J. King, M. Lotya, C. Wirtz, U. Khan, S. De, A. O'Neill, G. S. Duesberg, J. C. Grunlan, G. Moriarty, *Adv. Mater.* **2011**, *23*, 3944.
[100] H. Li, B. Zhou, Y. Lin, L. Gu, W. Wang, K. S. Fernando, S. Kumar, L. F. Allard, Y.-P. Sun, *J. Am. Chem. Soc.* **2004**, *126*, 1014.
[101] H. Song, C. Liu, J. Xu, Q. Jiang, H. Shi, *RSC Adv.* **2013**, *3*, 22065.
[102] Z. Zhu, C. Liu, H. Shi, Q. Jiang, J. Xu, F. Jiang, J. Xiong, E. Liu, *J. Polym. Sci., Part B: Polym. Phys.* **2015**, *53*, 885.
[103] T. Humphrey, M. O'Dwyer, H. Linke, *J. Phys. D: Appl. Phys.* **2005**, *38*, 2051.
[104] C. T. Hong, W. Lee, Y. H. Kang, Y. Yoo, J. Ryu, S. Y. Cho, K.-S. Jang, *J. Mater. Chem. A* **2015**, *3*, 12314.
[105] W. Lee, Y. H. Kang, J. Y. Lee, K.-S. Jang, S. Y. Cho, *RSC Adv.* **2016**, *6*, 53339.
[106] a) D. A. Mengistie, C.-H. Chen, K. M. Boopathi, F. W. Pranoto, L.-J. Li, C.-W. Chu, *ACS Appl. Mater. Interfaces* **2014**, *7*, 94; b) Y.-J. Lin, W.-S. Ni, J.-Y. Lee, *J. Appl. Phys.* **2015**, *117*, 215501.
[107] L. Li, F. Yan, G. Xue, *J. Appl. Polym. Sci.* **2004**, *91*, 303.
[108] J. Wang, K. Cai, S. Shen, J. Yin, *Synth. Met.* **2014**, *195*, 132.
[109] L. Liang, G. Chen, C.-Y. Guo, *Compos. Sci. Technol.* **2016**, *129*, 130.
[110] a) J. Zhang, X. Zhao, *J. Phys. Chem. C* **2012**, *116*, 5420; b) L. Sun, Y. Shi, L. Chu, Y. Wang, L. Zhang, J. Liu, *J. Appl. Polym. Sci.* **2012**, *123*, 3270.
[111] a) W. Lee, C. T. Hong, O. H. Kwon, Y. Yoo, Y. H. Kang, J. Y. Lee, S. Y. Cho, K.-S. Jang, *ACS Appl. Mater. Interfaces* **2015**, *7*, 6550; b) L. Wang, X. Jia, D. Wang, G. Zhu, J. Li, *Synth. Met.* **2013**, *181*, 79; c) S. Qu, Q. Yao, L. Wang, Z. Chen, K. Xu, H. Zeng, W. Shi, T. Zhang, C. Uher, L. Chen, *NPG Asia Mater.* **2016**, *8*, e292.
[112] C. Bounioux, P. Díaz-Chao, M. Campoy-Quiles, M. S. Martín-González, A. R. Goñi, R. Yerushalmi-Rozen, C. Müller, *Energy Environ. Sci.* **2013**, *6*, 918.
[113] C. T. Hong, Y. H. Kang, J. Ryu, S. Y. Cho, K.-S. Jang, *J. Mater. Chem. A* **2015**, *3*, 21428.
[114] a) Y. Wang, K. Cai, J. Yin, Y. Du, X. Yao, *Mater. Chem. Phys.* **2012**, *133*, 808; b) K. Zhang, M. Davis, J. Qiu, L. Hope-Weeks, S. Wang, *Nanotechnology* **2012**, *23*, 385701; c) H. Wang, S.-i. Yi, X. Pu, C. Yu, *ACS Appl. Mater. Interfaces* **2015**, *7*, 9589.
[115] Z. Zhang, G. Chen, H. Wang, X. Li, *Chem. Asian J.* **2015**, *10*, 149.
[116] F. Rivadulla, C. Mateo-Mateo, M. Correa-Duarte, *J. Am. Chem. Soc.* **2010**, *132*, 3751.
[117] C. Cho, B. Stevens, J. H. Hsu, R. Bureau, D. A. Hagen, O. Regev, C. Yu, J. C. Grunlan, *Adv. Mater.* **2015**, *27*, 2996.
[118] Y. Hiroshige, M. Ookawa, N. Toshima, *Synth. Met.* **2006**, *156*, 1341.
[119] B. Abad, I. Alda, P. Díaz-Chao, H. Kawakami, A. Almarza, D. Amantia, D. Gutierrez, L. Aubouy, M. Martín-González, *J. Mater. Chem. A* **2013**, *1*, 10450.
[120] a) K. Zhang, Y. Zhang, S. Wang, *Sci. Rep.* **2013**, *3*, 3448; b) T. Zou, X. Qin, D. Li, B. Ren, G. Sun, Y. Dou, Y. Li, L. Li, J. Zhang, H. Xin, *J. Appl. Phys.* **2014**, *115*, 053710; c) S. V. Faleev, F. Léonard, *Phys. Rev. B* **2008**, *77*, 214304.
[121] C. Cho, M. Culebras, K. L. Wallace, Y. Song, K. Holder, J.-H. Hsu, C. Yu, J. C. Grunlan, *Nano Energy* **2016**, *28*, 426.
[122] A. B. Bourlinos, V. Georgakilas, R. Zboril, T. A. Steriotis, A. K. Stubos, C. Trapalis, *Sol. State Commun.* **2009**, *149*, 2172.
[123] T. Nakashima, J. Zhu, M. Qin, S. Ho, N. A. Kotov, *Nanoscale* **2010**, *2*, 2084.
[124] a) M. Shim, A. Javey, N. W. S. Kam, H. Dai, *J. Am. Chem. Soc.* **2001**, *123*, 11512; b) M. Rastegaralam, M. Piao, G. Kim, U. Dettlaff-Weglikowska, S. Roth, *Phys. Status Solidi C* **2013**, *10*, 1183.
[125] B. Stevens, E. Dessiatova, D. A. Hagen, A. D. Todd, C. W. Bielawski, J. C. Grunlan, *ACS Appl. Mater. Interfaces* **2014**, *6*, 9942.
[126] a) L.-D. Zhao, S.-H. Lo, Y. Zhang, H. Sun, G. Tan, C. Uher, C. Wolverton, V. P. Dravid, M. G. Kanatzidis, *Nature* **2014**, *508*, 373; b) L.-D. Zhao, J. He, D. Berardan, Y. Lin, J.-F. Li, C.-W. Nan, N. Dragoe, *Energy Environ. Sci.* **2014**, *7*, 2900.
[127] T. M. Tritt, H. Böttner, L. Chen, *MRS Bull.* **2008**, *33*, 366.
[128] S. LeBlanc, *Sustainable Mater. Technol.* **2014**, *1*, 26.
[129] a) F. Jiao, C.-a. Di, Y. Sun, P. Sheng, W. Xu, D. Zhu, *Philos. Trans. R. Soc., A* **2014**, *372*, 20130008; b) R. R. Søndergaard, M. Hösel, N. Espinosa, M. Jørgensen, F. C. Krebs, *Energy Sci. Eng.* **2013**, *1*, 81; c) B. Dörling, J. D. Ryan, J. D. Craddock, A. Sorrentino, A. E. Basaty, A. Gomez, M. Garriga, E. Pereiro, J. E. Anthony, M. C. Weisenberger, *Adv. Mater.* **2016**.
[130] a) C. A. Hewitt, A. B. Kaiser, S. Roth, M. Craps, R. Czerw, D. L. Carroll, *Nano Lett.* **2012**, *12*, 1307; b) C. A. Hewitt, D. S. Montgomery, R. L. Barbalace, R. D. Carlson, D. L. Carroll, *J. Appl. Phys.* **2014**, *115*, 184502.
[131] S. L. Kim, K. Choi, A. Tazebay, C. Yu, *ACS Nano* **2014**, *8*, 2377.

 © 2017 WILEY-VCH Verlag GmbH & Co. KGaA, Weinheim

Pursuant to the DOE Public Access Plan, this document represents the authors' peer-reviewed, accepted manuscript. The published version of the article is available from the relevant publisher.